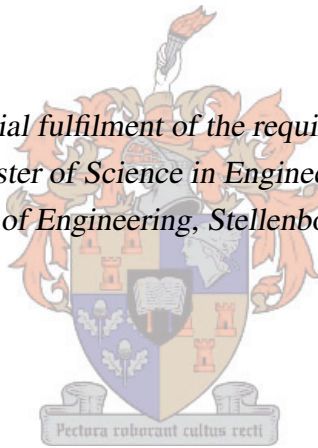


Electronically Adjustable Bandpass Filter

by

Phillip Terblanche

*Thesis presented in partial fulfilment of the requirements for the degree of
Master of Science in Engineering
at the Faculty of Engineering, Stellenbosch University*



Supervisors: Prof. Petrie Meyer and Dr. Dirk de Villiers
Department of Electrical and Electronic Engineering

December 2011

Declaration

By submitting this thesis electronically, I declare that the entirety of the work contained therein is my own, original work, that I am the sole author thereof (save to the extent explicitly otherwise stated), that reproduction and publication thereof by Stellenbosch University will not infringe any third party rights and that I have not previously in its entirety or in part submitted it for obtaining any qualification.

Date: December 2011

Copyright © 2011 Stellenbosch University
All rights reserved.

Abstract

This thesis presents the study, analysis and design of electronically tunable filters, that can be tuned over a wide frequency range (20-500MHz), for use in a direct sampling receiver. The final design does not have to be a single filter, but may be comprised of a filter bank which enables switching between the filters. The band of interest is too low to use normal transmission lines and lumped elements have to be used. Different topologies that can implement Coupled Resonator filters with lumped elements are investigated. Devices that can be used for tuning are also investigated and varactor diodes are found to be the most suitable tuning devices currently available. Two filters, one at the high-end and one at the low-end of the band, were designed and built, both using varactor diodes. These filters perform well in terms of tuning range, but achieving low losses with current technologies in this band remains difficult.

Uittreksel

Hierdie tesis meld die studie, analise en ontwerp van elektronies verstelbare filters, wat verstelbaar is oor 'n wye band (20-500MHz), vir gebruik in 'n direk-monster-ontvanger. Die finale ontwerp hoef nie 'n enkele filter te wees nie, maar kan bestaan uit 'n filterbank wat skakeling tussen die filters toelaat. Die betrokke band is te laag vir die gebruik van normale transmissielyne en diskrete komponente moet gebruik word. Verskillende topologieë wat gekoppelde resoneerder filters implementeer met diskrete komponente is ondersoek. Verstelbare komponente word ook ondersoek en varaktor diodes blyk die mees geskikte verstelbare komponent wat huidig beskikbaar is in hierdie band. Twee filters, een aan die hoë kant en een aan die lae kant van die band, is ontwerp en gebou, beide met varaktor diodes. Hierdie filters het wye verstelbare bereik, maar dit is steeds moeilik om verliese te beperk met die huidige tegnologie.

Acknowledgements

I would like to thank the following people and institutions for their contributions to this project:

- Prof. P. Meyer and Dr. D. de Villiers for their help and encouragement.
- Wessel Croukamp for building my filters and for his friendly help.
- Grintek Ewation for funding this project.
- The University of Stellenbosch for usage of their facilities.
- My girlfriend, Caroline, for her support and motivation.
- My family, for their support and prayers.
- David Prinsloo, Shamim Omar, David Smith and Theunis Beukman for their support and advice.

Table of Contents

Declaration	i
Abstract	ii
Uittreksel	iii
Table of Contents	v
List of Figures	viii
List of Tables	xi
List of Acronyms	xii
1 Introduction	1
1.1 Filter requirements for software defined radio	1
1.2 Literature overview	3
1.3 Objectives and Specifications	4
1.4 Contributions	5
1.5 Thesis layout	5
2 Coupled Resonator Filter Theory	8
2.1 Modern Filter Synthesis	8
2.1.1 Ideal Impedance and Admittance Inverters	8
2.1.2 Inverters in a low pass prototype	10
2.1.3 Bandpass transformation	11
2.2 Resonators	12
2.3 Inter-resonator Coupling	12
2.4 Input and output coupling (Q_e)	15
2.5 CR Filter Design	16
2.6 Designing for tunability	17
2.6.1 Constant relative bandwidth	18
2.6.2 Constant absolute bandwidth	18
2.7 Conclusion	18

3	Filter Implementation for Tunability	19
3.1	Tunable resonators	19
3.1.1	Parallel LC tank	19
3.1.2	Short-circuited transmission line loaded with a capacitor	20
3.1.3	Parallel-series LC resonator	20
3.2	Implementation of inverters	22
3.2.1	Capacitor pi-network	23
3.2.2	Inductor pi-network	24
3.2.3	Capacitor and Inductor pi-network	25
3.2.4	Parallel coupled transmission lines	26
3.3	Coupling tuned resonators	28
3.3.1	Capacitor pi-network coupling	29
3.3.2	Inductor-Capacitor pi-network coupling	30
3.3.3	Parallel coupled transmission lines	32
3.4	Coupling to source and load	33
3.5	Conclusion	35
4	Non-ideal components	37
4.1	Lumped elements	37
4.2	Transmission lines	38
4.3	Components for discrete tuning	39
4.3.1	PIN diodes	40
4.3.2	RF semiconductor switches	41
4.3.3	RF MEMS switches	42
4.4	Components for continuous tuning	43
4.4.1	Varactor diodes	43
4.4.2	YIG crystal resonator	45
4.4.3	RF MEMS varactors	45
4.5	Conclusion	46
5	Filter design	47
5.1	Prototypes with sharp cut-off	47
5.1.1	Elliptic prototype	47
5.1.2	Chebyshev prototype	49
5.2	Minimising insertion loss	49
5.2.1	Unloaded Q	49
5.2.2	Bandwidth	49
5.2.3	Filter order	50
5.2.4	Minimizing the loss of varactors diodes	51
5.3	Designing bandwidth and order for cut-off specification	52
5.4	Low side filter	52
5.4.1	Filter design procedure	53

5.4.2	Implementing the design	55
5.4.3	PCB design	58
5.4.4	Simulations and Measurements	58
5.5	High side filter	61
5.5.1	Filter design procedure	61
5.5.2	Implementation of inter-resonator coupling	64
5.5.3	Simulations and Measurements	65
5.6	Conclusion	68
6	Conclusions and recommendations	70
6.1	Recommended filter bank design	71
6.2	Future work	72
A	Lumped Element Inverter Implementations	73
B	Selected information from datasheets	75
B.1	Transmission lines	75
B.1.1	Trans-Tech™ ceramic resonators	75
B.1.2	Micro-coax semi-rigid line	77
B.1.3	SRC semi-rigid lines	78
B.2	Passive lumped elements	79
B.2.1	Coilcraft® Micro spring™ air core inductors	79
B.2.2	AVX Microwave MLC COG (NPO)	80
B.3	Varactor diodes	81
B.3.1	NXP BB179	81
B.4	RF switches	82
B.4.1	Randant MEMS	82
C	Numerical computation	83
D	Digital control system schematics	84
	List of References	88

List of Figures

1.1	The original spectrum and the shifted replicas [1]	2
1.2	Allowed and forbidden sampling rates for bandpass signals. The shaded regions indicate sample rates for bandpass signals that will not cause aliasing [2].	3
2.1	Low pass ladder prototype networks	9
2.2	The input impedance and input admittance of loaded impedance and admittance inverters	9
2.3	The working of an inverter	10
2.4	Coupled resonator low pass prototype networks	11
2.5	Coupled resonator bandpass prototype with admittance inverters	11
2.6	Two-port coupling with mutual capacitance	13
2.7	Capacitive coupling between two capacitors	14
2.8	Coupled parallel LC resonators coupled	14
2.9	Frequency response of the circuit in figure 2.8 for different coupling coefficient values	15
2.10	Frequency response showing the effect of different external Q values	16
2.11	CR bandpass prototype using admittance inverters	17
3.1	Susceptance of the capacitor, $\omega_0 C$, and negative of the transmission line susceptance, $-Y_0 \cot(\omega_0 T)/\omega_0$. The circuit resonates at the intersection point of the two curves, which represent zero susceptance.	21
3.2	LC circuit with parallel and series resonances	21
3.3	The admittance of a parallel-series-type resonator	22
3.4	Pi-network of admittances	22
3.5	Capacitor pi-network inverter	23
3.6	Comparison between an ideal inverter, a capacitor-pi inverter and inductor-pi inverter	24
3.7	Inductor pi-network inverter	25
3.8	CLC pi-network	25
3.9	Comparison of inductor and inductor-capacitor pi-network inverters	26
3.10	Parallel coupled transmission lines and equivalent circuit	27
3.11	Two resonators coupled with parallel transmission lines	27
3.12	Comparison of parallel coupled short-circuited stubs with different electrical lengths	28
3.13	LC resonators coupled with capacitor pi-network	29
3.14	Short circuited transmission lines coupled with capacitor pi-network	29

3.15	Frequency dependence of coupling between short-circuited transmission lines with capacitor pi-network in the range $\frac{\pi}{6} \leq \theta_0 \leq \frac{\pi}{2}$	30
3.16	LC resonators coupled with inductor-capacitor pi-network	30
3.17	Short circuited transmission line coupled with inductor-capacitor pi-network	31
3.18	Frequency dependence of coupling between short-circuited transmission lines with inductor-capacitor pi-network in the range $\frac{\pi}{6} \leq \theta_0 \leq \frac{\pi}{2}$	32
3.19	Parallel coupled short circuited transmission lines	32
3.20	Coupling coefficient between two resonators of a combline filter	33
3.21	Series and parallel equivalent impedance transformers	33
3.22	Impedance transformer coupled to LC-resonator	34
4.1	Tunable resonator that can be adjusted to four discrete resonant frequencies	39
4.2	Series resistance vs forward current for Skyworks SMP1322 PIN diode (measured at 100MHz)	40
4.3	Single-pole PIN diode switches in (a) series configuration and (b) shunt configuration	41
4.4	Single-pole, triple throw, PIN diode compound switch with diodes in the RF path (series configuration)	41
4.5	MEMS series switch configurations, broadside with (a) one electrode, (b) two electrodes, and (c) an in-line switch [3]	42
4.6	Typical voltage-capacitance curves for varactor diodes	44
4.7	Series resistance vs. biasing voltage of the M/A-COM MA4ST1300 Series	44
4.8	MEMS shunt switch to implement variable capacitor [4]	46
5.1	Example of circuit with many cross coupling paths	48
5.2	Triplet and quadruplet coupling configurations	48
5.3	Elliptic filter implemented with a quadruplet and compared with a fourth order Chebyshev filter	48
5.4	Comparison of lossless response and filters with finite Q_u	50
5.5	Effect of bandwidth on passband loss	50
5.6	Comparison of the insertion loss at the centre frequency of filters with different order	51
5.7	Maximum absolute bandwidth to meet specifications	52
5.8	Required unloaded resonator Q to meet insertion loss specification when using the maximum bandwidth	53
5.9	Fourth order filter prototype with inductor-capacitor pi-network inverters and LC resonators	53
5.10	Capacitor tuning curves	56
5.11	Varactor biasing circuits	57
5.12	Measured and data sheet capacitance of BB201 varactor	57
5.13	Improvement of filter response after adding vias in ground plane	58
5.14	Photo of the filter, scale 1:1	59
5.15	MWO circuit simulation	59
5.16	Measurements and simulated results for filter tuned to $f_0 = 23\text{MHz}$, $f_0 = 39\text{MHz}$ and $f_0 = 54\text{MHz}$	60
5.17	Effect of different filter order on passband insertion loss	62
5.18	Single resonator as simulated in AWR® Microwave Office® (MWO)	63
5.19	Resonator capacitor tuning curves	64

LIST OF FIGURES

5.20	EM simulation of interdigital capacitor	65
5.21	Photo of high side filter	66
5.22	Filter response before and after the resonators were shielded from each other	66
5.23	Simulated and measured results when filter is tuned to $f_0 = 498\text{MHz}$, $f_0 = 450\text{MHz}$ and $f_0 = 400\text{MHz}$	67
6.1	Maximum fractional bandwidth for different order Chebyshev filters to meet cut-off specification .	71
C.1	MATLAB® code for computation of chebyshev prototype values	83

List of Tables

3.1	Comparison of different inverter and resonator combinations	36
4.1	Unloaded Q factors of quarter wave length transmission lines at 500MHz in order of ascending Q_u	39
5.1	Summary of inductor values	55
5.2	Summary of capacitor values at different tuning points	56
5.3	Summary of insertion loss values at different tuning points	61
5.4	Summary of coupling capacitors and their interdigital capacitor design values	64
5.5	Capacitance values [pF] of interdigital capacitors according to design equations and simulations	65
5.6	Comparison of tunable and non-tunable filters in terms of their insertion loss	68
6.1	Minimum required tuning ranges for tunable filters in a filter bank covering the band from 20-500MHz	71
A.1	Pi-network inverter implementations for use with resonators with parallel type of resonance	73
A.2	T-network inverter implementations for use with resonators with series type of resonance	74

List of Acronyms

RF	Radio Frequency
SDR	Software Defined Radio
MEMS	micro electromechanical systems
SMD	Surface mount device
CR	Coupled Resonator
DC	Direct Current
LC	inductor-capacitor
TEM	Transverse Electromagnetic
ADC	Analog to Digital Converter
YIG	Yttrium-iron-garnite
IF	Intermediate frequency
SRF	self resonant frequency
GaAs	Gallium arsenide
CMOS	Complementary metal oxide semiconductor
BST	Barium-Strontium-Titanate
FET	Field-effect transistor
IC	Integrated circuit
CT	cascaded triplet
CQ	cascaded quadruplet
MWO	AWR® Microwave Office®
PCB	printed circuit board

LIST OF ACRONYMS

ESR equivalent series resistance

EM Electromagnetic

Chapter 1

Introduction

Electronically tunable bandpass filters are of great interest to the communication industry. They constitute one of the key hardware components needed to realise direct sampling receivers, which are used in Software Defined Radios (SDRs). The Radio Frequency (RF) signal may be sampled and perfectly reconstructed by making use of bandpass sampling, which is also known as undersampling.

A bandpass filter is needed to attenuate all the frequencies outside the band of interest in order to limit the bandwidth of the signal to be sampled. To keep the sampling rate down, a relatively narrow bandwidth is required for the filter. But this limits the use of the system, as it can only view a narrow band. For this reason the use of a tunable filter is preferable, as it extends the range of the system. A tunable filter will enable the direct sampling receiver to access a wide band by focussing on multiple narrower bands in turn.

Superheterodyne (superhet) receivers are currently in competition with direct sampling receivers, the latter of which are gaining competitiveness as the sampling rate of Analog to Digital Converters (ADCs) increase. The superhet receiver use mixers to down-convert the RF signal, and then filters it at an Intermediate frequency (IF) where crystal filters can be used. The mixers can be tuned to give this system the same flexibility as the direct sampling receiver. The most important advantage of a direct sampling receiver is that filtering and demodulation can be done with computer software, which is much easier and cheaper to change than special-purpose hardware.

1.1 Filter requirements for software defined radio

Digital systems attempt to sample analog signals without loss of information due to aliasing. The correct sampling rate is sufficient to prevent this type of distortion.

The Nyquist rate for lowpass signals is [1]:

$$F_N = 2B = 2F_H \quad (1.1)$$

where B is the bandwidth and F_H is the highest frequency contained in the sampled signal. The original signal can be perfectly reconstructed with the samples if the signal is sampled at a the Nyquist rate, or faster. But for a bandpass signal, the highest frequency does not equal the bandwidth. The Nyquist rate for such a signal reduces to $F_N = 2B$. The technique of exploiting this fact, and sampling at a rate less than twice the highest frequency is known as bandpass sampling (or undersampling).

A bandpass signal, $x_a(t)$, sampled at $F_s = 1/T_s$ produces a sequence $x(n) = x_a(nT_s)$. The frequency spectrum of this signal is given by:

$$X(F) = F_s \sum_{k=-\infty}^{\infty} X_a(F - kF_s) \quad (1.2)$$

where k is an integer. The positioning of the shifted copies of $X_a(F - kF_s)$ is only controlled by the sampling frequency, F_s . Care should be taken in the choice of F_s to avoid aliasing, as a bandpass signal has two spectral bands.

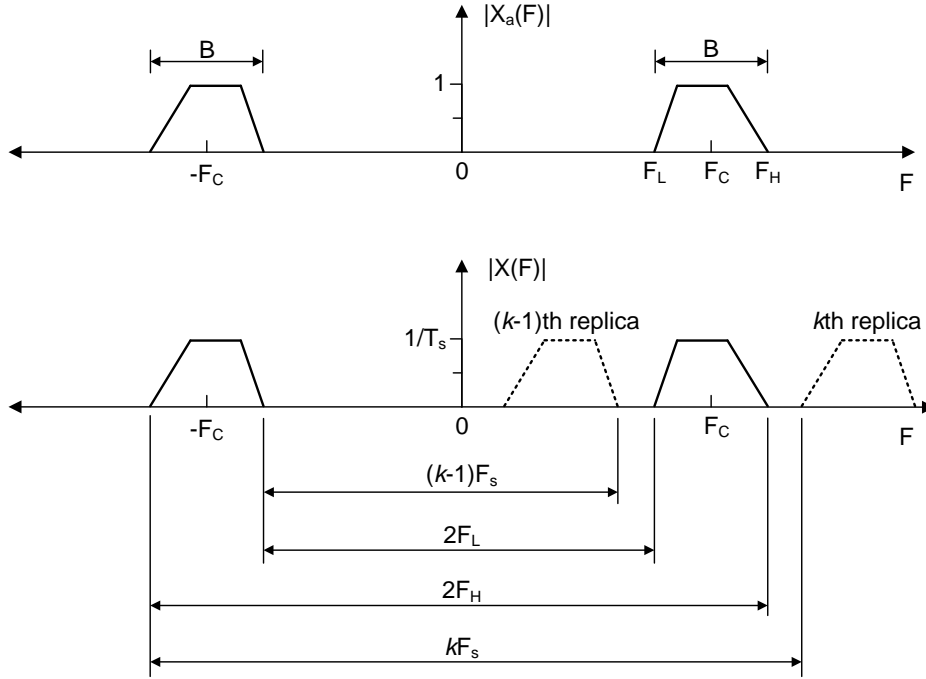


Figure 1.1: The original spectrum and the shifted replicas [1]

"To avoid aliasing, the sampling frequency should be chosen such that the $(k - 1)$ th and the k th shifted replicas of the "negative" spectral band do not overlap with the "positive" spectral band" [1], see figure 1.1.

From figure 1.1, the range of suitable sampling rates is determined by [1]

$$\frac{2F_H}{k} \leq F_s \leq \frac{2F_L}{k-1} \quad (1.3)$$

where F_L is the lowest frequency in the bandpass signal, and F_H is the highest. The integer k is given by

$$1 \leq k \leq \left\lfloor \frac{F_H}{F_H - F_L} \right\rfloor \quad (1.4)$$

The conditions given in equations (1.3) and (1.4) can be shown in a graph as shown in figure 1.2.

The largest possible value for k gives the lowest possible sampling rate. This rate places the maximum number of frequency spectrum replicas between 0 and F_H , where k is the number of bands. The close spacing leaves a small margin for error for the sampling frequency, and the maximum k is seldom used.

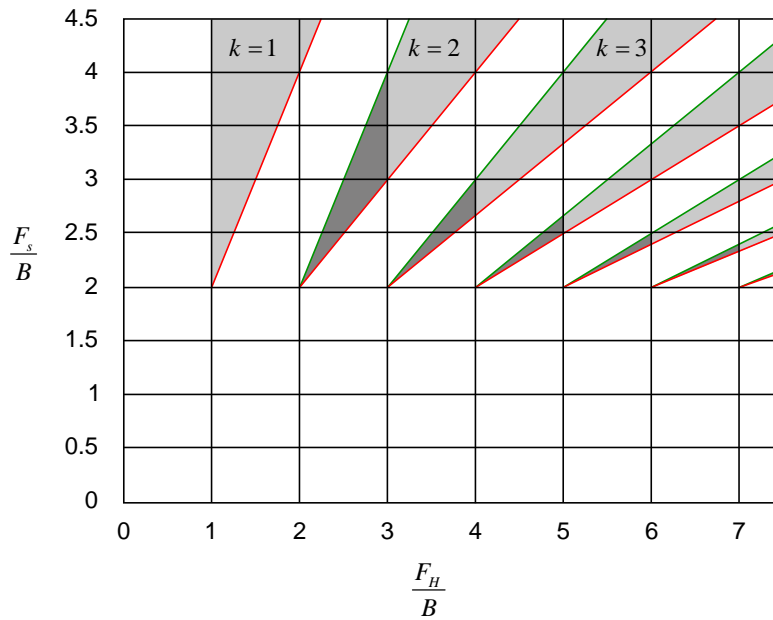


Figure 1.2: Allowed and forbidden sampling rates for bandpass signals. The shaded regions indicate sample rates for bandpass signals that will not cause aliasing [2].

The bandwidth and the cut-off rate of the bandpass filter directly determines the lower bound of the required sampling rate, according to equations (1.3) and (1.4). The frequencies, F_H and F_L , are not the band edges, but the stopband edges where the signal has been attenuated to such a degree that their influence is deemed negligible. A filter with a steep cut-off rate will consequently be given preference.

The dynamic range of an ADC is the ratio between smallest and largest possible signal values that can be detected. Frequencies outside the band of interest must be attenuated by more than the dynamic range in order to differentiate between the smallest signals in the passband and the largest signals in the stopband. For this reason an ADC with wide dynamic range necessitates a filter with considerable attenuation in the stopband.

A tunable bandpass filter will enable a SDR to access a wide band by sampling different sections of the frequency band at a time. The tuning speed specification of the filter is determined by the tempo at which the ADC can output the digital data. The narrower the bandwidth of the filter, the slower it will be able to tune. This argument cautions against using a very narrow band filter when designing for the minimum sampling rate.

1.2 Literature overview

Coupled Resonator (CR) theory is a mature design technique and well covered in literature [5–9]. The theory was extended to tunable filters, and implemented with mechanical and magnetic tuning at microwave frequencies [5, ch. 17]. There is not much literature available on tunable filters in the band below 500MHz. The tunable filters found in literature are mostly in the range around 1GHz and implemented in stripline or microstrip.

As example, Hunter and Rhodes [10] present a combline filter of which the centre frequency may be tuned over a broad bandwidth. The filter incorporates novel input and output coupling networks to enable tuning of the centre frequency with minimal degradation in passband performance. The reason why this filter is able to tune with so little change in passband characteristics is of key interest and will accordingly be thoroughly

investigated.

Distributed filter implementations are not suitable for frequencies below 500MHz, as the wavelength becomes too long to be deemed practical. This limits the suitable designs to lumped element implementations. Tuning elements are of key importance in tunable filters.

"An [ideal] tuner is a variable capacitive device (analog varactor, a switched capacitor, a low-loss switch followed by a fixed capacitor) with low series resistance (high-Q), zero power consumption, large power handling (watt level), very high linearity, and fast switching speeds (μ s). It is small and lightweight, temperature insensitive, and can be integrated in a planar fashion and with a simple and accurate equivalent circuit model." [11]

A comparison between tuning elements was done by Uher and Hofer [12]. They found that the best tuning device is the Yttrium-iron-garnite (YIG) tuner. This is an expensive tuner that requires a lot of current (0.3-3A), as well as a magnet, and cannot be integrated in a planar fashion. The second best device is RF micro electromechanical systems (MEMS) [3] switches and varactors. MEMS switches may be used to switch discrete components in and out of a circuit [11]. Variable capacitors may also be constructed with MEMS technology. Yet MEMS still remains a relatively expensive option, and is therefore not the ideal choice.

Varactor diodes are relatively cheap and widely available. They are small and available in Surface mount device (SMD) packages. These diodes are consequently the tuning device of choice for this project although they are relatively lossy and create non-linear distortion. These drawbacks have been investigated by Brown and Rebeiz [13]. They measured varactor loss and found it to vary with applied bias and frequency. Their tunable combline filter measurements are comparable to state-of-the-art YIG filters. Varactors, MEMS and YIG circuit elements are discussed in more depth in chapter 4.

1.3 Objectives and Specifications

This thesis presents the study, analysis and design of electronically tunable filters, that can be tuned over a wide frequency range, for use in a direct sampling receiver. The final design does not have to be a single filter, but may be comprised of a filter bank which enables switching between the filters. The specifications are as follows:

- Range: 20MHz to 500MHz
- Bandwidth: 2MHz to 20MHz
- Pass-band attenuation: less than 3dB
- Stop-band attenuation: more than 80dB 10MHz from pass-band edge
- Tuning speed: 100MHz/s
- Power handling: +30dBm

The primary objective of this project is to investigate if the above specifications can be achieved with available technology by designing and building a set of tunable filters. The secondary objectives that serve as guide to reach the primary objective are as follows:

- Review modern filter theory, in order to see how optimal tuning may be achieved.
- Evaluate different filter implementations that may enable such tuning.
- Investigate different components across the band of interest to minimize pass band loss.
- Design, build and measure tunable filters that confirm the simulated results.
- Design a digital control system to select and tune the different filters.

The completed system should then be able to electronically select a filter and tune its centre frequency, whilst keeping the bandwidth within the desired range.

1.4 Contributions

This project makes a number of contributions to the design and implementation of tunable filters in lumped element technology. The specific contributions may be stated as follows:

- Applicability of tunable microwave filter design theory to lumped element filters.
- A discussion of the areas where the theory and implementation diverges because of the use of practical lumped elements.
- Comparison of state-of-the-art tuning components to be used in the frequency range 20MHz to 500MHz.
- The design and measurement of two filters, one at the low end of the 20-500MHz band, and one at the high end. The fourth order low-end filter can be tuned from 23MHz to 54MHz with insertion loss at f_0 decreasing from 2.22 to 1.55. The sixth order high-end filter was designed at 500MHz, where it has 8.6dB insertion loss at f_0 and can tune down to where the passband disappears into the noise floor at 250MHz.

1.5 Thesis layout

This investigation commences with the discussion of Coupled Resonator theory to be used in the design of tunable filters. The parameters that determine the bandwidth and centre frequency of a CR filter are conveniently expressed in the design equations. The impact on these two properties when changing filter elements can be deduced from these equations. Chapter 2 (page 8) states CR theory with an emphasis on inter-resonator coupling. This coupling influences the bandwidth and is implemented with impedance and admittance inverters, as discussed in section 2.3 (page 12).

The resonators are the elements that determine the centre frequency and that are tuned to change it. But this adjustment also changes the filter response and so the inter-resonator coupling and input/output coupling needs to be adjusted accordingly to ensure a good response. Chapter 2 concludes by discussing optimal tuning methods in section 2.6 (page 17). These respective methods are able to accomplish constant relative bandwidth or constant absolute bandwidth.

The ideal CR filter design can be implemented in a variety of forms, finding the optimal combination for a tunable filter is the subject of chapter 3 (page 19). Impedance and admittance inverters cannot be implemented

with lumped elements, as these circuits require constant impedances and admittances. Lumped elements are only a good approximation in the passband and make the stopband response deviate from the ideal response as discussed in section 3.2. This difference can, for example, be used to increase the attenuation in the higher stopband, while decreasing the attenuation in the lower stopband of a bandpass filter.

An important result of chapter 3 is the summary of how the coupling coefficients of different inverter-resonator combinations change as the resonators are tuned, shown in table 3.1 (page 36). These curves give an indication as to how the bandwidth will change if only the resonators are tuned.

Finding low loss components in the 20-500MHz frequency band to build tunable filters proved to be difficult. Several technologies are available to implement tunable components, a comparison of these can be found in chapter 4 (page 37). Fixed components that are switched in and out of the circuit (digital tuning) or variable impedance components (continuous tuning) can be used. The switches add too much losses to the resonator circuit, but can be considered to tune the inverter. Yttrium-iron-garnite (YIG) crystal tuners have very high unloaded Q , but are not suitable to the frequency band below 500MHz. Varactor diodes were chosen as tuning element for this project, because of their low losses and availability.

Inductor-capacitor resonant circuits have to be used in the lower part of the 20-500MHz band, as transmission lines are simply too long. At the higher end of the band transmission lines loaded with varactor diodes can be used. Low loss ceramic resonators that have high unloaded Q was chosen after a comparison with other transmission lines, as shown in table 4.1 (page 39).

Two filters were designed and built to demonstrate the best results that can be achieved with currently available components and also show the different challenges at the lower and higher ends of the band. These designs are reported in chapter 5 (page 47). The Chebyshev prototype is compared to elliptic prototypes, but the former was chosen because it is easier to implement and also simplifies tuning. The combination of fixed attenuation and variable bandwidth specifications means the passband loss is minimised by maximising the bandwidth and choosing an eighth order Chebyshev filter, see section 5.3 (page 52).

The low-end filter can be tuned from 23MHz to 54MHz, with insertion loss at the centre frequency varying from 2.22dB to 1.55dB and the bandwidth increases from 4.12MHz to 9.62MHz, see section 5.4.4 (page 58). This filter was designed for constant relative bandwidth so that only the resonator capacitors need to be tuned, but causes the bandwidth to increase and the cut-off rate to decrease as the filter is tuned to a higher frequency. Low passband insertion loss is achieved because this filter is only fourth order and has wide relative bandwidth. The losses are mostly due to the low Q_u of the inductors in the resonant circuit. The final interesting fact to note about this filter is the symmetry of the stopband, almost identical attenuation is achieved 10MHz away from the passband edges.

The high-end filter was designed at 500MHz, where it has 8.6dB insertion loss at f_0 and can tune down to where the passband disappears into the noise floor at 250MHz. This filter achieves very sharp cut-off at the higher band-edge, approaching 80dB 10MHz from the passband-edge. The cut-off rate is much slower at the lower band-edge because of unwanted inductive coupling. The losses in this sixth order Chebyshev filter is determined by the varactor diodes, as their Q_u is much lower than the ceramic coaxial transmission lines. The inter-resonator coupling is implemented with microstrip interdigital capacitors and not tunable. Consequently the passband degrades as the filter is tuned down from the 500MHz design frequency.

Ultimately the insertion loss specification proved unrealistic in the light of currently available components. Varactor diodes were shown to be good tuning devices and achieved octave tuning. A filter bank consisting of

five tunable filters will cover the 20-500MHz band and will be a suitable RF front-end for a SDR system.

Chapter 2

Coupled Resonator Filter Theory

This project will use Coupled Resonator (CR) theory as point of departure to design lumped element filters that can be tuned over wide bandwidths. This theory is very attractive from a tuning perspective because of the alternating coupler and resonator topology. Tuning of the centre frequency may be achieved by tuning the resonant frequency of the resonators, and the bandwidth can be controlled by adjusting the couplers.

The aim of the chapter is to state the CR theory and show what parameters have to be changed in order to tune a filter, while retaining the desired frequency response. Firstly, impedance and admittance inverters are introduced as one of the basic concepts in CR theory. These components lead to a different low pass prototype which can be impedance - and frequency scaled. Frequency transformation shows that bandpass filters need resonators, the second basic concept in CR theory. The concept of coupling its relationship to filter bandwidth is examined. The chapter concludes with the design procedure for tunable CR filters.

2.1 Modern Filter Synthesis

The modern design procedure for filters is the insertion loss method. This method enables the design of filters with a completely specified frequency response [9]. This procedure leads to a low pass prototype that is normalized in terms of frequency and impedance. Impedance and frequency transformations can be applied to this prototype to give the desired frequency response and impedance match.

The low pass prototypes of Butterworth and Chebyshev (all-pole) filters are ladder networks consisting of series inductors and parallel capacitors as shown in figure 2.1. The Chebyshev filter is most popular because it is the all-pole filter that has the steepest cut-off rate [6]. Tables for the element values of these prototypes are compiled in [5].

2.1.1 Ideal Impedance and Admittance Inverters

Coupled Resonator filter theory relies on inverting an impedance or admittance. The working of an inverter is defined by equations (2.1) and (2.2) [9]

$$Z_{in} = \frac{K^2}{Z_L} \quad (2.1)$$

$$Y_{in} = \frac{J^2}{Y_L} \quad (2.2)$$

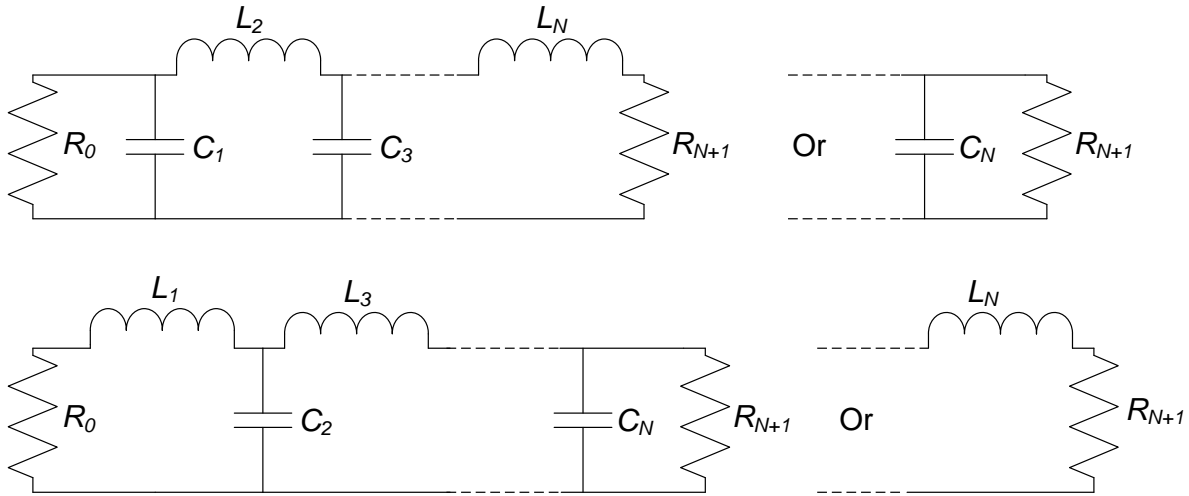


Figure 2.1: Low pass ladder prototype networks

where Z_{in} and Y_{in} are shown in figure 2.2. Admittance inverters are in principal the same as impedance inverters, but it is convenient to describe them with a characteristic admittance rather than an impedance [5]. The inverter is a two-port network that inverts the terminating load (Z_L or Y_L) as shown in equations (2.1) and (2.2). The inverter is described by its characteristic impedance (K) or admittance (J). The property not evident from equations (2.1) and (2.2) is that the inverter also changes the phase by $\pm 90^\circ$.

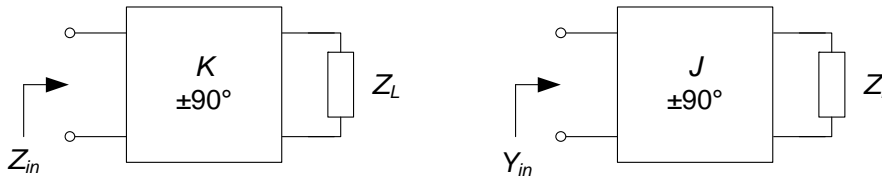


Figure 2.2: The input impedance and input admittance of loaded impedance and admittance inverters

These equations also show that the input impedance of an impedance inverter terminated with an inductor is capacitive. Analogously, the input admittance of an admittance inverter terminated with a capacitor is inductive.

The inverter is a lossless reciprocal two port network, and can be defined in a more general manner by the transfer matrices [8].

$$[T_K] = \begin{bmatrix} 0 & jK \\ \frac{j}{K} & 0 \end{bmatrix} \quad (2.3)$$

$$[T_J] = \begin{bmatrix} 0 & \frac{j}{J} \\ jJ & 0 \end{bmatrix} \quad (2.4)$$

The characteristics of an ideal inverter remains the same (J and K are constant) as frequency changes.

2.1.2 Inverters in a low pass prototype

When a series inductor is placed between two impedance inverters, the resulting transfer matrix is given by

$$[T_{network}] = \begin{bmatrix} 0 & jK \\ \frac{j}{K} & 0 \end{bmatrix} \cdot \begin{bmatrix} 1 & jX_L \\ 0 & 1 \end{bmatrix} \cdot \begin{bmatrix} 0 & -jK \\ -\frac{j}{K} & 0 \end{bmatrix} \quad (2.5)$$

$$= \begin{bmatrix} 1 & 0 \\ \frac{jX_L}{K^2} & 1 \end{bmatrix} \quad (2.6)$$

This transfer matrix of the network is recognized as equivalent to a parallel capacitor with $Y_C = j\frac{Z_L}{K^2}$. A low pass prototype may now be implemented using only impedance inverters and series inductors, because these inverters are able to transform series inductors to parallel capacitors (see figure 2.3). The dual network consists of parallel capacitors and admittance inverters.

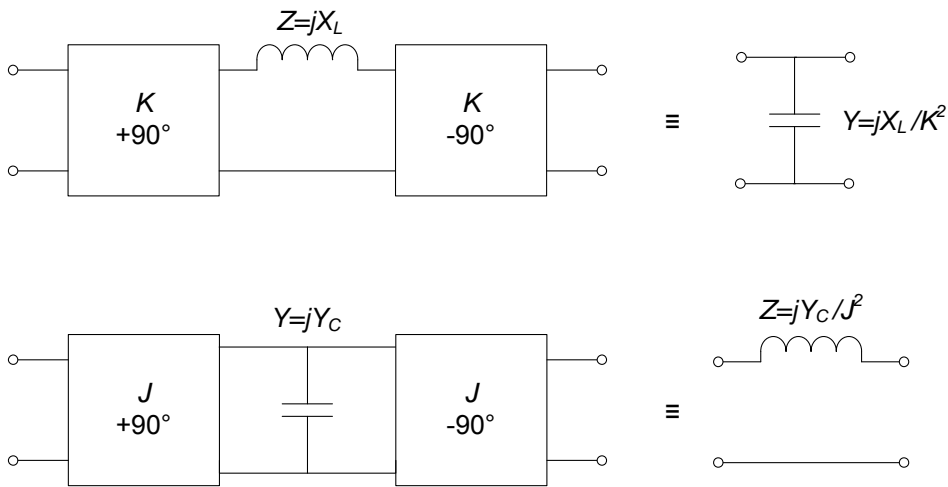


Figure 2.3: The working of an inverter

A alternative realisation of ladder networks is now possible by using the properties of the inverters [8]. The coupled resonator low pass prototypes are shown in figure 2.4.

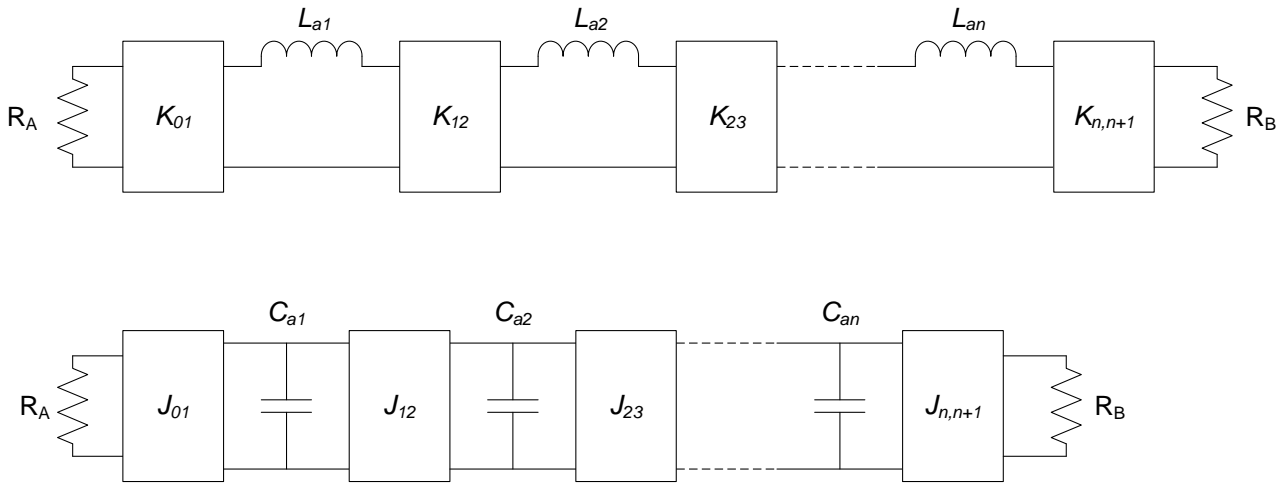


Figure 2.4: Coupled resonator low pass prototype networks

The inverters, in addition to their inverting property, also scales the impedance. This simplifies the matching at the terminating ports, and it introduces another degree of freedom in the design [5]. The design equations (stated in section 2.5) show this design freedom. This freedom allows for identical reactive elements, which in turn leads to identical resonators in bandpass realisations.

2.1.3 Bandpass transformation

A low-pass prototype network implemented with parallel capacitors and admittance inverters may be transformed to a bandpass filter by using a bandpass transformation. The resulting network consists of parallel resonators and admittance inverters. Similar steps may be followed to find a bandpass filter consisting of impedance inverters and series resonators.

The band pass transformation to transform low pass filters to band pass filter is [9]:

$$\omega \leftarrow \frac{\omega_0}{\omega_1 - \omega_2} \left(\frac{\omega}{\omega_0} - \frac{\omega_0}{\omega} \right) = \frac{\omega_0}{\Delta\omega} \left(\frac{\omega^2 - \omega_0^2}{\omega_0 \omega} \right) \quad (2.7)$$

Here ω_1 and ω_2 are the bandpass edges, and $\Delta\omega$ is the absolute bandwidth. This transformation converts series inductors to series LC resonators, and also parallel capacitors to parallel LC resonators [9]. These results show that a bandpass CR filter is comprised of alternating resonator and inverter (coupler) sections as shown in figure 2.5.

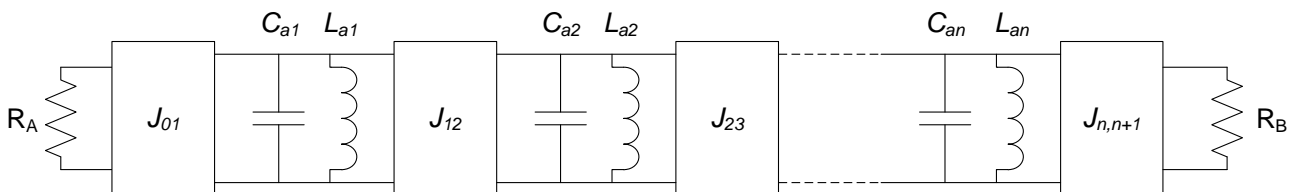


Figure 2.5: Coupled resonator bandpass prototype with admittance inverters

2.2 Resonators

A resonator is a device that stores energy, but in two different ways. The system resonates by exchanging the energy stored from one way to another. In a LC resonator the energy is exchanged between the inductor, where it is stored as magnetic energy, and the capacitor, where it is stored as electric energy. Resonance occurs at the frequency where the average stored magnetic and electric energies are equal [9].

The resonant frequency can be varied by changing the average amount of electric or magnetic energy stored. In a LC resonator this translates to either changing the inductance or the capacitance.

Many different resonators exist and it is convenient to define the resonant frequency, ω_0 , and the slope parameter in order to specify resonance properties [5]. The reactance slope is used for resonators with a series-type resonance (zero reactance at ω_0):

$$\hat{x} = \frac{\omega_0}{2} \left. \frac{dX}{d\omega} \right|_{\omega=\omega_0} \quad (2.8)$$

where X is the reactance of the resonator. The susceptance slope parameter is used for resonators with parallel-type resonance (zero susceptance at ω_0):

$$\hat{b} = \frac{\omega_0}{2} \left. \frac{dB}{d\omega} \right|_{\omega=\omega_0} \quad (2.9)$$

where B is the susceptance of the resonator.

All practical resonators have losses, which can be quantified by the unloaded Q-factor, denoted Q_u . It can be shown that [5]:

$$Q_u = \frac{\hat{x}}{R_s} \quad (2.10)$$

for series resonators, where R_s is the series resistance, and

$$Q_u = \frac{\hat{b}}{G_n} \quad (2.11)$$

for parallel resonators, where G_n is the parallel conductance [5].

Resonator losses are of great concern, as it is the primary source of loss in CR filters. The currents circulating in the resonators are largest at resonance, due to the fact that the magnitude of the impedance in the LC loop reaches a minimum. The losses are of importance, as the specifications (section 1.3) put tight constraints on attenuation in the pass band.

2.3 Inter-resonator Coupling

The concept of a coupling coefficient is not necessary in the design of lumped element filters, but it is a useful quantity to use when considering bandwidth. The most general definition of coupling is the tempo of energy exchange between coupled resonators [14]. This statement is supported by the fact that the coupling coefficient can be measured by analysing the time energy takes to enter and exit an electronic filter [15].

Coupling in electrical circuits is caused by mutual inductance or mutual capacitance and subsequently defined as inductive (magnetic) or capacitive (electric) coupling. Inductive coupling occurs when a current change in one inductor induces a voltage in another conductor by means of some mutual inductance (L_m).

$$v_2 = L_m \frac{di_1}{dt} \quad (2.12)$$

This is recognised as Faraday's law of magnetic induction. Capacitive coupling induces a current as a result of a voltage change.

$$i_2 = C_m \frac{dv_1}{dt} \quad (2.13)$$

Using equation (2.13) a two-port network can be constructed to show coupling with mutual capacitance.

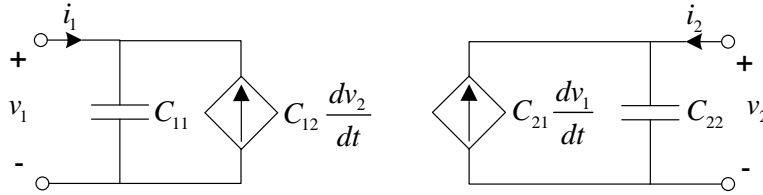


Figure 2.6: Two-port coupling with mutual capacitance

The mesh currents for the network is given by:

$$i_1 = C_{11} \frac{dv_1}{dt} - C_{12} \frac{dv_2}{dt} \quad (2.14)$$

$$i_2 = C_{22} \frac{dv_2}{dt} - C_{21} \frac{dv_1}{dt} \quad (2.15)$$

Transform the network from the time domain to the frequency domain, and write it in matrix format, to get

$$\begin{bmatrix} I_1 \\ I_2 \end{bmatrix} = \begin{bmatrix} sC_{11} & -sC_{12} \\ -sC_{21} & sC_{22} \end{bmatrix} \begin{bmatrix} V_1 \\ V_2 \end{bmatrix} \quad (2.16)$$

A normalized variable, the coupling coefficient, can be defined to express the amount of coupling [16],

$$k = \frac{L_m}{\sqrt{L_1 L_2}} \quad (2.17)$$

where L_1 and L_2 are the (self) inductances of the coupled conductors. Here $k = 0$ denotes no coupling and $k = 1$ denotes maximum coupling. A similar definition is used for the capacitive coupling coefficient:

$$k = \frac{C_m}{\sqrt{C_1 C_2}} \quad (2.18)$$

The simplifications, $C_{11} = C_{22} = C_0$ and $C_{12} = C_{21} = C_m$, may be made to give

$$\begin{bmatrix} I_1 \\ I_2 \end{bmatrix} = \begin{bmatrix} sC_0 & -sC_m \\ -sC_m & sC_0 \end{bmatrix} \begin{bmatrix} V_1 \\ V_2 \end{bmatrix} \quad (2.19)$$

This development of the idea of capacitive coupling is illustrated by a circuit with two coupled capacitors as shown in figure 2.7. The circuit in figure 2.7 shown in dotted lines is an inverter. This shows that coupling can be achieved by an inverter circuit.

The question of the relationship between coupled resonators and the bandwidth of a filter remains. The analysis of two LC resonators coupled with an inverter will answer this question, as this circuit behaves as a band pass filter. It is convenient to choose the LC resonators to be identical, without any loss of generality. The mutual capacitance can now be defined in terms of the coupling coefficient using equation (2.18):

$$C_m = kC_0 \quad (2.20)$$

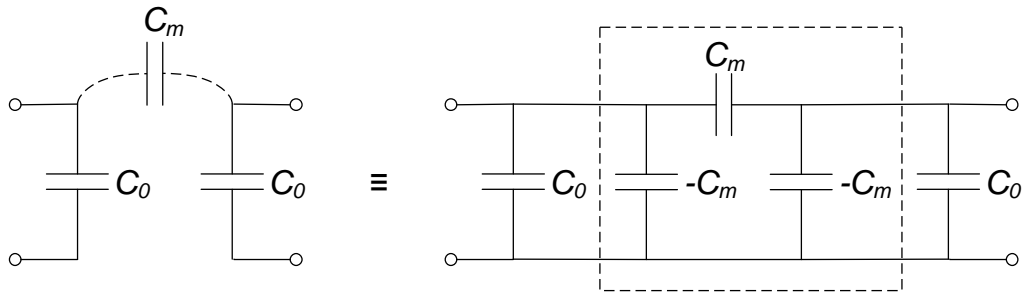


Figure 2.7: Capacitive coupling between two capacitors

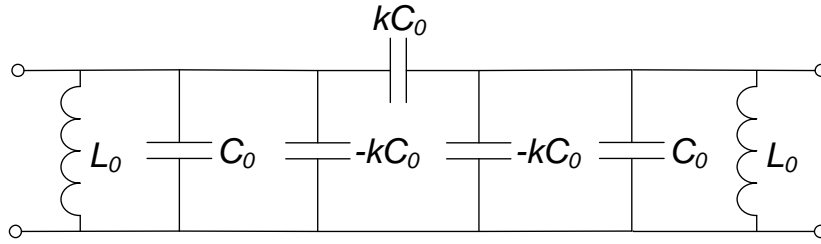


Figure 2.8: Coupled parallel LC resonators coupled

The nodal equations for the network are:

$$\begin{bmatrix} I_1 \\ I_2 \end{bmatrix} = \begin{bmatrix} sC_0 + \frac{1}{sL_0} & -skC_0 \\ -skC_0 & sC_0 + \frac{1}{sL_0} \end{bmatrix} \cdot \begin{bmatrix} V_1 \\ V_2 \end{bmatrix} \quad (2.21)$$

Using the admittance matrix, the input admittance of the network is:

$$Y_{in} = y_{11} - \frac{y_{12}y_{21}}{y_{22}} = \frac{(1-k^2)s^4C_0^2L_0^2 + 2s^2C_0L_0 + 1}{s^3C_0L_0^2 + sL_0} \quad (2.22)$$

Solving for the zeros of 2.22 gives the resonant frequencies of the system

$$s_{1,2} = \pm \frac{j}{\sqrt{C_0L_0(1-k)}} \quad (2.23)$$

$$s_{3,4} = \pm \frac{j}{\sqrt{C_0L_0(1+k)}} \quad (2.24)$$

These two zero pairs correspond to the odd and even resonant frequencies

$$\omega_{0o} = \frac{\omega_0}{\sqrt{1-k}} \quad (2.25)$$

$$\omega_{0e} = \frac{\omega_0}{\sqrt{1+k}} \quad (2.26)$$

where $\omega_0 = \frac{1}{\sqrt{C_0L_0}}$. Solving for k using equations 2.25 and 2.26 gives

$$k = \frac{\omega_{0o}^2 - \omega_{0e}^2}{\omega_{0o}^2 + \omega_{0e}^2} \quad (2.27)$$

This equation gives some insight into what a variation in coupling coefficient will have on the frequency response of the system. If the coupling is increased (k is increased) then the difference between ω_{0o} and ω_{0e} will

also increase. The resonant frequencies of the circuit (ω_{0o} and ω_{0e}) moves away from the resonant frequency of the resonators (ω_0). The bandwidth is consequently increased by this increase in coupling, as is shown in figure 2.9 [17].

This graph is the response of the circuit in figure 2.8 as the coupling coefficient is changed. From figure 2.9 it is evident that stronger coupling increases the bandwidth. For this comparison the load and source impedances was chosen as $R_L = R_S = \frac{1}{k}$. This choice keeps $Q_e k = 1$, to give a maximally flat (Butterworth) response.

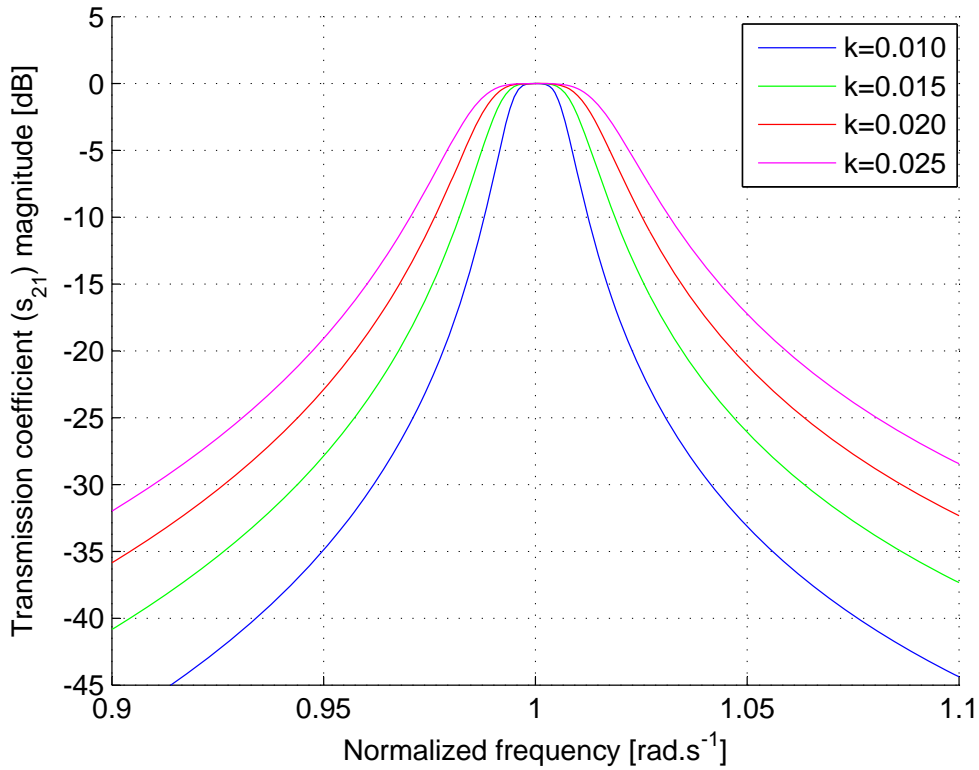


Figure 2.9: Frequency response of the circuit in figure 2.8 for different coupling coefficient values

2.4 Input and output coupling (Q_e)

The inverter circuit introduced in section 2.1.1 is an impedance transformer, and by choosing the correct characteristic impedance a circuit can be matched to an arbitrary system. From equation (2.11), the external Q s for the input and output coupling is

$$(Q_e)_{in} = \hat{b}_1 R_S \quad (2.28)$$

$$(Q_e)_{out} = \hat{b}_n R_L \quad (2.29)$$

For the filter in figure 2.8, with $k = 0.02$, the effect of changing the external Q s can be seen in figure 2.10.

Figure 2.10 shows that the matching is determined by Q_e , but also that the filter response is defined by this coupling. The degree of matching is not determined by Q_e alone, but the product, $Q_e k$. A maximally flat

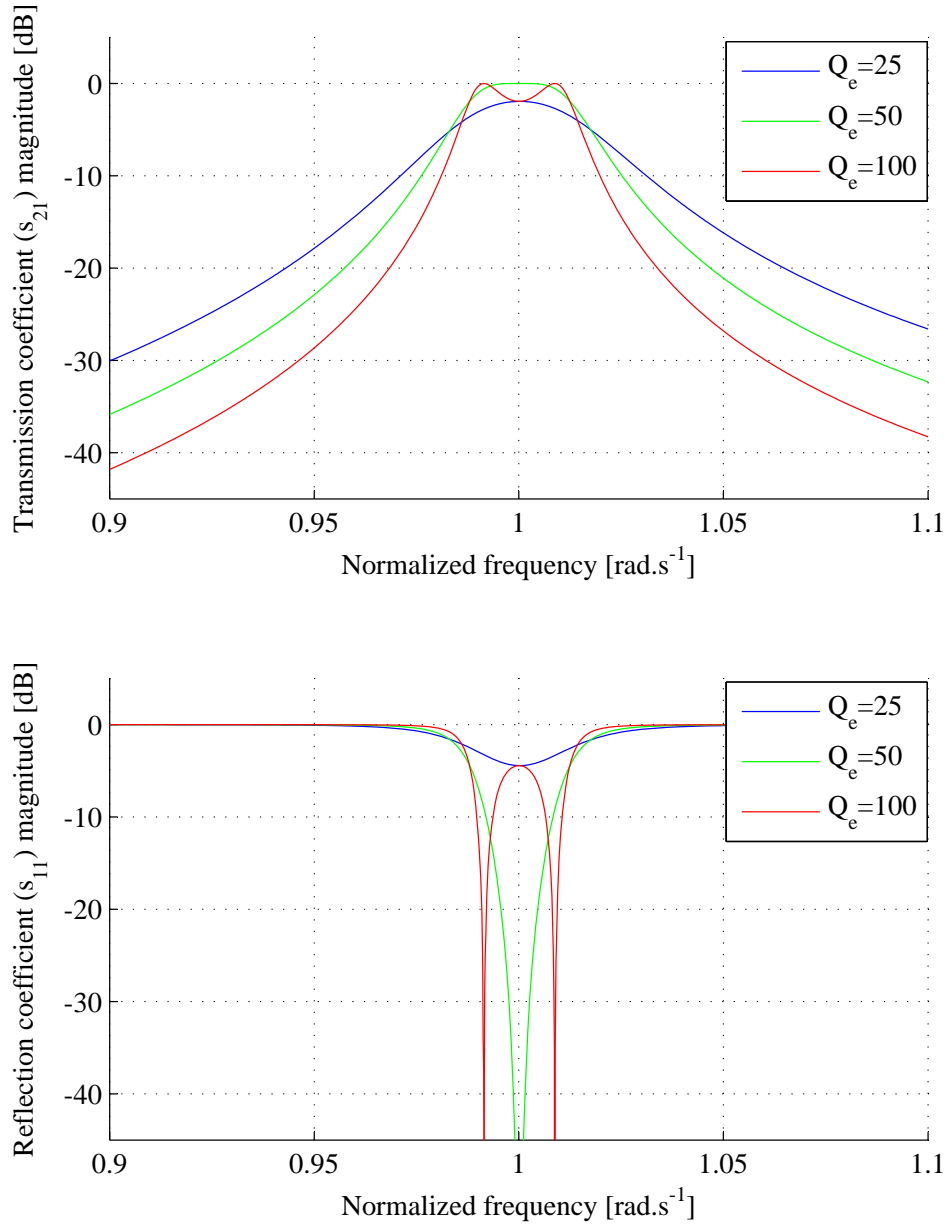


Figure 2.10: Frequency response showing the effect of different external Q values

(Butterworth) response is obtained if $Q_e k = 1$ ($Q_e = 50$), this is termed critical coupling. A Chebyshev response is obtained if the coupling coefficient increases ($Q_e k > 1$), and over coupling is achieved.

A CR filter prototype can be completely specified with only coupling coefficients (k -values), and the input and output coupling (Q_e -values).

2.5 CR Filter Design

The design equations for the design of an CR bandpass prototype is repeated here for convenience [5].

$$\hat{b}_j = \frac{\omega_0}{2} \left. \frac{dB_j(\omega)}{d\omega} \right|_{\omega=\omega_0} \quad (2.30)$$

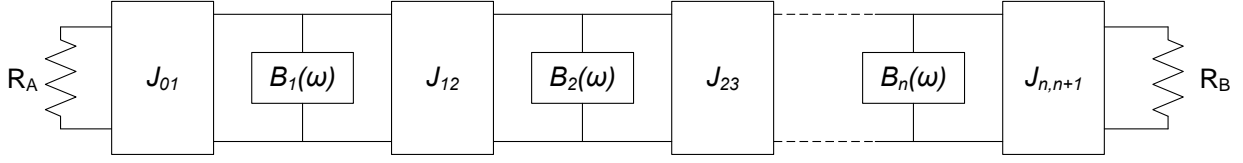


Figure 2.11: CR bandpass prototype using admittance inverters

$$J_{01} = \sqrt{\frac{\hat{b}_1 \Delta \omega}{g_0 g_1 \omega_0 R_A}} \quad (2.31)$$

$$J_{n,n+1} = \sqrt{\frac{\hat{b}_n \Delta \omega}{g_n g_{n+1} \omega_0 R_B}} \quad (2.32)$$

$$J_{j,j+1} = \frac{\Delta \omega}{\omega_0} \sqrt{\frac{\hat{b}_j \hat{b}_{j+1}}{g_j g_{j+1}}} \quad (2.33)$$

$$(Q_e)_A = \frac{\hat{b}_1}{\left(\frac{J_{01}^2}{G_A}\right)} = \frac{\hat{b}_1}{J_{01}^2 R_A} \quad (2.34)$$

$$(Q_e)_B = \frac{\hat{b}_n}{\left(\frac{J_{n,n+1}^2}{G_B}\right)} = \frac{\hat{b}_n}{J_{n,n+1}^2 R_B} \quad (2.35)$$

$$k_{j,j+1} \Big|_{j=1, \dots, j=n-1} = \frac{J_{j,j+1}}{\sqrt{\hat{b}_j \hat{b}_{j+1}}} \quad (2.36)$$

The values, $g_1, \dots, g_j, g_{j+1}, \dots, g_n$, are the normalized lowpass prototype element values. The absolute bandwidth given by $\Delta \omega = \omega_2 - \omega_1$, with ω_1 and ω_2 the band-edges.

2.6 Designing for tunability

The coupling values, k - and q -values, has been shown to determine filter response. An investigation as to how these values should change to achieve tunability will now commence. The coupling coefficient between two parallel LC resonators is given by [5]

$$k_{n,n+1} \Big|_{n=1, \dots, n=N-1} = \frac{J_{n,n+1}}{\sqrt{\hat{b}_n \hat{b}_{n+1}}} = \frac{\frac{\Delta \omega}{\omega_0}}{\sqrt{g_n g_{n+1}}} \quad (2.37)$$

This design equation also shows that the coupling coefficient determines the relative bandwidth ($\frac{\Delta \omega}{\omega_0}$). The Q_e -value for a filter with parallel type resonators is:

$$Q_e = \frac{\hat{b}_1}{J_{01}^2 R_0} = g_0 g_1 \frac{\omega_0}{\Delta \omega} \quad (2.38)$$

2.6.1 Constant relative bandwidth

Constant relative bandwidth is achieved when $\frac{\Delta\omega}{\omega_0}$ stays constant as ω_0 changes. The shape of the filter response should also stay the same as the low pass prototype, thus g_n and g_{n+1} must also remain unchanged. These two conditions imply that the coupling coefficient must not change when the centre frequency is adjusted.

Constant relative bandwidth also means that the absolute bandwidth is a linear function of the centre frequency. An increase in bandwidth also decreases the absolute cut-off rate of the filter, neither of which is normally desired. Constant absolute bandwidth does not have these problems.

2.6.2 Constant absolute bandwidth

From equation (2.37) it is clear that the coupling coefficient is dependent on the centre frequency, ω_0 , if the absolute bandwidth, $\Delta\omega$, is kept constant. To achieve the same filter response while the centre frequency is changed therefore requires the coupling coefficient to change with $\frac{1}{\omega_0}$. Ideally, for constant absolute bandwidth the following equations should hold.

$$k(\omega_0) = \left(\frac{\Delta\omega}{\sqrt{g_n g_{n+1}}} \right) \frac{1}{\omega_0} \quad (2.39)$$

$$q(\omega_0) = \left(\frac{g_0 g_1}{\Delta\omega} \right) \omega_0 \quad (2.40)$$

2.7 Conclusion

The CR theory was shown to be a attractive design technique for synthesising tunable filters. Lumped element filters implement coupling by using impedance and admittance inverters. The resonant frequency of the resonators are adjusted to enable tuning of the filter, while the amount of coupling determines the bandwidth.

The ideal tunable filter has constant absolute bandwidth, and design equations for such a filter was stated.

Chapter 3

Filter Implementation for Tunability

This chapter aims to compare the various alternative circuits to implement tunable Coupled Resonator (CR) filters.

CR theory assumes ideal, frequency invariant components, which are not realisable in practice. The effect frequency dependant components have on CR filter response is examined. Different coupling implementations are discussed with the goal of achieving constant absolute bandwidth while tuning the filter. The advantages of, and the requirements for achieving this was discussed in chapter 2.

An important fact to reiterate is that the coupling coefficient is determined by the properties of the inverter as well as the properties of the resonator. Different resonator-inverter combinations (section 3.3), to be used as filter sections, will be examined after different resonators (section 3.1) and inverters (section 3.2) were investigated on their own.

3.1 Tunable resonators

The susceptance slope parameter is a useful quantity for determining the coupling coefficient between resonators. The two resonators that will be used in this project are the parallel inductor-capacitor (LC) tank and short circuited transmission lines loaded with capacitors. Both these resonators are tuned by changing the value of the capacitor in the circuit. The admittance slope parameter can be calculated with [5]

$$\hat{b} = \frac{\omega_0}{2} \left. \frac{dB}{d\omega} \right|_{\omega_0} \quad (3.1)$$

3.1.1 Parallel LC tank

Consider a inductor, of inductance L , and a capacitor of capacitance C in parallel. The susceptance of this LC circuit is:

$$B_{LC} = \omega C - \frac{1}{\omega L} \quad (3.2)$$

Apply (3.1) to this susceptance to obtain:

$$\hat{b}_{LC} = \frac{\omega_0}{2} \left(C + \frac{1}{\omega_0^2 L} \right) \quad (3.3)$$

From the equation for the resonant frequency, $\omega_0^2 = \frac{1}{LC}$, follows that

$$C = \frac{1}{\omega_0^2 L} \quad (3.4)$$

Substitute (3.4) into (3.3)

$$\hat{b}_{LC} = \omega_0 C = \frac{1}{\omega_0 L} \quad (3.5)$$

It is evident from equation (3.5) that, in the case of the resonator being tuned by varying only the capacitance, the susceptance slope will change inversely proportional to the centre frequency, as L is constant.

Important to note here as well is how much the value of the capacitor needs to change to tune the centre frequency of the resonator. From equation (3.4) it can be seen that C has to tune

$$C(\omega_0) \propto \frac{1}{\omega_0^2} \quad (3.6)$$

3.1.2 Short-circuited transmission line loaded with a capacitor

Consider now a transmission line, grounded at one end, and connected to ground through a capacitor at the other end. The susceptance of this circuit is:

$$B_{TL} = \omega C - \frac{1}{Z_0 \tan(\omega T)} = \omega C - Y_0 \cot(\omega T) \quad (3.7)$$

Apply (3.1) to this susceptance to obtain:

$$\hat{b}_{TL} = \frac{\omega_0}{2} (C + T \operatorname{cosec}^2(\omega T)) \quad (3.8)$$

This circuit exhibits a parallel type of resonance where $B_{TL} = 0$ at ω_0 . The capacitor value may be expressed as:

$$C = \frac{Y_0 \cot \omega_0 T}{\omega_0} \quad (3.9)$$

Substituting (3.9) in (3.8) yields [7] (Note $\omega_0 T = \theta_0$)

$$\hat{b}_{TL} = \frac{Y_0}{2} (\omega_0 T \operatorname{cosec}^2(\omega_0 T) + \cot(\omega_0 T)) \quad (3.10)$$

The susceptances of the capacitor and the negative of the transmission line susceptance is shown in figure 3.1, to show the resonant frequency as the capacitor is tuned.

A small change in capacitor value gives a big change in resonant frequency if the resonant frequency is close to the frequency where the transmission line is a quarter of a wavelength long. A shorter transmission line will consequently require smaller changes in capacitor value to tune the centre frequency, but much larger values capacitance values are required.

3.1.3 Parallel-series LC resonator

A similar type of multi-resonance behaviour as that of a transmission lines, can be achieved with LC circuits by adding another type of resonance. Such a circuit can have a series and parallel type of resonance, circuit shown in figure 3.2.

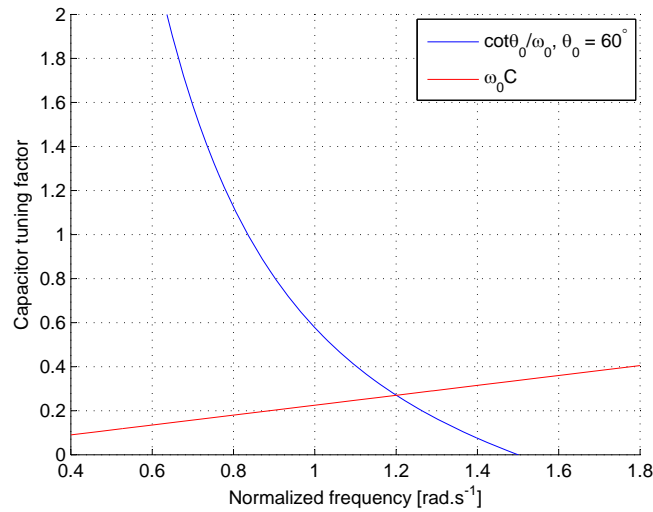


Figure 3.1: Susceptance of the capacitor, $\omega_0 C$, and negative of the transmission line susceptance, $-Y_0 \cot(\omega_0 T)/\omega_0$. The circuit resonates at the intersection point of the two curves, which represent zero susceptance.

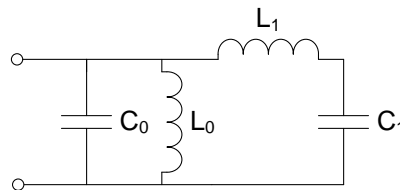


Figure 3.2: LC circuit with parallel and series resonances

This additional resonant circuit will give some freedom to adjust the susceptance slope at the original resonance [5]. The admittance of this circuit is shown in 3.3, the parallel and series resonances can be seen. The susceptance slope at the parallel resonance can be changed by adjusting the series resonance.

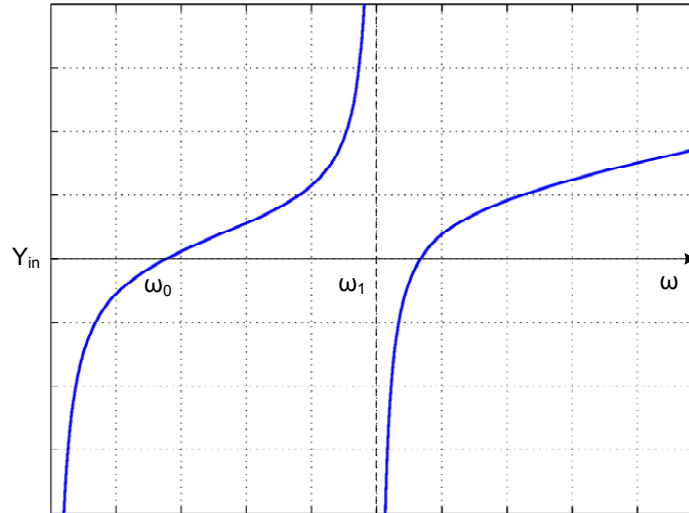


Figure 3.3: The admittance of a parallel-series-type resonator

3.2 Implementation of inverters

The non-ideal circuits investigated here are a good approximation to the ideal circuit in a relatively narrow band. The goal of this section is to investigate the wide band response of non-ideal inverters. This information will aid the understanding of the stopband response of filters constructed with these inverters.

The ideal inverter was discussed in section 2.1.1. An ideal admittance inverter may be described by the following transmission matrix

$$[T_B] = \begin{bmatrix} 0 & \frac{j}{B} \\ jB & 0 \end{bmatrix} \quad (3.11)$$

Consider the problem of realising an admittance inverter of characteristic admittance, Y_0 , from a general pi-network of lumped admittances.

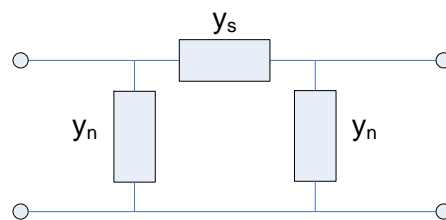


Figure 3.4: Pi-network of admittances

The transmission matrix of this general circuit is:

$$T = \begin{bmatrix} 1 + \frac{y_n}{y_s} & \frac{1}{y_s} \\ y_n \cdot \left(2 + \frac{y_n}{y_s}\right) & 1 + \frac{y_n}{y_s} \end{bmatrix} \quad (3.12)$$

The goal here is to choose the element values of the general admittance pi-network (figure 3.4) so that it is equivalent to the ideal inverter (3.11). It follows from this goal that $\frac{y_n}{y_s} = -1$, so that

$$T = \begin{bmatrix} 0 & \frac{1}{y_s} \\ y_n & 0 \end{bmatrix} \quad (3.13)$$

This is the same form as (3.11), which was the aim. We choose $Y_0 = jB$ and

$$y_n = jB = -y_s \quad (3.14)$$

which yields

$$T = \begin{bmatrix} 0 & \frac{j}{B} \\ jB & 0 \end{bmatrix} \quad (3.15)$$

This is the transmission matrix for an ideal inverter with $J = B$ [8]. An ideal inverter with constant admittances as required by equation (3.14) is not realisable with lumped or distributed elements. The approximations for pi-network inverters applicable in the frequency band of the project will be discussed. The discussion can be extended to T-network inverters.

3.2.1 Capacitor pi-network

Consider the inverter approximation consisting of a capacitor pi-network. Solve equation (3.14) by setting $y_s = j\omega C$ and $y_n = -j\omega C$. This gives

$$J_C = \omega C \quad (3.16)$$

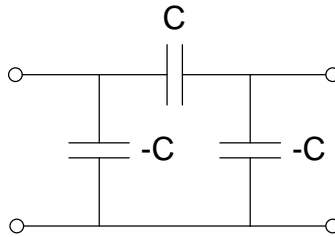


Figure 3.5: Capacitor pi-network inverter

The characteristic admittance is not constant, but a linear function of frequency. The circuit will still work as an inverter as long as the capacitor values are unchanged. This implementation displays high-pass characteristics when compared to the ideal inverter. Considering that this inverter has a series capacitor, this makes intuitive sense.

To illustrate this consider two identical LC resonators with $L = 1H$ and $C = 1F$ so that $\hat{b} = 1$. Plot the frequency response when the two resonators are coupled with an ideal inverter, with constant characteristic admittance, $B = Y_0$. Compare this with the same resonators, but coupled with a admittance inverter with $B = \omega kC$, where $\omega_0 kC = Y_0$. The bandwidth of these inverters should be the same, but the stopband responses differ, as seen in figure 3.6. The cut-off rate at the lower band-edge is steeper than the ideal case, but more gradual than the ideal case at the higher band-edge. This is what is meant by high pass behaviour.

The negative capacitances can be absorbed by the resonators on either sides of the inverter. These negative capacitances are normally much smaller than the resonator capacitor. Alternatively the series capacitor may be chosen to be negative (see table A.1), but this is not realisable with lumped elements, and not a practical implementation.

The negative capacitor is a problem at the source and the load, as there is no resonator to absorb the capacitance. This can be solved with a single frequency matching network, as will be discussed in section 3.4.

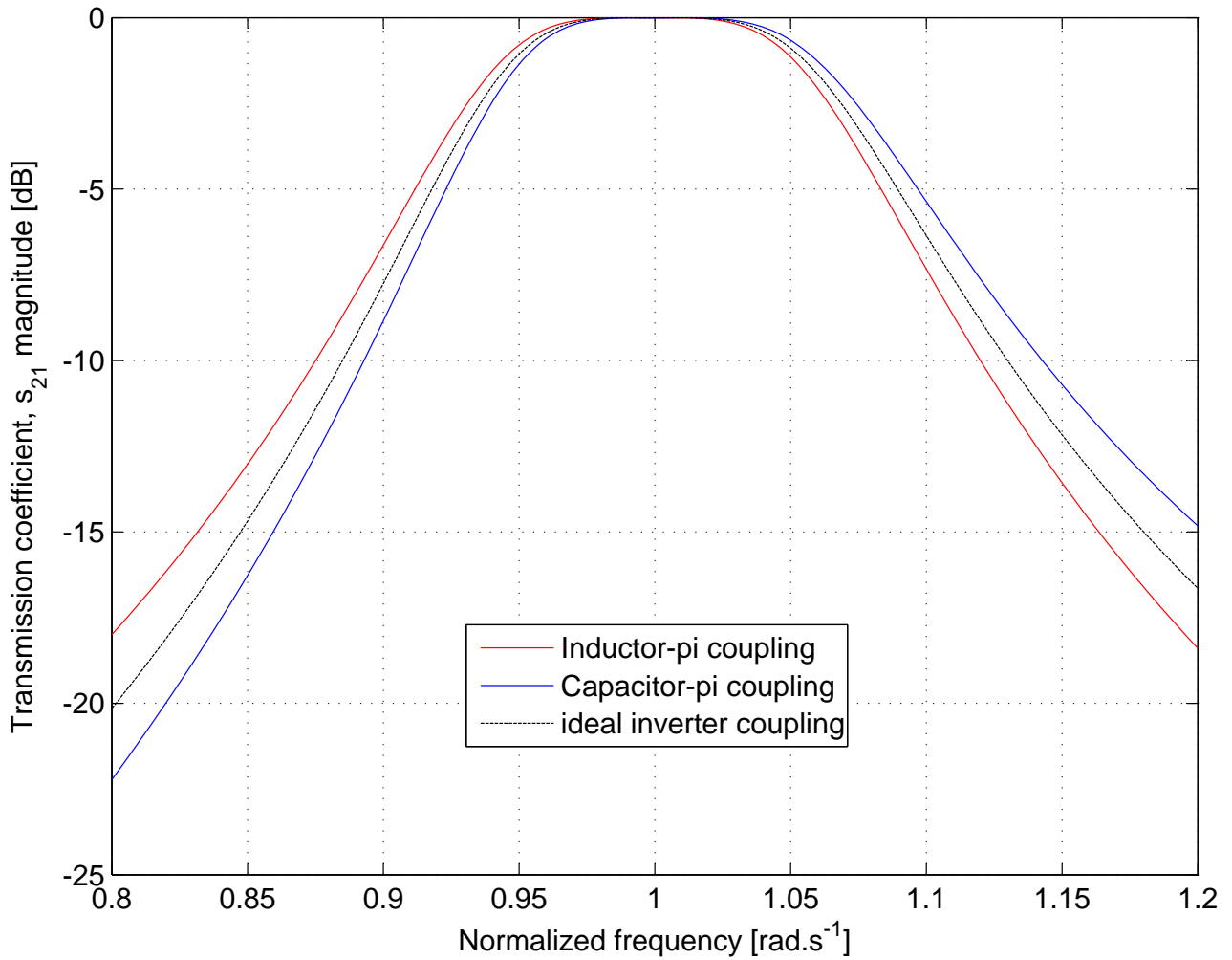


Figure 3.6: Comparison between an ideal inverter, a capacitor-pi inverter and inductor-pi inverter

3.2.2 Inductor pi-network

An inverter may also be constructed with an inductor pi-network. Solve equation (3.14) by setting $y_s = \frac{1}{j\omega L}$ and $y_n = -\frac{1}{j\omega L}$. This gives

$$J_L = \frac{1}{\omega L} \quad (3.17)$$

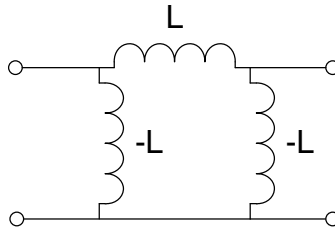


Figure 3.7: Inductor pi-network inverter

The characteristic admittance of this inverter is also frequency dependant, but it is inversely proportional to the frequency. The circuit will still function as an inverter at other than the design frequency, but with another characteristic admittance. The series inductor in this inverter gives the network low-pass characteristics, see figure 3.6.

Analyse an inductor admittance inverter, that has $B = \omega kL$, and compare it with an ideal inverter, that has $B = Y_0$. The inductor inverter approximates the ideal inverter perfectly at the centre frequency, where $\omega_0 kL = Y_0$. In this case the inductor inverter has more gradual cut-off at the lower band-edge, and steeper cut-off at the higher band-edge when compared to the ideal inverter. The network has lowpass characteristics when compared to the ideal inverter.

The negative inductors can be absorbed into adjacent resonators in similar fashion to the capacitor pi-network.

3.2.3 Capacitor and Inductor pi-network

The need for negative circuit elements in the previous two inverters can be eliminated by using a combination of inductors and capacitors. Solve equation (3.14) by setting $y_s = -j\left(\frac{1}{\omega_0 L_s}\right)$ and $y_n = j\omega_0 C_n$ (note that ω_0 is used here in stead of ω to show the narrow band working). This gives

$$J_{LC} = \frac{1}{\omega_0 L_s} \tag{3.18}$$

$$= \omega_0 C_n \tag{3.19}$$

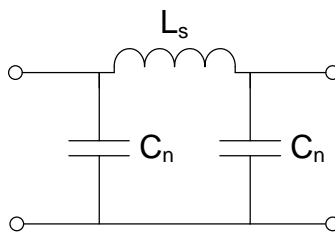


Figure 3.8: CLC pi-network

This circuit only functions as an ideal inverter when $J = \omega_0 C_n = \frac{1}{\omega_0 L_s}$. For this circuit there is only one frequency where $y_n = -y_s$, consequently the circuit is a more narrow band approximation than was the case for

the inductor pi-network (see figure 3.9). The comparison in figure 3.9 is between two circuits coupling identical resonators. The only difference being the type of inverter used. The inverters have identical characteristic admittance at the centre frequency. A Chebyshev response, with sharper cut-off, is chosen for the analysis to emphasise the difference between the circuits.

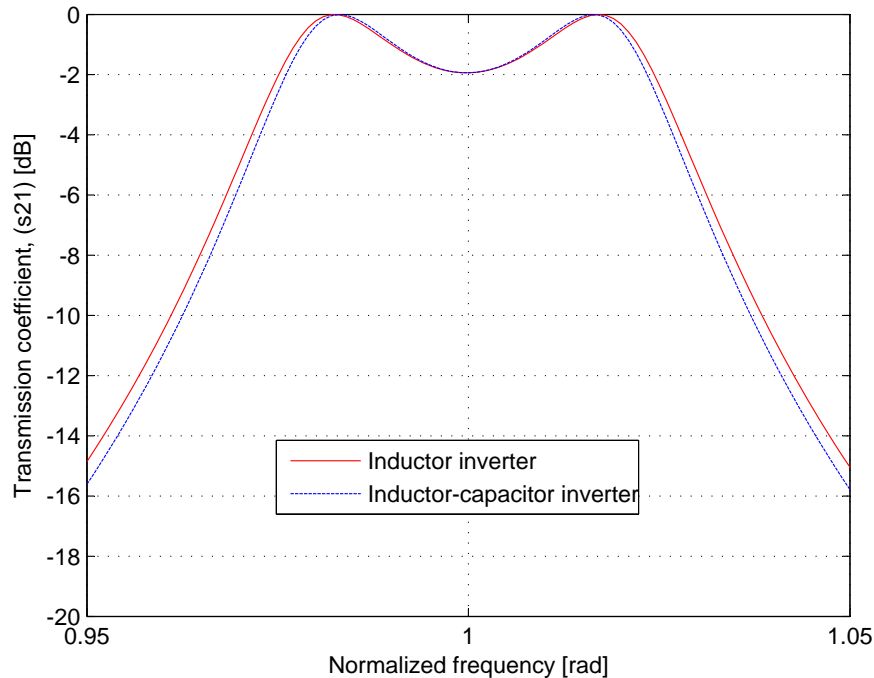


Figure 3.9: Comparison of inductor and inductor-capacitor pi-network inverters

The main cause of the difference between the inductor-pi and inductor-capacitor-pi inverters is that the impedances of the inductor and capacitor in the latter inverter scales differently with frequency. This is irrelevant for normal filter working, as the impedances do not change much over the pass band of the filter. This detuning of the inverter becomes important if the filter has to be tuned, but this problem is solved by tuning the parallel capacitors, ensuring $\frac{1}{\omega_0 L_s} = \omega_0 C_n$.

3.2.4 Parallel coupled transmission lines

An inverter can be constructed with parallel coupled Transverse Electromagnetic (TEM) transmission lines, grounded at the same end. It can be shown that the equivalent circuit of this network is a pi-network consisting of short circuited stubs [18], see figure 3.10 (The symbols used here are the same as used by Hunter [8]). To realise an inverter using the equivalent circuit, the parallel stubs have to have negative admittance, so that

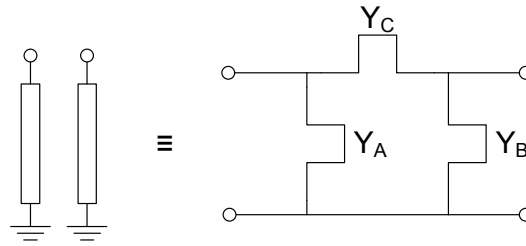


Figure 3.10: Parallel coupled transmission lines and equivalent circuit

$Y_C = -Y_A = -Y_B = j \frac{Y_0}{\tan \theta}$. The transmission matrix of such a network is:

$$[T_{network}] = \begin{bmatrix} 1 & 0 \\ j \frac{Y_0}{\tan \theta} & 1 \end{bmatrix} \cdot \begin{bmatrix} 1 & j \frac{\tan \theta}{Y_0} \\ 0 & 1 \end{bmatrix} \cdot \begin{bmatrix} 1 & 0 \\ j \frac{Y_0}{\tan \theta} & 1 \end{bmatrix} \quad (3.20)$$

$$= \begin{bmatrix} 0 & j \frac{\tan \theta}{Y_0} \\ j \frac{Y_0}{\tan \theta} & 0 \end{bmatrix} \quad (3.21)$$

This is the transmission matrix of an admittance inverter with characteristic admittance

$$J = j \frac{Y_0}{\tan \theta} \quad (3.22)$$

If θ is chosen to be 90° long at the centre frequency, then this will be an all-stop network [18], as $\tan \theta_0 \rightarrow \infty$. For this reason the lines are designed to be less than a quarter of a wavelength long at ω_0 . The effect the electrical length of the stubs has on the response of this circuit is investigated by coupling two resonators with different line lengths. The circuit is shown in figure 3.11 and the circuit response is shown in figure 3.12.

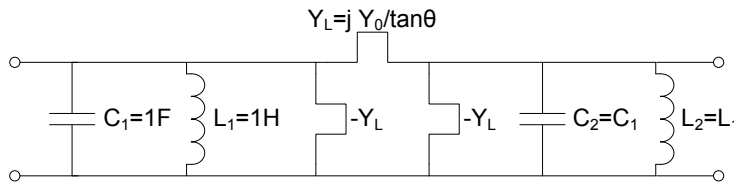


Figure 3.11: Two resonators coupled with parallel transmission lines

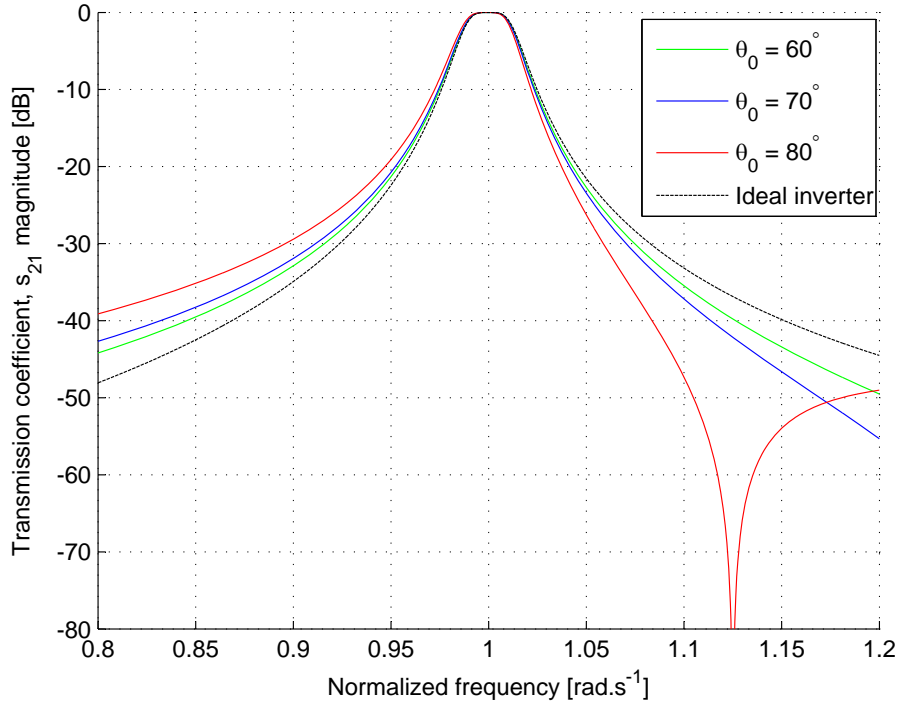


Figure 3.12: Comparison of parallel coupled short-circuited stubs with different electrical lengths

The characteristic admittance of this inverter, $\frac{Y_0}{\tan \theta_0}$, is comparable to $\frac{1}{\omega_0}$ in the range $0^\circ \leq \theta_0 \leq 90^\circ$. This inverse proportionality to frequency is very desirable, as it is the behaviour needed from the coupling to achieve constant absolute bandwidth. The coupling of this inverter will be investigated more thoroughly in section 3.3.3.

3.3 Coupling tuned resonators

Equations for the coupling coefficient will be found that describes this variable only in terms of the centre frequency, ω_0 , irrelevant of the capacitive element that will be tuned. This approach will enable comparison of different coupling implementations as the centre frequency of the circuit is tuned.

The coupling coefficient between two resonators in a CR filter can be described by [5]

$$k_{n,n+1} = \frac{J_{n,n+1}}{\sqrt{\hat{b}_n \hat{b}_{n+1}}} \quad (3.23)$$

In practical circuits both $J_{n,n+1}$ and b_n change when the centre frequency changes. The analysis may be simplified by assuming that the resonators are identical. This simplifies the coupling coefficient to

$$k = \frac{J}{\hat{b}} \quad (3.24)$$

Resonators in CR filters are usually very similar in characteristics, which justifies this simplification.

3.3.1 Capacitor pi-network coupling

Parallel LC-tank

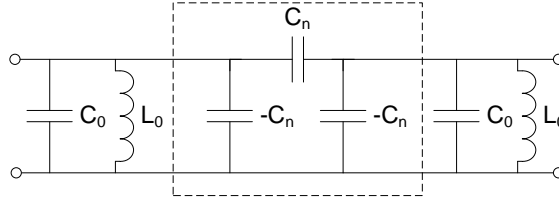


Figure 3.13: LC resonators coupled with capacitor pi-network

Calculate the coupling coefficient by substituting (3.5) and (3.16) in (3.24):

$$k = \frac{J}{\hat{b}} = \frac{\omega_0 C_n}{\frac{1}{\omega_0 L_0}} = \omega_0^2 C_n L_0 \quad (3.25)$$

This coupling factor shows that this configuration has a quadratic dependence on frequency. This is unfortunately far from the desired inverse proportionality required for constant absolute bandwidth. If the inverter capacitors can also be tuned, then absolute bandwidth can be achieved with this implementation by tuning the inverter capacitors in the following way:

$$C_n'(\omega_0) \propto \frac{1}{\omega_0^3} \quad (3.26)$$

This will then give the desired inverse proportionality to frequency.

Short-circuited Transmission Line

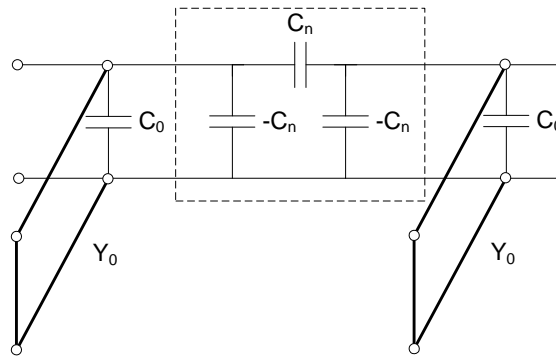


Figure 3.14: Short circuited transmission lines coupled with capacitor pi-network

Find the coupling coefficient by substituting (3.10) and (3.16) into (3.24):

$$k = \frac{2C_n}{Y_0} \cdot \frac{\omega_0}{\omega_0 T \csc^2(\omega_0 T) + \cot(\omega_0 T)} \quad (3.27)$$

The amount of frequency dependence here is not clearly visible. The denominator has no zero in $0 < \omega_0 T < \frac{\pi}{2}$ and the variable, k , is therefore continuous in this region. This region corresponds to an electrical length of $0 < \theta_0 < \frac{\pi}{2}$, and this is where the network will be operating.

In this qualitative analysis it is convenient to multiply (3.27) by $\frac{Y_0 T}{2C_n}$ and substitute $\omega_0 T = \theta_0$. This variable, k' , is therefore proportional to the exact coupling factor k .

$$k' = \frac{\theta_0}{\theta_0 \csc^2(\theta_0) + \cot(\theta_0)} \tag{3.28}$$

The graph of k' is shown in fig. 3.15.

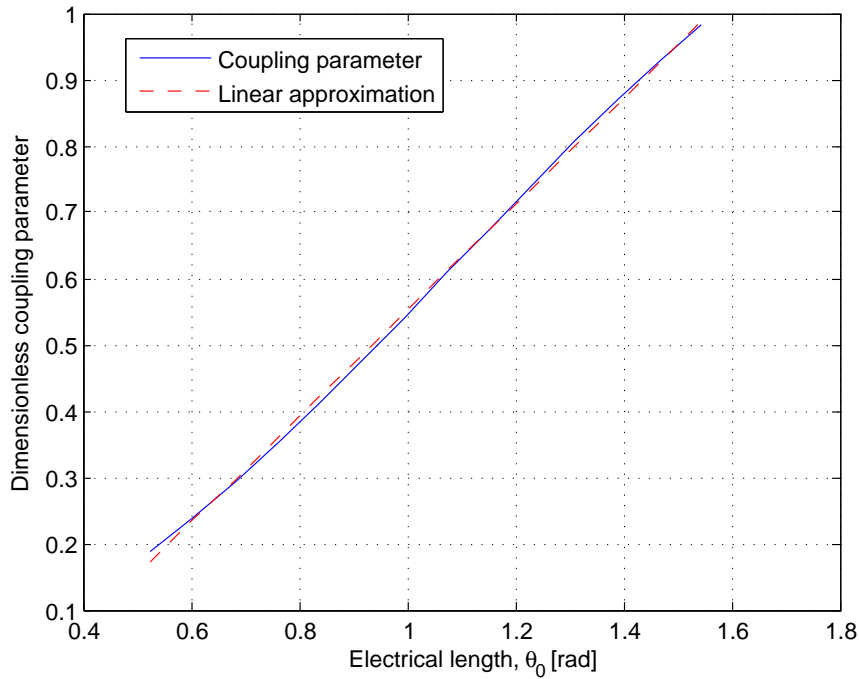


Figure 3.15: Frequency dependence of coupling between short-circuited transmission lines with capacitor pi-network in the range $\frac{\pi}{6} \leq \theta_0 \leq \frac{\pi}{2}$

This graph shows that this configuration is close to linear, in the range $\frac{\pi}{6} \leq \theta_0 \leq \frac{\pi}{2}$. A linear variation is not ideal, but it is better than the quadratic variation of coupling LC resonators with a capacitor pi-network.

3.3.2 Inductor-Capacitor pi-network coupling

Parallel LC-tank

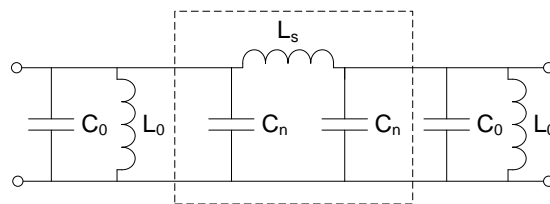


Figure 3.16: LC resonators coupled with inductor-capacitor pi-network

Examining the LC parallel tanks coupled with the inductor-capacitor pi-network shown in 3.8, the simplified formula for the coupling coefficient, (3.24), is used. Substitute (3.5) and (3.18) into this coupling coefficient equation:

$$k = \frac{\frac{1}{\omega_0 L_s}}{\omega_0 C_0} = \frac{1}{L_s \omega_0^2 C_0} \quad (3.29)$$

The value of the resonant frequency of the parallel LC tank, $\omega_0^2 = \frac{1}{L_0 C_0}$, is rearranged to give:

$$\frac{1}{\omega_0^2 C_0} = L_0 \quad (3.30)$$

which is substituted into (3.29) to give:

$$k = \frac{L_0}{L_s} \quad (3.31)$$

This result shows a constant coupling coefficient. The parallel capacitors have to be tuned to change the centre frequency as well as keeping the coupling coefficient constant. This configuration will enable constant relative bandwidth, but not constant absolute bandwidth.

Short-circuited Transmission Line

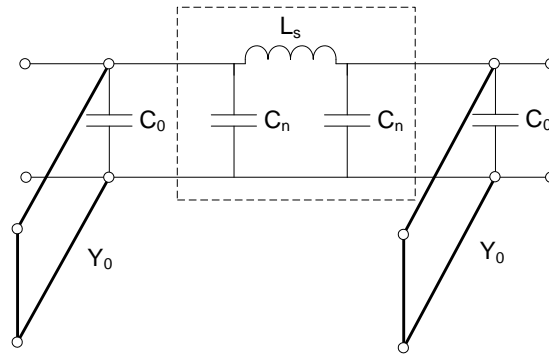


Figure 3.17: Short circuited transmission line coupled with inductor-capacitor pi-network

Substitute the equation for the characteristic admittance of the inductor-capacitor pi-network (3.18) and the susceptance slope of the short-circuited transmission line (3.5) into (3.24):

$$k = \frac{1}{\omega_0 L_s \frac{1}{2} Y_0 (\omega_0 T \csc^2(\omega_0 T) + \cot(\omega_0 T))} \quad (3.32)$$

This coupling value is multiplied by $\frac{L_s Y_0}{2T}$ for convenience and $\omega_0 T$ is substituted by θ_0 . This manipulation yields:

$$k' = \frac{1}{(\theta_0 (\theta_0 \csc^2(\theta_0) + \cot(\theta_0)))} \quad (3.33)$$

This frequency dependence is shown in fig. 3.18.

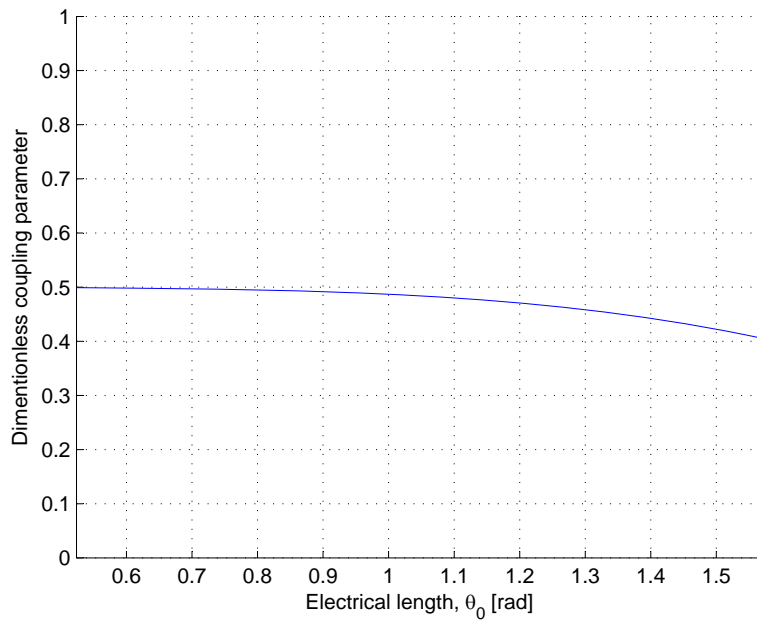


Figure 3.18: Frequency dependence of coupling between short-circuited transmission lines with inductor-capacitor pi-network in the range $\frac{\pi}{6} \leq \theta_0 \leq \frac{\pi}{2}$

This near constant coupling coefficient of this configuration is to be expected since the LC resonators with the same inverter had constant coupling factor.

3.3.3 Parallel coupled transmission lines

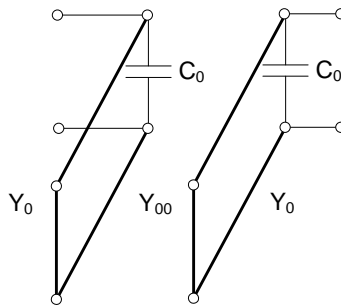


Figure 3.19: Parallel coupled short circuited transmission lines

Compline filters implement coupled transmission line resonators, which are short-circuited on the one end and loaded by capacitors on the other end. These filters have been shown to retain good filter response when tuned over broad bandwidths [10]. Compute the coupling coefficient of this network by substituting (3.10) and (3.22) in (3.24). Also set $Y_{00} = Y_0$ for numerical convenience.

$$k = \frac{2}{(\theta_0 \csc^2 \theta_0 + \cot \theta_0) \tan \theta_0} \tag{3.34}$$

The coupling coefficient is graph in figure 3.20.

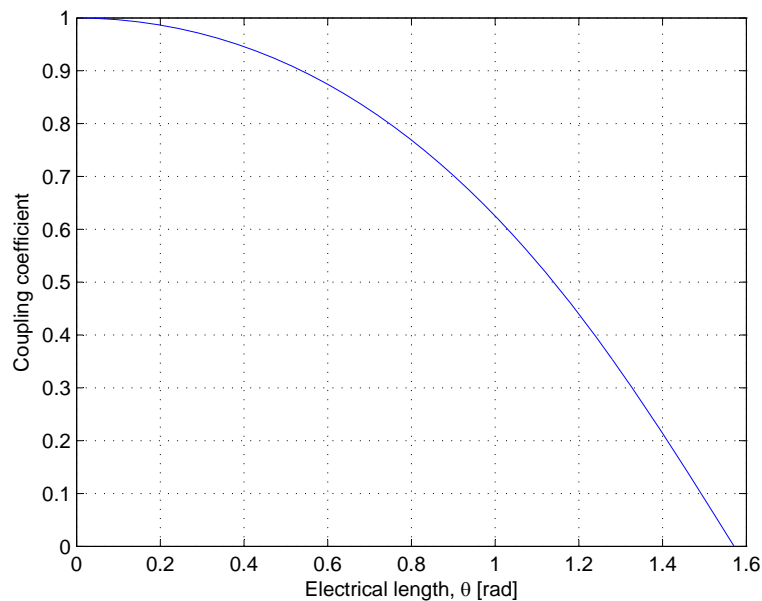


Figure 3.20: Coupling coefficient between two resonators of a combline filter

This configuration is the closest to the inverse frequency dependency that is required, and explains the good tuning results that have been reported for combline filters [10].

3.4 Coupling to source and load

The nature of the end-coupling is different, as a resonator needs to be coupled to a constant resistance (or conductance). A convenient approach is to use the external Q -factors, the Q_e factor for a parallel resonant circuit is [9]:

$$Q_e = \frac{R_L}{\omega_0 L_0} \quad (3.35)$$

Inverters that have negative parallel elements cannot be used for matching, as there is no reactive element at the source or load to absorb the negative element. A filter implementing this type of inverter can use single frequency matching instead.

Adding a series reactive element and adjusting the nearest resonator is sufficient to enable matching to a parallel resonator at a specific frequency. Consider the equivalent parallel and series impedance transformers, shown in figure 3.21, to be able to compare parallel and series element values.

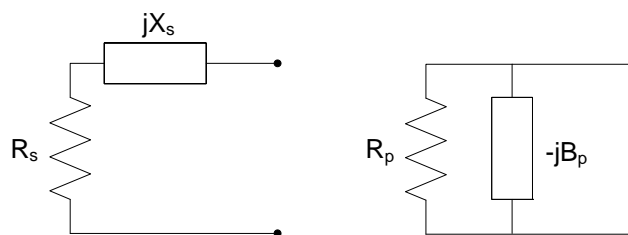


Figure 3.21: Series and parallel equivalent impedance transformers

The input impedance of the series network is:

$$Z_s = R_s + jX_s \quad (3.36)$$

Equate the to input impedances by setting $Y_p = \frac{1}{Z_s}$:

$$Y_p = \frac{1}{R_s + jX_s} = \frac{R_s - jX_s}{R_s^2 + X_s^2} = G_p + jB_p \quad (3.37)$$

The two circuits shown in fig 3.21 are equivalent the following two conditions are met:

$$G_p = \frac{1}{R_p} = \frac{R_s}{R_s^2 + X_s^2} \quad (3.38)$$

$$B_p = \frac{X_s}{R_s^2 + X_s^2} \quad (3.39)$$

Use this circuit to couple to the end resonators, as shown in figure 3.22.

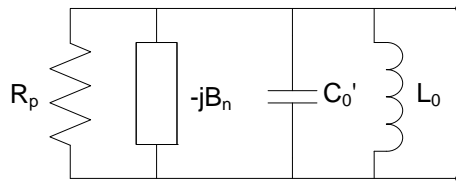


Figure 3.22: Impedance transformer coupled to LC-resonator

The matching circuit should not change the resonant frequency of the resonant circuit, in addition to providing an impedance match. The two conditions following from these requirements are:

$$-jB_n + j\omega_0 C_0' = j\omega_0 C_0 \quad (3.40)$$

$$Q_e = \frac{R_p}{\omega_0 L_0} \quad (3.41)$$

The resonator capacitor, C_0 , will be tuned, and the first condition, (3.40), can be met by adjusting the tuning curve of C_0' . Investigating the second condition, substitute (3.38) into (3.41):

$$Q_e = \frac{1}{\omega_0 L_0} \left(\frac{R_s^2 + X_s^2}{R_s} \right) = \frac{R_s}{\omega_0 L_0} \left(1 + \frac{X_s^2}{R_s^2} \right) \quad (3.42)$$

Normally L_0 would be chosen to achieve a high resonator Q -value, calculate C_0 for resonance and fix $R_s = 50\Omega$. The coupling values ($k_{n,n+1}$) and external q -values were determined by the filter response and bandwidth, leaving the designer only the type of element used for X_s as a free parameter. However, an additional degree of freedom can be introduced when using optimisation and allowing the inductance value of the input and output resonators to differ from the inner ones.

For narrow bandwidth, $\frac{X_s^2}{R_s^2} \gg 1$

$$Q_e = \frac{X_s^2}{\omega_0 L_0 R_s} \quad (3.43)$$

For capacitive coupling, $X_s = -\frac{1}{\omega C_s}$

$$Q_e = \frac{1}{\omega_0^3 L_0 R_s C_s^2} \quad (3.44)$$

For inductive coupling, $X_s = \omega L_s$

$$Q_e = \frac{\omega_0 L_s^2}{L_0 R_s} \quad (3.45)$$

The inductive coupling gives the linear frequency dependency required for constant absolute bandwidth. The capacitive coupling seems the worst choice due to the ω_0^3 term, but C_s can be electronically tuned, while for inductive coupling L_s is very difficult to tune in this way. The tuning curve for C_s to achieve constant absolute bandwidth is inverse quadratic:

$$C_s(\omega_0) \propto \frac{1}{\omega_0^2} \quad (3.46)$$

This is the same ratio of tuning as required for the resonator capacitor of a LC resonator.

3.5 Conclusion

The coupling coefficients, that determine the filter response, is effected by the susceptance slope of the resonator as well as the characteristics of the inverter. Both these circuits were investigated to find the combination that comes closes to achieving constant absolute bandwidth when the circuit is tuned, see table 3.1 for comparison.

The most suitable combination is parallel coupled transmission line resonators. This option is unfortunately not practical at frequencies lower than 500MHz. The inductor-capacitor inverter performs much better than the capacitor pi-network. This should be the option of choice if suitable inductors can be found.

Two different options for matching were investigated in a similar manner to find a suitable circuit that will enable the retention of good filter response. Here the series inductor seems to be the best option, though the series capacitor has the advantage that it can be electronically tuned.

Table 3.1: Comparison of different inverter and resonator combinations

Circuit	k vs f

Chapter 4

Non-ideal components

The most important factor that limits the use of lumped elements at microwave frequencies is the parasitic resistance, inductance and capacitance inherent in the component construction. Parasitic inductance or capacitance causes the device to resonate, as it creates a parallel or series inductor-capacitor (LC) tank. The frequency at which this resonance occurs is called the self resonant frequency (SRF).

Parasitic resistance cause component Q -values to be reduced, often drastically, as is the case for inductors. Expressions for the unloaded Q -values for resonators were given in section 2.2. The equations can be changed to include the impedance or admittance, rather than the slopes of these values, to give

$$Q_u = \frac{X}{R_s} \quad (4.1)$$

$$Q_u = \frac{Y}{G_n} \quad (4.2)$$

This chapter investigates the influence of parasitics, specifically in terms of the project at hand. The effect on both fixed and tuning elements are discussed.

4.1 Lumped elements

Surface mount device (SMD) capacitor technology is well suited to the lower half of the frequency band in this project, that is frequencies lower than 250MHz. The SRF of ordinary ceramic multilayer capacitors are between 250MHz and 350MHz. But capacitors made specifically for Radio Frequency (RF) and microwave frequencies, that resonate above 1GHz, are available.

In the case of SMD capacitors, their SRF is limited by the inductance of the package. Dielectric loss is the primary cause of dissipation in such a capacitor. This loss is frequently specific as equivalent series resistance (ESR) and is normally less than 0.1Ω in the range below 1GHz.

The principal problem when constructing a RF filter is to find inductors with a high unloaded Q value. These losses are caused by the finite conductance of the inductor windings. For inductors, the SRF is limited by the amount of inter-winding capacitance.

SMD inductors are wound around ferrite cores to reduce size. The small size is advantageous because it results in high SRF. This technique focuses the majority of the magnetic field inside the magnetic core, and

minimises the scattered field around the inductor. The strength of the scattered magnetic field is of importance when designing for stopband attenuation of 80dB, as it creates unwanted coupling between resonators. Unfortunately these inductors have relatively low Q_u in the order of 50.

Air core inductor coils have the highest Q_u , the values range from 100 to 150. Small inductors that have higher SRF than similar ferrite core inductors are available. The inductors can be shielded to some extent, but this lowers the Q_u . Care should be taken to ensure these magnetic fields do not couple, as this will surely degrade the passband performance.

4.2 Transmission lines

The smallest air core inductors have SRF well above 1GHz, but a Q_u in the order of 100 at 500MHz (see section B.2.1, page 79). Fortunately transmission lines can be considered as an alternative to inductors at this frequency.

The physical length of transmission lines are unattractive at frequencies as low as 300MHz. Consider for example a line with, $v_{rel} = 66\%$, where the guided length of a quarter wavelength is 16,5cm. Consequently transmission lines will only be considered for the filter that will tune to 500MHz. This filter may have tuning centre frequency of 420MHz. Calculating the length of a line with electrical length, $\theta = 53^\circ$ (as suggested by Hunter and Rhodes [10]), and also with $v_{rel} = 66\%$

$$\lambda_g = \frac{53}{360} \cdot \frac{0.66c}{420 \times 10^6} = 6,94cm \quad (4.3)$$

This is a much more practical length to consider.

Where semi-rigid coaxial transmission line exhibits relatively low loss, ceramic coaxial resonators have superior dissipation characteristics, and are therefore the first choice. Table 4.1 shows a comparison of these two technologies.

The Q_u values of the ceramic coaxial resonators are given, and the attenuation factor is computed for comparison with the semi-rigid transmission lines. The susceptance slope of a quarter wavelength transmission line, equation (3.8), is substituted in equation (2.11) to find the Q_u factor of such a line

$$Q_u = \frac{\frac{Y_0\pi}{4}}{G} = \frac{\pi Y_0}{4G} \quad (4.4)$$

where G is the conductance per unit length. The conductance of the line is given by [5]

$$G = Y_0\alpha\ell \quad (4.5)$$

with α the attenuation constant. Substitute (4.5) into (4.4) and rearrange to give

$$\alpha = \frac{\pi}{4\ell Q_u} \quad (4.6)$$

The resulting answer is in nepers per meter, and it is simply multiplied by 8,686 to convert it to dB per meter.

The Q_u factors of the semi-rigid lines are also computed for easy comparison. The attenuation factors of the transmission lines are given, and the Q_u factors are computed using

$$Q_u = \frac{\beta}{2\alpha} \quad (4.7)$$

where β is given by

$$\beta = \frac{2\pi f}{v_{rel}c} \quad (4.8)$$

Care should be taken to convert the attenuation factor to nepers when using equation (4.7).

The data in the following table was found in data sheets from the manufactures. Selected pieces the transmission line data sheets can be found in B.1.

Table 4.1: Unloaded Q factors of quarter wave length transmission lines at 500MHz in order of ascending Q_u

	Length [mm]	v_{rel} [%]	α [$dB.m^{-1}$]	Q_u
Micro-Coax UT-141C-LL	115.5	77.0	0.230	256
Microstrip on Taconic TLY-3F	106.8	71.2	0.174	367
Trans-Tech 9000 EP	15.8	10.5	1.016	425
SRC semi-rigid 0.250	105.0	70.0	0.151	430
Trans-Tech 9000 HP	15.8	10.5	0.785	550

The semi-rigid lines in this comparison have far superior attenuation characteristics, but are also much longer than the coaxial resonators. The large dielectric constant of the ceramic material shortens the physical length and less loss occurs in this reduced length of line. Consequently, the Trans-Tech 9000 HP series has the highest unloaded Q in this comparison.

4.3 Components for discrete tuning

Components that are used as switches require banks of reactive components to facilitate a change in resonant frequency. The reactive component can be chosen to be SMD capacitors to minimise the board space needed for these tuning banks. The tuning range will be determined by the number of elements in such a bank. Switches need to be of the single-pole, multiple-throw type to switch between an array of elements. A single-pole, four-throw switch configuration is shown in figure 4.1.

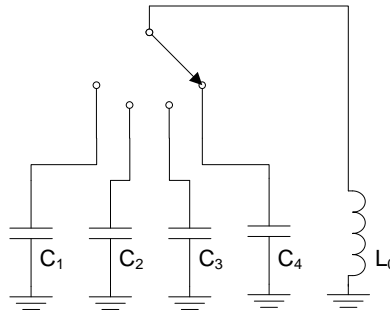


Figure 4.1: Tunable resonator that can be adjusted to four discrete resonant frequencies

The losses for this type of tuning is due to the loss in the fixed capacitor in the tuning bank, and the ON resistance of the switch.

The way in which the switches are controlled are also of great importance. Preference will be given to switches that can be easily controlled with a voltage, as this is the easiest to implement. The switching speed will be considered, but it is not of critical importance.

4.3.1 PIN diodes

The PIN diode V-I curve is designed to have characteristics that make it a good RF switch. In the ON state, the diode is operated in the forward bias state, and behaves like a variable resistor at RF and microwave frequencies. Reverse biasing the diode sets up a small junction capacitance and puts the diode in a high impedance or OFF state. The ON resistance is investigated as it will effect the resonator Q_u .

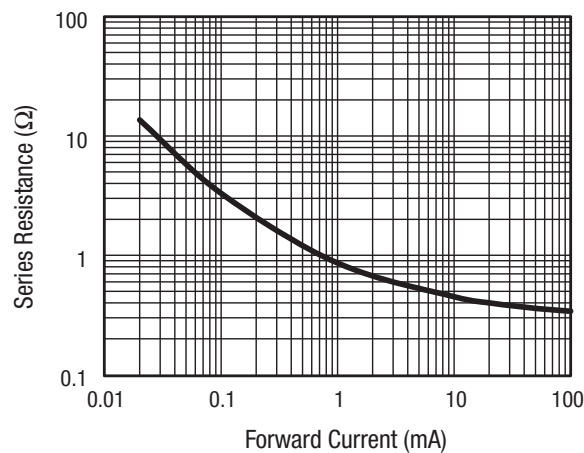


Figure 4.2: Series resistance vs forward current for Skyworks SMP1322 PIN diode (measured at 100MHz)

The value of this resistance is controlled by the forward bias current through the diode. A small current puts the diode in a high impedance state, and a large current puts the diode in a low impedance state. This inverse proportional relationship is shown in figure 4.2.

The forward bias current is typically 10 – 30mA [9], and must be applied to the diode with RF chokes and Direct Current (DC) blocks to enable isolation from the RF signal. These biasing networks for two different configurations is shown in figure 4.3.

For tunable filters, single-pole, multi-throw switches are required. Each PIN diode in a multi-throw switch has to be biased separately to control individual diodes. A biasing network for a single-pole, multi-throw PIN diode switch, that switches capacitors, C_1 , C_2 and C_3 , in and out a circuit is shown in figure 4.4.

Large biasing currents are needed to lower the resistance of the diode in the ON state. This extra resistance, typically 1Ω [11], would add to the loss in the signal path the diode is in. In a tunable filter, this will add to the resonator losses. This drawback, together with substantial current biasing networks, makes this switch unappealing.

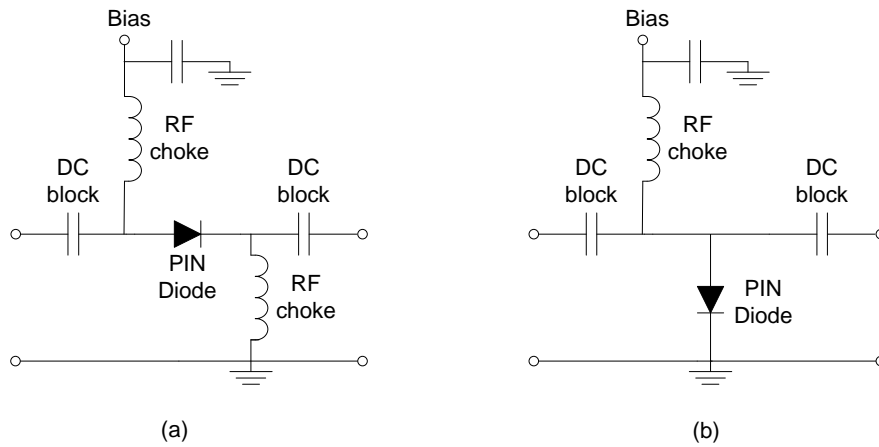


Figure 4.3: Single-pole PIN diode switches in (a) series configuration and (b) shunt configuration

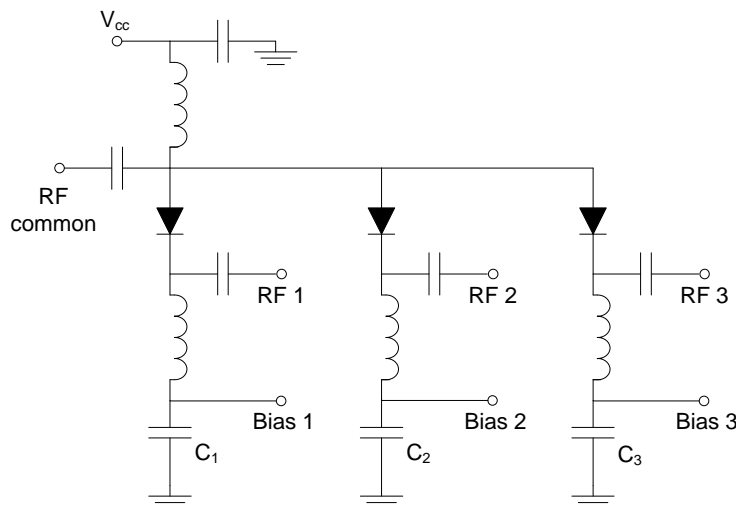


Figure 4.4: Single-pole, triple throw, PIN diode compound switch with diodes in the RF path (series configuration)

4.3.2 RF semiconductor switches

Si junction or Gallium arsenide (GaAs) Field-effect transistors (FETs) make good RF switches because the ratio between the ON and OFF resistances of the channel is quite high. A FET that is correctly sized for the application can have a ON resistance of 1Ω , which is comparable to a PIN diode [19].

The biasing of a FET is simple as it does not require any power. It is a three terminal device and the DC voltage is isolated from the RF path by the inherent DC blocking of the gate. On the negative side it causes more intermodulation distortion than a PIN diode.

Integrated RF switch Integrated circuits (ICs), like the range from Peregrine are investigated as an example of a transistor switch. These switches are based on Complementary metal oxide semiconductor (CMOS) technology and can be controlled with 1.8V or 2.75V logic levels. The range includes switches from single-pole, single-throw up to single-pole, six-throw packages. Such a multi-throw switch increases the tunable range that can be achieved with switches.

The switches are optimised for isolation and linearity. Their third order intermodulation intercept point is

67dBm. Insertion loss of about 0.45dB at 500MHz, which translates to a series resistance of about 4.9Ω , using equation (4.9).

A switch has to use a bank of capacitors to enable tuning. Peregrine integrated their RF switches and a capacitor bank into a single package. The equivalent series resistance of the capacitors is in the range of 1.33Ω to 1.40Ω , not including the series resistance of the switch. This technology is quite new and only limited capacitance ranges are available.

4.3.3 RF MEMS switches

These switches work by pulling a flexible electrode towards a fixed electrode. The actuation force can be electrostatic, magnetic or thermal [9, p.531]. This mechanical actuation connects or disconnects two terminals from each other. Figure 4.5 shows three different configurations that work with electrostatic actuation. In the ON state a voltage is applied to the pull-down-electrode to pull the flexible metal beam downwards, connecting the switch contacts. The moveable electrode is spring loaded so that it returns to the resting position the OFF state. To switch off, the pull-down-electrode is grounded and the beam moves away from the switch contacts to disconnect the terminals. In this OFF state the switch can be represented by a small capacitance, depending on the electrode spacing.

The cantilever beam in the in-line configuration carries the RF signal, and the whole beam has to be fabricated as a relatively thick metal layer to minimise losses. In the broadside configurations the RF signal only passes through contact portion of the switch, and only this part needs to be metallised.

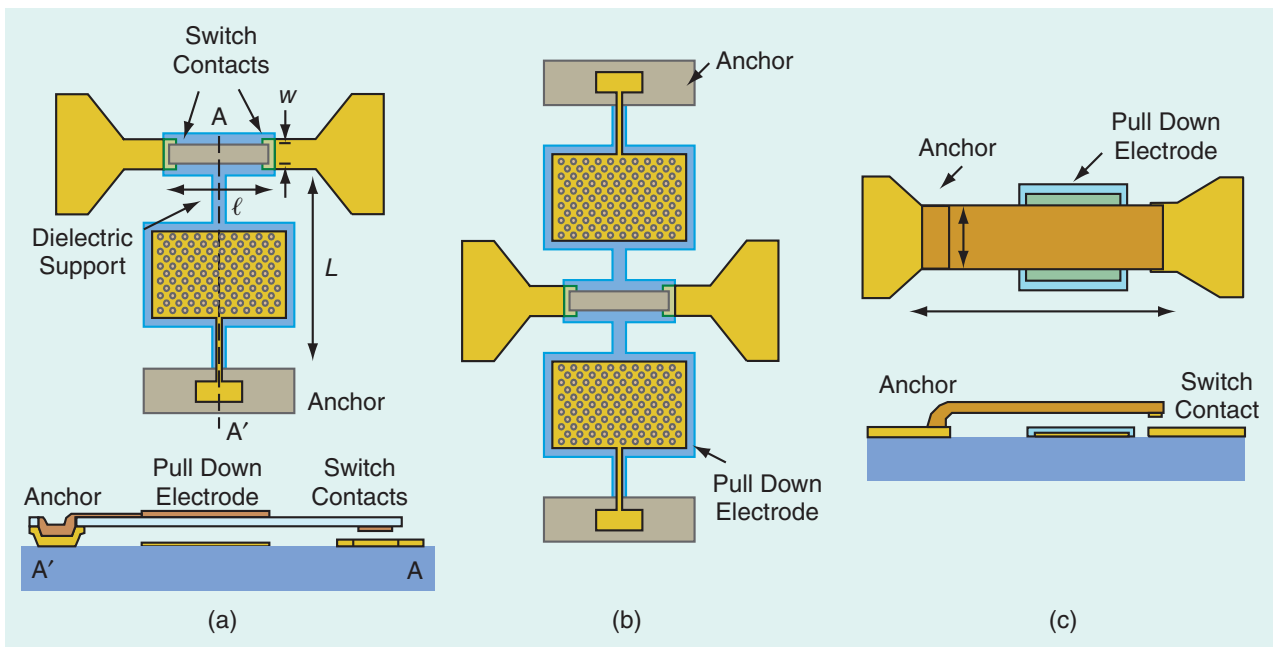


Figure 4.5: MEMS series switch configurations, broadside with (a) one electrode, (b) two electrodes, and (c) an in-line switch [3]

The equivalent circuit model of an series micro electromechanical systems (MEMS) switch is a series

capacitor in the OFF state, and a small series resistance in the ON state. The insertion loss is [3]

$$|s_{21}|^2 = 1 - \frac{R_s}{Z_0} \quad (4.9)$$

where Z_0 is the transmission line characteristic impedance and R_s is the contact resistance of the switch. For a typical contact resistance of 1Ω this gives a loss of less than 0.1dB. The insertion loss for a Radant MEMS RMSW221 is roughly 0.3dB at 500MHz, which translates to 3.3Ω when applying equation 4.9, and increases to 4Ω at DC (see section B.4.1, page 82).

The major advantage of MEMS switches for this project is their low loss in the ON state. They also have small capacitance in the OFF state, in the order of 2-16fF [11], which gives them high isolation. They are very linear, and their third-order intercept point is 20-50dB better than GaAs or CMOS devices.

The two disadvantages for MEMS in this project are the control voltage and price. The most reliable MEMS require high voltages (25-90V) to drive the circuits. The Radant MEMS, mentioned earlier, require 90V. Reliability is the biggest concern for MEMS at the moment, but continued research is making significant advances in this regard [11].

Filters which operate as low as 25MHz have been successfully implemented using binary-weighted switched capacitor banks [20].

4.4 Components for continuous tuning

The components in this section have reactance that can be varied continuously by some electronic means. Thin film Barium-Strontium-Titanate (BST) varactors are not included in this comparison, as they are not readily available. These devices have losses comparable with semiconductor varactors. They are more linear, but their reactance can not be varied as much as their semiconductor counterparts.

4.4.1 Varactor diodes

This diode is operated in reverse bias mode, and the capacitance across the pn junction is controlled with the reverse bias voltage. This behaviour provides a voltage controlled capacitive component. The reverse bias voltage and the junction capacitance is related by [9,21]

$$C_j(V_r) = \frac{C_{j0}}{\left(1 + \frac{V_r}{V_{bi}}\right)^\gamma} \quad (4.10)$$

where C_{j0} is the junction capacitance at zero bias and V_{bi} is the built-in potential barrier. The exponent, γ , is dependant on the doping profile of the diode. From equation 4.10 it can be seen that γ determines the slope of the voltage-capacitance curve. If γ is large then a small change in voltage causes a big change in capacitance. Such varactors, which have $\gamma > 0.5$, are named hyperabrupt varactors, while an abrupt varactor has $\gamma \approx 0.5$ [22]. The ratio of minimum and maximum capacitance, C_{max}/C_{min} , of a hyperabrupt varactor can be as high as 12 [19].

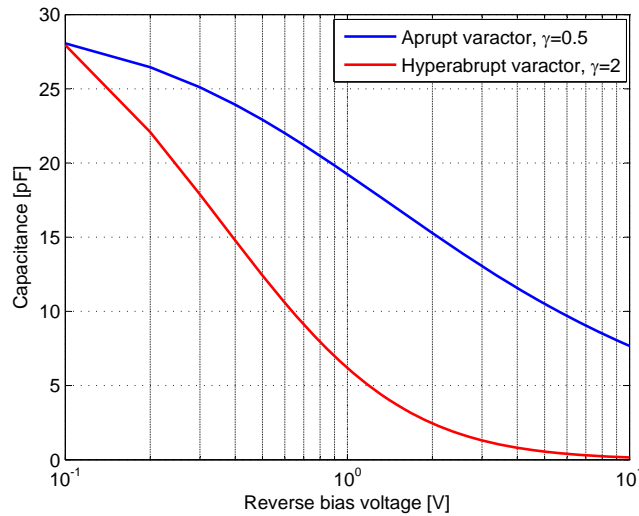


Figure 4.6: Typical voltage-capacitance curves for varactor diodes

The simplified equivalent circuit for a varactor diode is a resistor (R_s) and capacitor (C_j) in series with each other [9]. The loss of the diode can be quantified by the series resistance or the Q_u factor, related by [19]

$$Q_u = \frac{1}{2\pi f R_s C_j} \quad (4.11)$$

The Q_u factor is an unfortunate choice for a comparison, as it is directly related to the junction capacitance, which changes with biasing. The series resistance is therefore a better figure of merit to compare different diodes, although it does also vary with biasing. Manufactures specify the series resistance or the Q_u factor of the diode typically only at one frequency-biasing point. This means simulations cannot predict the measured losses very accurately.

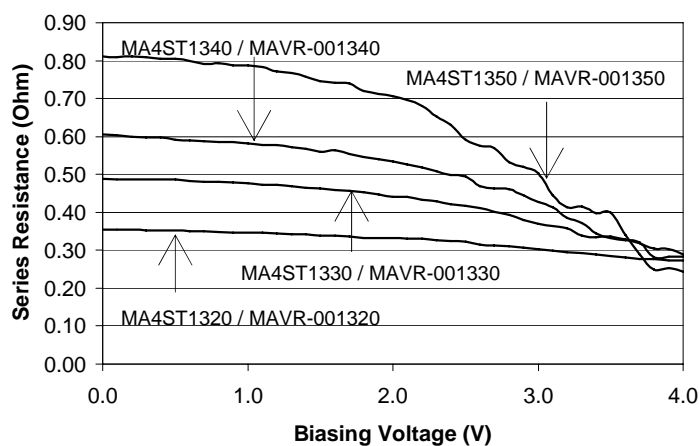


Figure 4.7: Series resistance vs. biasing voltage of the M/A-COM MA4ST1300 Series

Figure 4.7 shows the junction capacitance and series resistance of some typical varactor diodes. It is clear that the series resistance decreases as bias voltage increases [19], as is also evident from the work of Brown and

Rebeiz [13]. Operating the diode close to the maximum reverse voltage will minimise the series resistance and junction capacitance. And this will, according to equation (4.11), maximise the Q_u .

Varactor diodes are popular because of their low cost, availability and simple control circuits. Filters tuning over relatively broad bandwidths have been built [10, 13]. It is particularly this wide tuning ability and their simple control circuits that make this technology appealing for this project.

The inherent non-linear behaviour of this semiconductor diode is its main drawback. Intermodulation distortion in an interdigital filter using varactor diodes have been investigated by Brown and Rebeiz [13]. The fourth order filter they constructed tunes from 700 MHz to 1.33 GHz and the input third-order intermodulation product intercept point was measured to be better than 17 dBm across the tuning range [13].

4.4.2 YIG crystal resonator

The current-tuned Yttrium-iron-garnite (YIG) resonator is the dual of the voltage-tuned varactor diode. A YIG is a synthetic crystal of a ferrimagnetic material. The synthetic crystals are grown and subsequently sliced into small YIG cubes, and finally shaped into spheres. These spheres are in the order of 0.5mm in diameter and consist of a single crystal.

For resonance to occur the crystal must be immersed in an magnetic field to magnetise it - the direction of the magnetic dipoles depend on the crystal alignment and the direction of the applied magnetic field. Inductively coupling a RF signal to the sphere will cause the dipoles to precess. Precession is the rotation of the axis of a spinning object. A net magnetic moment is produced and secondary RF inductive coupler can be used to harness this energy. Resonance occurs at the Lamor frequency [23]

$$\omega_0 = \gamma B \quad (4.12)$$

where γ is a constant, the gyromagnetic ratio, and B is the magnitude of the magnetic field.

The great strength of the YIG is the high unloaded Q values that can be achieved, values as high as 2000 are possible [11]. Depending on the material composition, size, and applied field, a resonance of 500MHz to 50GHz can be achieved [19]. YIGs can be made to tune over a decade, while varactors can only manage about an octave of tuning [9]. This wide tuning ability is made possible by the nearly linear dependence of resonant frequency and applied DC magnetic field [23], approximated by equation (4.12).

The auxiliary systems needed to support the proper working and tuning of a YIG is quite substantial. Temperature control is required for good performance. The crystal has to be carefully positioned and orientated. Large magnetic fields are needed, and consequently large coils conducting large currents. For this reason YIGs are not able to tune as fast as varactors diodes [12] or RF MEMS varactors [11].

Tunable filters built with YIGs are common in microwave measuring equipment. Coupling techniques have been investigated [23] and used in different filters [5]. This technology still remains an expensive option.

4.4.3 RF MEMS varactors

This component is also known as a capacitive shunt switch. The working is very similar to the working of the MEMS series switch, as discussed in section 4.3.3. The difference is that the electrodes of this MEMS do not touch. It is a capacitor that is tuned by adjusting the distance between the two electrodes. A thin layer of

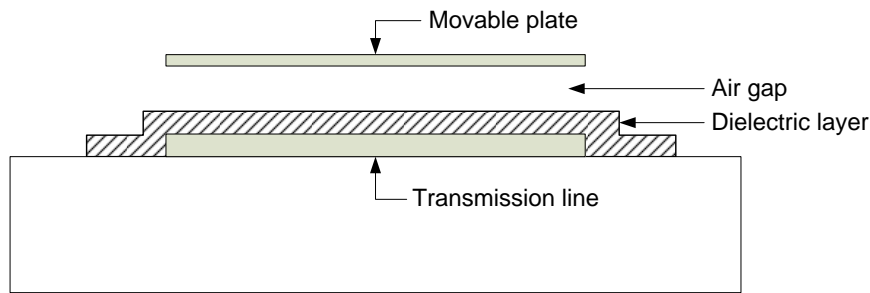


Figure 4.8: MEMS shunt switch to implement variable capacitor [4]

dielectric is placed on the one electrode to keep the electrodes from touching when the switch is in the down state - minimum distance and maximum capacitance.

MEMS capacitive switches with down state capacitance as high as 50pF have been reported [4] using dielectrics with high ϵ_r .

These capacitive switch MEMS have the same advantages and disadvantages as the series contact MEMS in section 4.3.3. The capacitive switches have high Q_u values, ideal for tunable filters. The important advantage is the linearity, which is much better (20-50dB) than varactor diodes [11]. MEMS are unfortunately not able to tune as fast as varactor diodes.

4.5 Conclusion

Lumped inductors have very low Q_u values and start to resonate well under 500MHz. The best option is to use small air core inductors. Most SMD capacitors have SRF in the order of 300MHz. Care must be taken to use RF capacitors, especially if large capacitance values are needed.

The discussion on tunable components does not point to an outright winner. MEMS switches and varactors have excellent linearity, while maintaining very low losses. MEMS are still quite expensive, as they require expensive packaging and are not yet mass produced. As their cost and availability increase they will become the tuning devices of choice in the future.

The CMOS switches from Peregrine that was evaluated compares well with MEMS, but although they are cheaper, they have more losses. PIN diodes is a viable option for single-pole, single-throw switches. This project will require many multiple-throw switches and the biasing networks and large biasing currents become unattractive.

YIG filters are expensive, bulky and power hungry, but have very low losses. This makes this technology a serious contender at frequencies above 500MHz. If tuning speed and price is the main consideration, then varactor diodes is the logical choice. This mature technology is available for wide frequency ranges, including the relevant band for this project. The varactor diode will consequently be used as tuning element in all the filters in this project.

Chapter 5

Filter design

It is clear from the component study in chapter 4 that a single filter solution does not exist for such a wide frequency range as 20-500MHz. For the purposes of this thesis, two filters were designed and implemented, one at the high end of the band and one at the low end.

A few design considerations are discussed that need to be taken into account when designing for the specifications set by the project. The detail design of the two filters will follow this initial discussion.

5.1 Prototypes with sharp cut-off

The all pole filter with the sharpest cut-off is the Chebyshev filter. An elliptic filter has a very sharp initial cut-off, but further from the band-edge the Chebyshev filter has more stopband attenuation, see figure 5.3. The synthesis of a Chebyshev prototype is straightforward, as it only makes use of adjacent coupling, where the elliptic prototype requires non-adjacent coupling and the synthesis is more complex [9].

5.1.1 Elliptic prototype

The synthesis of elliptic filters is not elementary and methods for direct synthesis are possible but cumbersome [24]. The basic idea of achieving an elliptic response with coupled resonators is explained in a simple manner by Thomas [25]. He outlines a simple procedure for determining the type (inductive or capacitive) of cross coupling between non adjacent resonators to control the position of the transmission zeros, and consequently suggests a synthesis by optimisation.

The order of the elliptic response required to meet the specifications, like the synthesis process, is not simple to calculate. Tables have been compiled for the design of elliptic filters [26], and this data can serve as starting point in the design.

The optimisation synthesis of Thomas [25] and the direct synthesis by Reeves [24] enables a design with the minimum number of resonators and the maximum number of cross couplings. Such a design will be very compact and will also have the least amount of insertion loss, but at a cost of complexity. Many coupling paths increases sensitivity to changes in resonator values, which need to be tuned. This level of sensitivity will make tuning a long and difficult process.

A more conservative and structured approach to designing filters with cross coupling is using cascaded triplet (CT) or cascaded quadruplet (CQ) sections [27], shown in figure 5.2. Cross coupling is limited to fewer

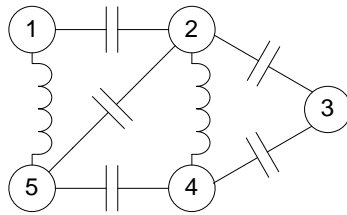


Figure 5.1: Example of circuit with many cross coupling paths

paths than mentioned previously to simplify the synthesis, which will make the filter easier to design and tune.

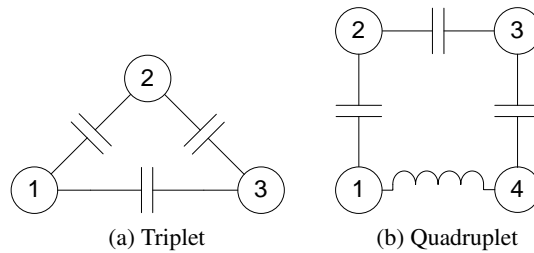


Figure 5.2: Triplet and quadruplet coupling configurations

A single quadruplet gives two transmission zeros (see figure 5.3), one on either side of the passband. To get two transmission zeros on either side of the passband with triplets, two in cascade are needed, one with positive and one with negative cross coupling. The problem with using these structures in tunable filters is implementing the negative coupling needed to realise transmission zeros. Either the main or cross couplings has to be inductive, and will therefore not be tunable.

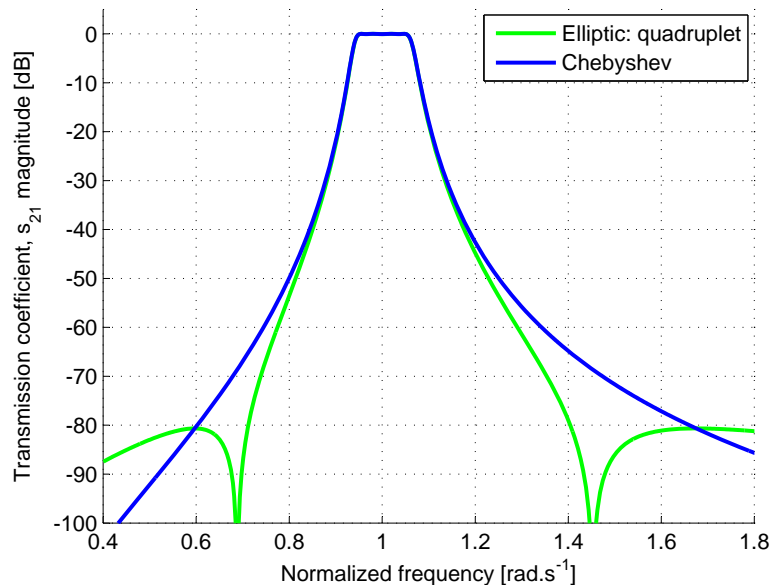


Figure 5.3: Elliptic filter implemented with a quadruplet and compared with a fourth order Chebyshev filter

5.1.2 Chebyshev prototype

The synthesis of this all pole prototype is straightforward. Formulas to compute the prototype values can be found in any text on electronic filters [5–7, 9, 10]. MATLAB code to compute the prototype values can be found in appendix C.

The order required to realise a specific cut-off rate may be computed for a Chebyshev response by using the following formula [8]:

$$N \geq \frac{L_A + L_R + 6}{20 \log \left(S + \sqrt{S^2 - 1} \right)} \quad (5.1)$$

where

L_A = stopband insertion loss [dB]

L_R = passband return loss [dB]

$$S = \frac{\omega_s}{\omega_p} \text{ (normalized } \omega_s \text{ and } \omega_p) \quad (5.2)$$

The lowpass prototype response to which (5.1) refers has passband edge, $\omega_p = 1$. The lowpass to bandpass transformation (equation (2.7)) is used to normalize the the passband (ω_p) and stopband (ω_s) frequencies.

5.2 Minimising insertion loss

Most of the losses in Coupled Resonator (CR) filters are due to currents in the resonators at their resonance, as discussed in section 2.2. All of the resonators in a bandpass CR filter resonate at some point in the passband. Consequently, most of the losses are confined to the passband.

5.2.1 Unloaded Q

A filter comprised of resonators that have high unloaded Q_u have low losses, and little degradation of the passband shape. The filters of figure 5.4 are Chebyshev bandpass prototypes with $RL = 20\text{dB}$ and 10% bandwidth. The graph shows that the losses in the filter only affect the passband, while the attenuation in the stopband remains unchanged.

5.2.2 Bandwidth

The bandwidth has a big impact on the amount of losses in the passband, as can be seen from figure 5.5. It shows a comparison of three fourth order Chebyshev bandpass prototypes ($RL = 20\text{dB}$) with resonators that have the same unloaded Q , but with different bandwidths.

A filter with narrower bandwidth has more loss in the passband, as the resonator losses are confined to a smaller band. This is a true catch-22, as a broader bandwidth decreases the cut-off rate of the filter. The best solution will be to make the bandwidth as wide as possible, while still maintaining the required cut-off rate.

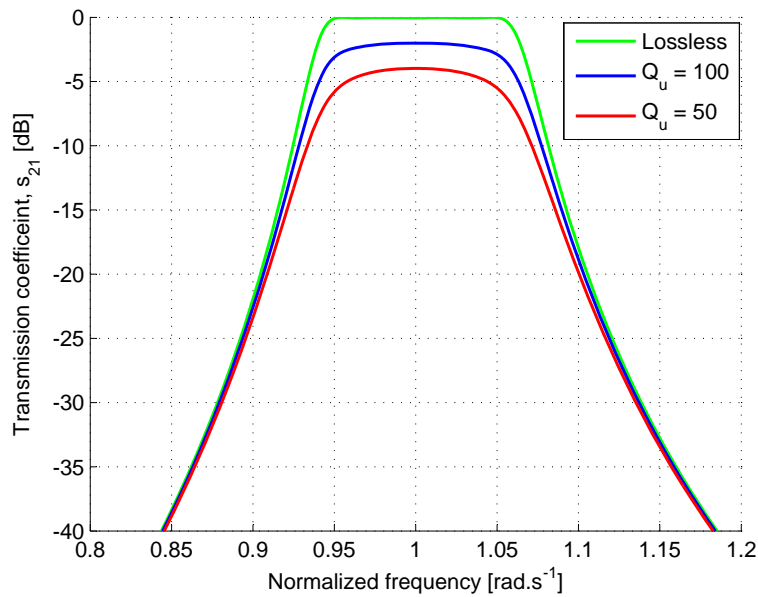
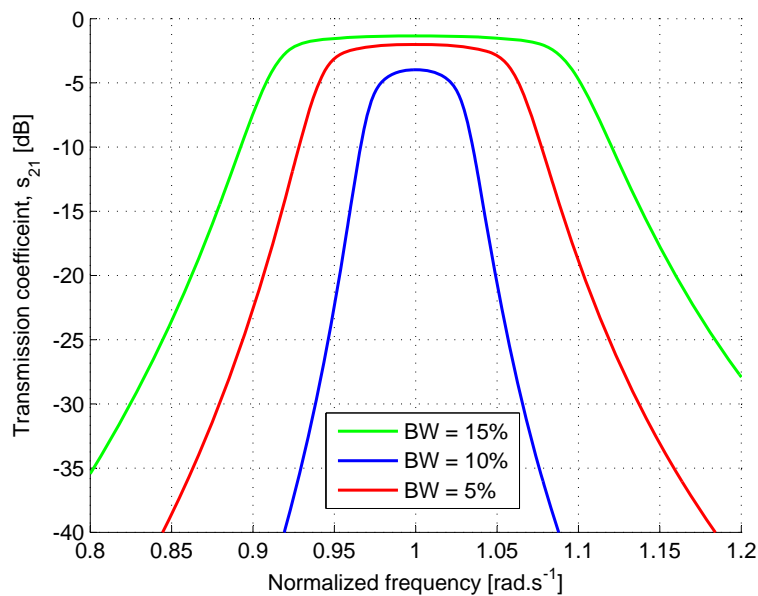
Figure 5.4: Comparison of lossless response and filters with finite Q_u 

Figure 5.5: Effect of bandwidth on passband loss

5.2.3 Filter order

The order of the filter also influences the cut-off rate and the losses, and has to be taken into account in the above mentioned problem. Increasing the order of the filter will make it possible to widen the bandwidth, without sacrificing cut-off rate. But increasing the order will increase the size and the tuning complexity.

Consider filters that have the same bandwidth, but different order. Analysis shows that there is a linear relationship between the insertion loss and the order of the filters, the result of the analysis is shown in figure 5.6. This is what was expected, as adding more resonators in the same confined band, will concentrate the

losses in that band.

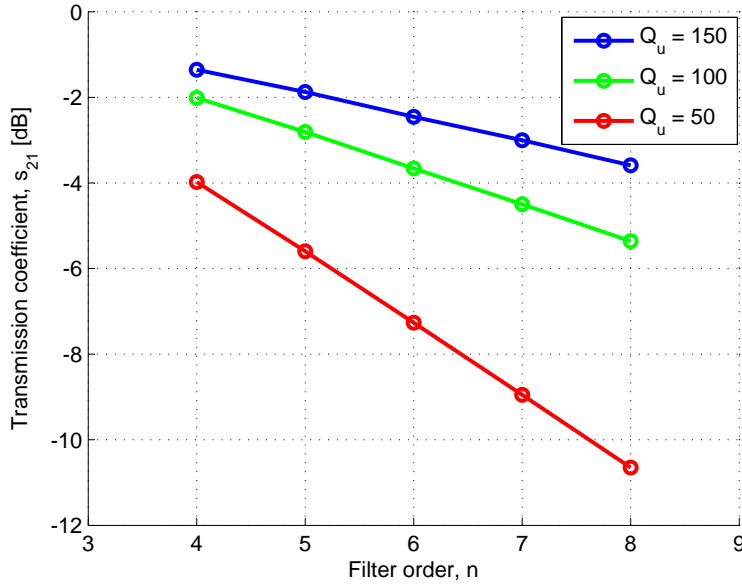


Figure 5.6: Comparison of the insertion loss at the centre frequency of filters with different order

5.2.4 Minimizing the loss of varactors diodes

Varactors are the tuning component of choice for this project. Their losses can be modelled by a series resistor. Adding two varactors in parallel will not change their Q_u value. Consider two varactors in parallel and compute the total impedance

$$Z_{tot} = \frac{Z_{var}}{2} = \frac{1}{2} \left(R_s + \frac{1}{j\omega C_0} \right) = \frac{R_s}{2} + \frac{1}{j\omega(2C_0)} \quad (5.3)$$

And the Q_u factor is simply

$$Q_u = \frac{1}{\omega(2C_0) \frac{R_s}{2}} = \frac{1}{\omega C_0 R_s} \quad (5.4)$$

However for a given R_s , the Q -factor increases as C decreases. The use of two varactor diodes of lower capacitance therefore results in an increased Q , as shown in equation (5.5). A varactor is tuned to a capacitance value of $C_0/2$, and two of these are used in parallel to obtain C_0 .

$$Q_u' = \frac{1}{2 \left(\frac{\omega C_0}{2} \right) \frac{R_s}{2}} = \frac{2}{\omega C_0 R_s} = 2Q_u \quad (5.5)$$

This is exactly double the Q_u value when compared with a single varactor. The series resistance is dependant on the biasing voltage as well, as shown in section 4.4.1. A better Q_u factor will be obtained for larger biasing voltages, where the junction capacitance is small.

The best way to use varactors for minimum loss is to add a few in parallel and operate them close to their minimum capacitance where the series resistance is lowest.

5.3 Designing bandwidth and order for cut-off specification

The order together with the bandwidth of a filter influence the cut-off rate of the filter, illustrated in figure 5.5. The specification gives a fair amount of freedom in the choice of bandwidth, but the cut-off requirement is very strict. An analysis was done to discover what bandwidth-order combinations will be able to meet the specifications. Equation (5.1) was used while tuning the bandwidth to ensure the cut-off rate is met. The maximum bandwidth for a given order to meet the cut-off requirement is shown in figure 5.7.

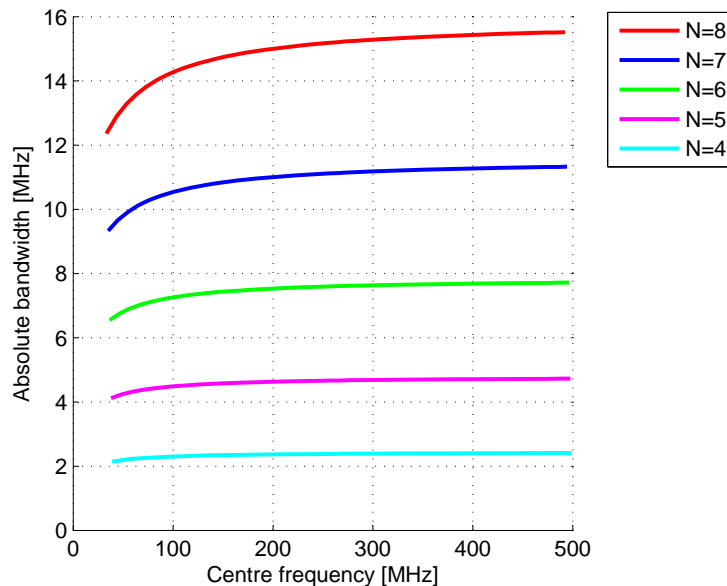


Figure 5.7: Maximum absolute bandwidth to meet specifications

The result shows that only a eighth order filter will come close to utilising the the maximum 20MHz bandwidth.

The insertion loss and cut-off specification (section 1.3) are not realisable at the same time. Figure 5.8 shows the required resonator Q needed to guarantee less than 3dB of attenuation in the passband.

This analysis was done for Chebyshev bandpass filters with return loss of 15dB and using the maximum bandwidth as shown in figure 5.7. Considering that the best inductors have $Q_u = 150$ and the best coaxial resonators have $Q_u = 550$ it can be seen that this specification is unrealistic in view of current technology.

5.4 Low side filter

The main purpose of this filter is to experiment with varactor diodes, and asses their tunability and losses. Meeting the 3dB insertion loss specification was a priority. Investigating if 80dB of attenuation is possible with the given components was also important.

This filter makes use of the inductor-capacitor pi-network and inductor-capacitor (LC) resonators, as discussed in section 3.3.2. The constant coupling factor achieved by this combination is used to implement a fourth order Chebyshev filter with constant relative bandwidth.

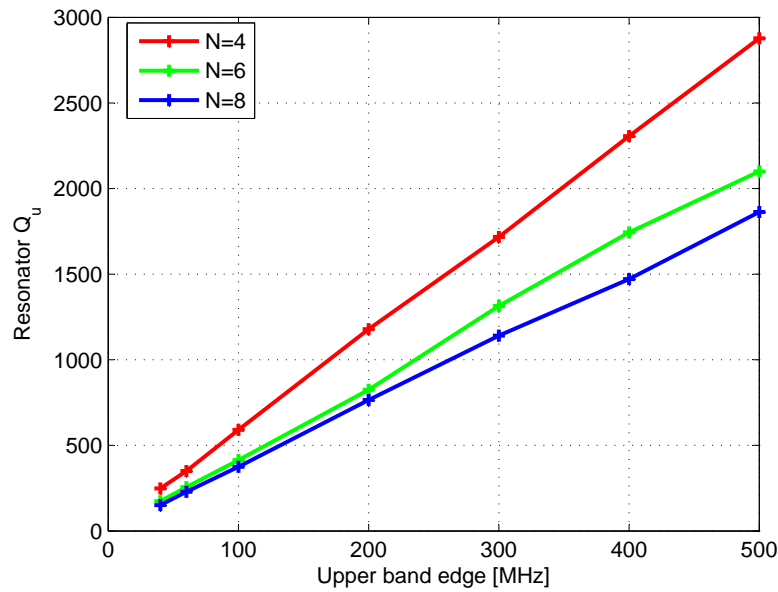


Figure 5.8: Required unloaded resonator Q to meet insertion loss specification when using the maximum bandwidth

5.4.1 Filter design procedure

The design procedure and equations for the design of this filter is outlined, as will be used in the following section for an specific design.

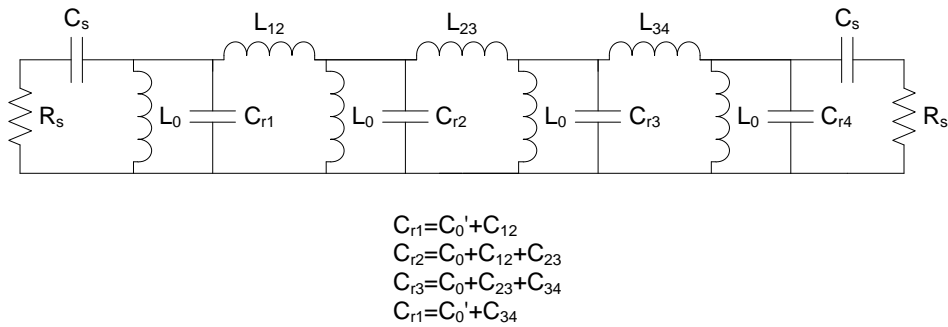


Figure 5.9: Fourth order filter prototype with inductor-capacitor pi-network inverters and LC resonators

The filter specification contains the following

- ω_0 - the centre frequency
- $\frac{\Delta\omega}{\omega_0}$ - the fractional bandwidth

Choose a lowpass prototype of order n and obtain the element values $g_0, g_1, \dots, g_n, g_{n+1}$. Use the formula for the inter-resonator coupling coefficient, equation (2.37), as restated here:

$$k_{j,j+1} = \frac{\frac{\Delta\omega}{\omega_0}}{\sqrt{g_j g_{j+1}}} \tag{5.6}$$

Resonator

Choose a resonator inductor, L_0 , with maximum unloaded Q , and compute the required resonator capacitor value:

$$C_0 = \frac{1}{\omega_0^2 L_0} \quad (5.7)$$

Inter-resonator coupling

According to equation (3.24), the coupling coefficient for this combination is

$$k = \frac{J}{b} = \frac{L_0}{L_s} \quad (5.8)$$

The values of the coupling inductors can now be computed as

$$L_{j,j+1} = \frac{L_0}{k_{j,j+1}} \quad (5.9)$$

The parallel capacitors that complete the inverter can also be computed by solving (3.18) and (3.19) as

$$C_{j,j+1} = \frac{1}{\omega_0 L_{j,j+1}} \quad (5.10)$$

Input/output coupling

To match the filter to external loads we need (from section 3.4)

$$Q_e = \frac{R_n}{\omega_0 L_0} \quad (5.11)$$

where

$$R_n = \frac{R_s^2 + X_s^2}{R_s} \quad (5.12)$$

Choose a capacitor as input and output coupling element, so that

$$X_s = \frac{-1}{\omega C_s} \quad (5.13)$$

Solve equations (5.11), (5.12) and (5.13) for C_s to give

$$C_s = \frac{1}{\omega_0 \sqrt{\omega_0 R_s L_0 Q_e - R_s^2}} \quad (5.14)$$

To ensure that the resonant frequency of the adjacent resonator is not shifted the following condition also has to hold (also from section 3.4):

$$-jB_n + j\omega_0 C_0' = j\omega_0 C_0 \quad (5.15)$$

with

$$B_n = \frac{X_s}{X_s^2 + R_s^2} \quad (5.16)$$

Combining equations (5.15) and (5.16) above and solving for C_0' gives

$$C_0' = \frac{\sqrt{\omega_0 R_s L_0 Q_e - R_s^2} + R_s Q_e}{\omega_0^2 R_s L_0 Q_e} \quad (5.17)$$

The square root in equations (5.14) and (5.17) puts a theoretical limit on the minimum frequency of operation

$$\omega_0 > \frac{R_s}{L_0 Q_e} \quad (5.18)$$

This limits the designer on the minimum size of L_0 that can be used.

These steps not only show the design procedure, but also state equations for the tuning curves of the capacitors. All the capacitors in this filter have to be tuned to ensure proper filter working.

5.4.2 Implementing the design

The following values were chosen to minimise the passband insertion loss

- $\frac{\Delta\omega}{\omega_0} = 0.27$
- $L_0 = 100\text{nH}$
- Fourth order Chebyshev with $RL = 20\text{dB}$

The resonator inductor was chosen as large as possible to minimise the size of the resonator capacitors, as varactors with large capacitance values are hard to find. The ceiling of the inductor value was determined by the size of the coupling inductors, $L_{j,j+1}$, which are larger than L_0 by a factor of $\frac{1}{k_{j,j+1}}$. These coupling inductors have to be tunable to fine tune the inter-resonator coupling, the largest tunable inductors were selected.

The fractional bandwidth was chosen as large as possible to minimise the difference between L_0 and $L_{j,j+1}$, as larger bandwidth means large coupling values, and smaller difference between difference between L_0 and $L_{j,j+1}$. The ceiling of this was set by the maximum bandwidth according to the project specification. At a fractional bandwidth of 27%, the bandwidth limit of 20MHz will be reached at a centre frequency of $\frac{20}{0.27} = 74.07\text{MHz}$. Making the bandwidth too large also degrades the filter response, as CR theory is a narrow band approximation and is not suited to wide band filter design.

Using the design procedure in section 5.4.1 and the specific values chosen above, the following component values are obtained:

Table 5.1: Summary of inductor values

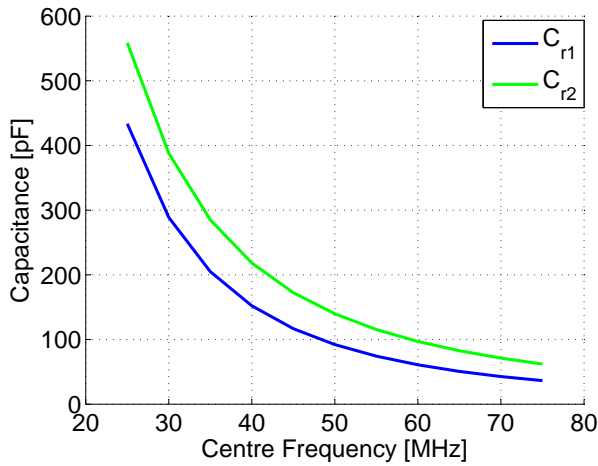
Inductor	value [nH]
L_0	100
L_{12}, L_{34}	523
L_{23}	622

The largest difference in capacitance will limit the tuning range of the filter. Adding capacitors in parallel only enlarges the minimum and maximum attainable values, but does not increase the tuning range. This tuning range is determined by the specific varactor diode.

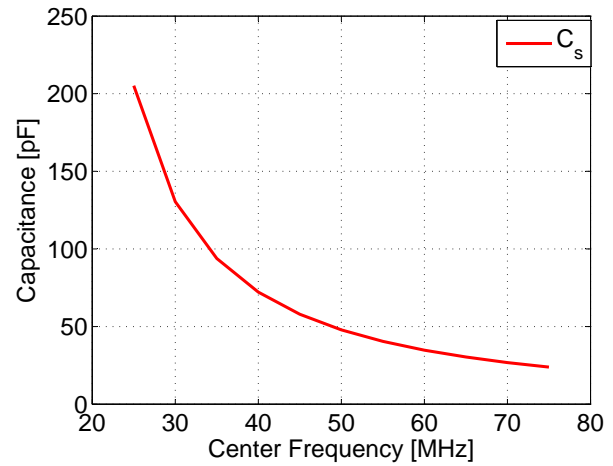
The capacitor tuning curves are shown in figure 5.10. These curves show that large changes in capacitance are needed to tune the filter from 25MHz to 30MHz, but small changes are needed to tune the filter from 70MHz to 75MHz.

Table 5.2: Summary of capacitor values at different tuning points

Capacitor	value [pF]		C_{max}/C_{min}
	$f_0 = 23\text{MHz}$	$f_0 = 74\text{MHz}$	
C_s	156	21	7.4
C_{r1}, C_{r4}	502	44	11.8
C_{r2}, C_{r3}	647	70	9.2



(a) Resonator capacitors



(b) Input and output coupling capacitors

Figure 5.10: Capacitor tuning curves

Biasing the varactors in a RF circuit

The varactor diodes in the circuit needs to be biased with a Direct Current (DC) voltage, without interfering with the Radio Frequency (RF) signal. One of the terminals of the varactor should be kept at a constant DC voltage and the voltage at the other terminal can be adjusted to change the voltage over the diode and hence change the capacitance. The easiest way to do this is to ground the anode and apply the biasing voltage to the cathode. A large DC blocking capacitor can be used to isolate the RF and DC signals.

This is easily done in the case of the resonators, as the resonator capacitor must be grounded, see figure 5.11a. For the input and output coupling capacitors, C_s , the anode can be connected to DC ground through the resonator inductor, see figure 5.11b.

For this filter the DC blocking capacitor, C_{DC} , is chosen to be 100nF, which is more than a hundred times bigger than the largest varactor capacitance, and it acts like a RF short circuit. Surface mount device (SMD) capacitors have self resonant frequency (SRF) far above this frequency band, and normal SMD capacitors can be used. The RF blocking resistors are chosen sufficiently large so that none of the RF power flows to ground via the DC path. This minimum value was determined by simulation in AWR® Microwave Office® (MWO) and found to be 100k Ω .

The NXP (Philips) BB201 varactor, a package with two diodes in common cathode configuration, was selected for this filter. It has low series resistance, typical value of 0.25 Ω at $f = 100\text{MHz}$ and $V_r = 3\text{V}$. The measured and data sheet voltage-capacitance curves for a single diode of a BB201 is shown in figure 5.12.

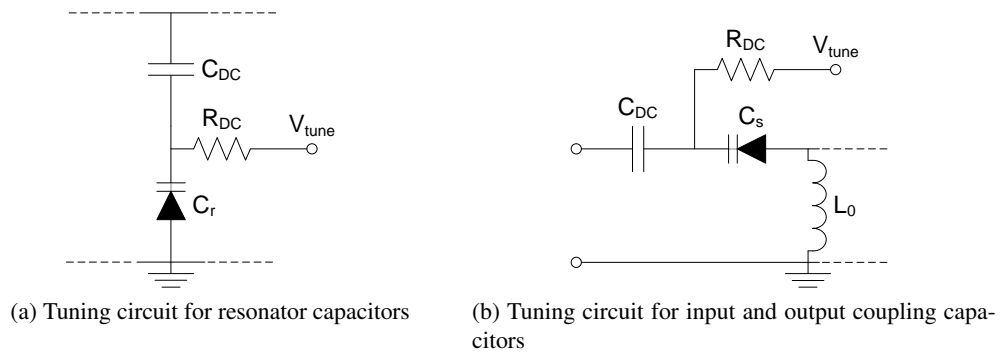


Figure 5.11: Varactor biasing circuits

The data was obtained by measuring s_{11} of the circuit shown in figure 5.11a. The maximum reverse voltage that was used, is the maximum reverse bias voltage specified in the data sheet, 15V. The maximum measured capacitance was $C_{max} = 111$ pF and the minimum was $C_{min} = 16.75$ pF. This translates to a usable tuning range of $C_{max}/C_{min} = 6.63$.

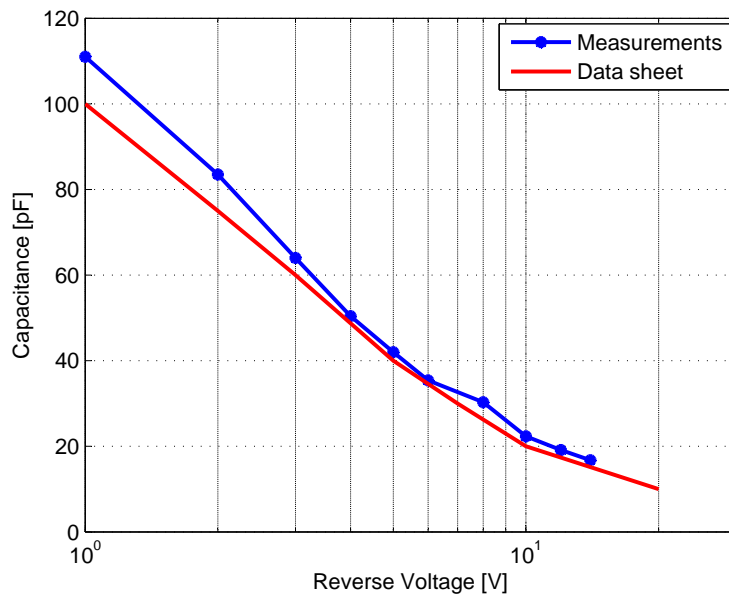


Figure 5.12: Measured and data sheet capacitance of BB201 varactor

This filter aims to tune from the lower band edge (20MHz) to as high as the varactor diodes allow. Analysing the capacitance curves in figure 5.10, it can be seen that one double package is required for C_s , two packages for C_{r1} and C_{r4} , and three packages for C_{r2} and C_{r3} . The second conclusion drawn from this analysis of these two graphs is that the filter will only be able to tune to about 55MHz or 60MHz, as limited by the varactor tuning range.

5.4.3 PCB design

The primary concern in the design of the printed circuit board (PCB) layout was to ensure that the magnetic fields of the inductors do not couple with each other and decrease the attenuation in the stopband. They were spaced relatively far apart and adjacent inductors were rotated 90° with regard to one another. Initial measurements did not correspond well to simulated results, as the problem was proven to be extra inductance in the grounding path of the varactors. Adding vias close to the the varactors solved the problem. The filter response before and after vias were added in shown in figure 5.13. A photo of the filter is shown in figure 5.14.

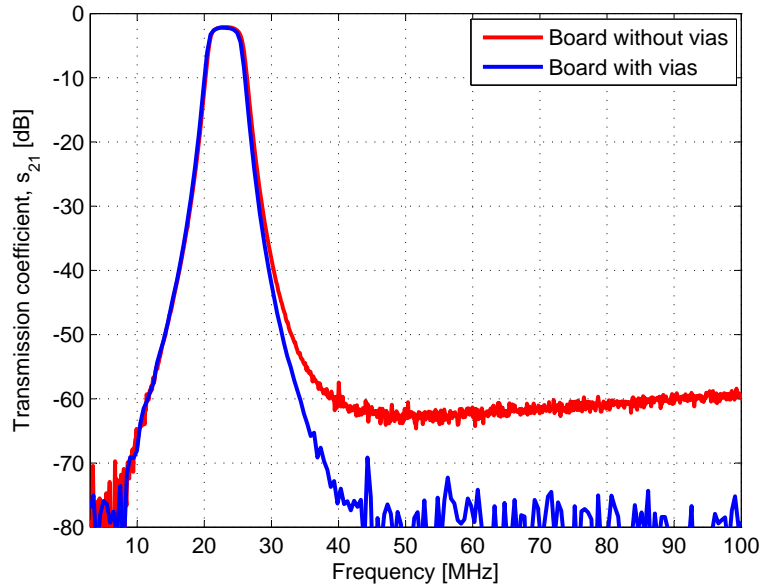


Figure 5.13: Improvement of filter response after adding vias in ground plane

5.4.4 Simulations and Measurements

The filter was simulated with MWO and included the resonator inductor losses by using s -parameters from the manufacturer. The varactor loss was modelled by adding a series resistor to a lossless capacitor. The MWO circuit is shown in figure 5.15.

The measurements were done on a Rhode and Schwarz ZVB vector network analyser. DC biasing networks consisted of resistor voltage dividers.

The simulated and measured results are shown in figure 5.16, and show good correlation up to the 80dB noise floor of the network analyser. The simulation predicts slightly more loss in the passband, but the simulation is not very accurate in this regard because the varactor loss is only specified at one bias-frequency point. The difference in the reflection coefficient is due to different tuning or optimising done by MWO, in the case of the simulation, and manual tuning in the case of the measurement.

The filter is able to tune from 23MHz continuously to 54MHz, which is slightly more than an octave (2:1). The passband edges are taken where the return loss is less than 20dB.

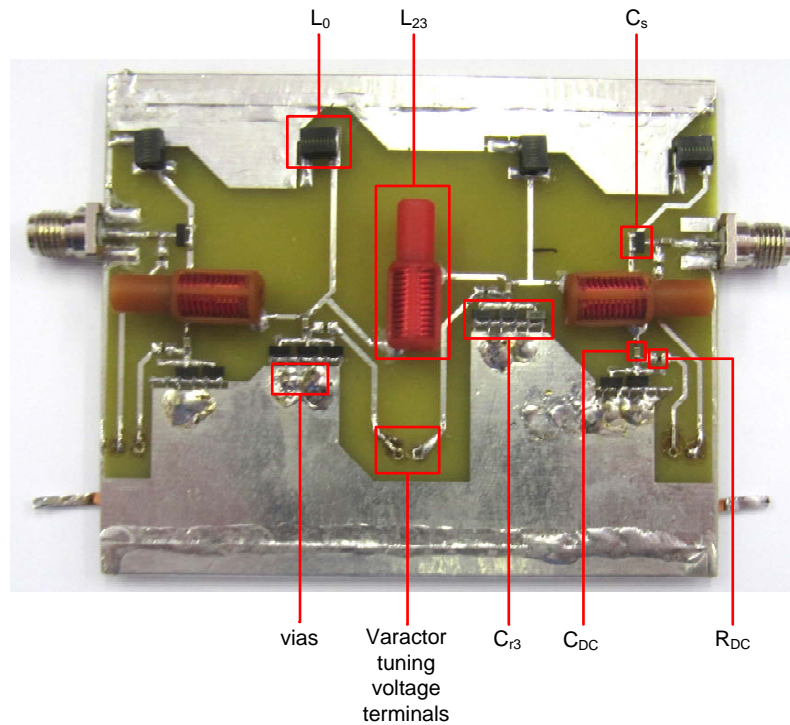


Figure 5.14: Photo of the filter, scale 1:1

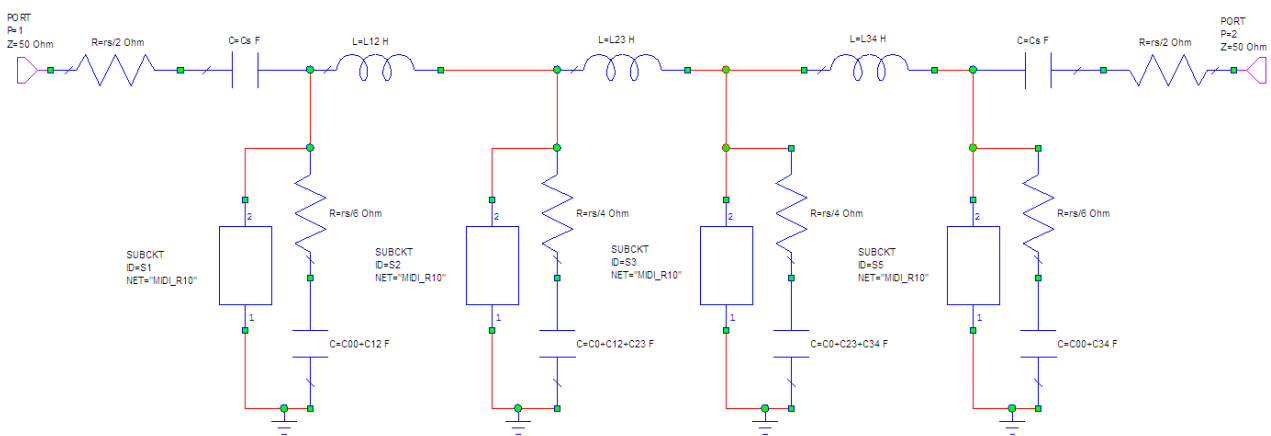


Figure 5.15: MWO circuit simulation

The losses in the passband are relatively low. The insertion loss specification (see section 1.3) of less than 3dB is met from 39MHz to the 54MHz limit. The cut-off specification is not met and the cut-off rate decreases as the centre frequency and bandwidth increases.

An important result is the symmetry achieved about the centre frequency, which is not the case for an ideal bandpass filter. Paying attention to the stopband edges, it can be seen that the upper and lower stopband have very similar attenuation. This is a direct consequence of the lowpass characteristic of the inductor-capacitor inverter, see section 3.2.3 and figure 3.6.

A filter that is not able to tune can use SMD capacitors instead of varactors, which will decrease the loss in the passband. Low equivalent series resistance (ESR) capacitors were found with (see appendix B.2.2),

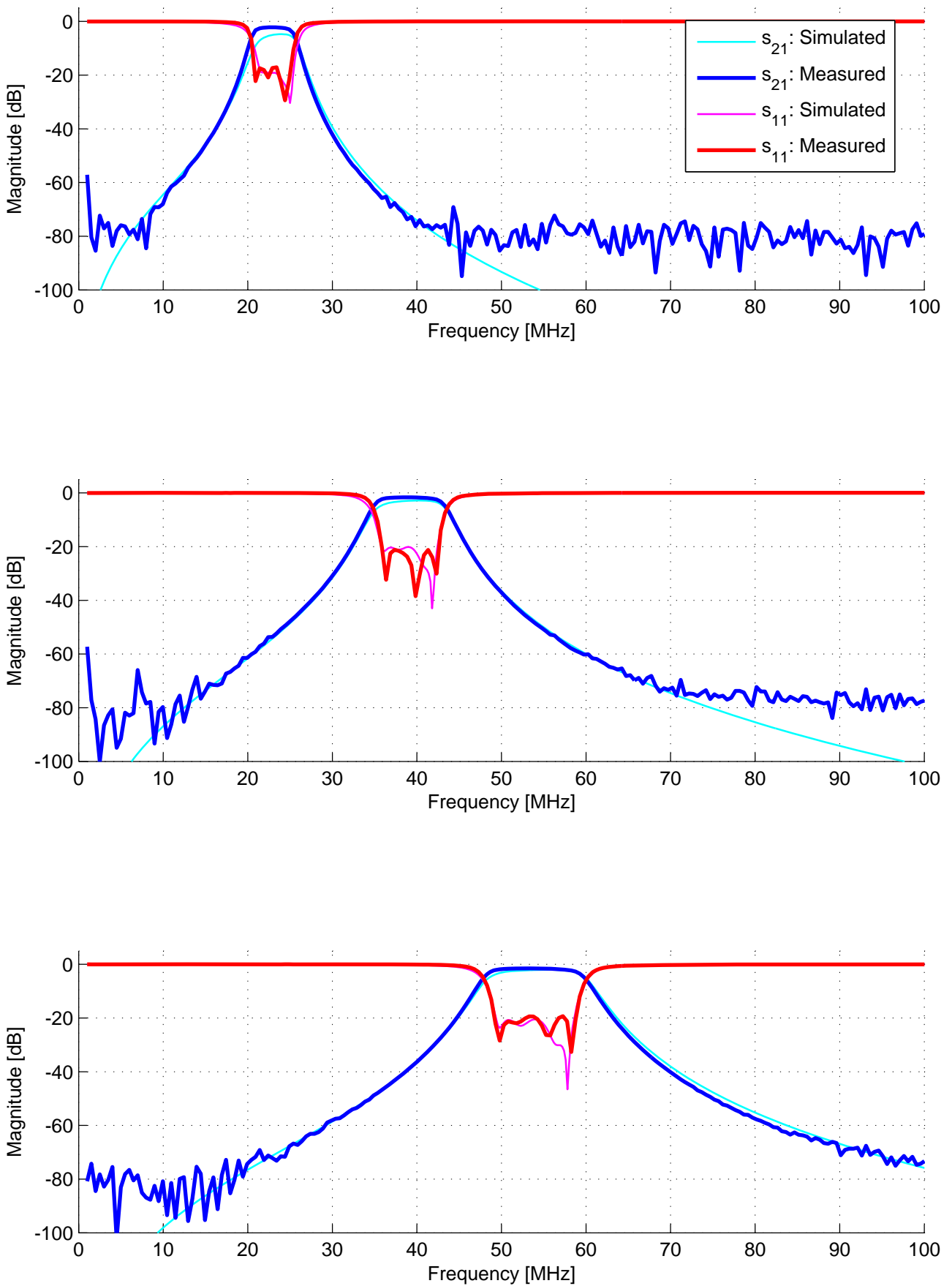


Figure 5.16: Measurements and simulated results for filter tuned to $f_0 = 23\text{MHz}$, $f_0 = 39\text{MHz}$ and $f_0 = 54\text{MHz}$

Table 5.3: Summary of insertion loss values at different tuning points

f_0 [MHz]	Δf [MHz]	Insertion loss [dB]				
		f_0	f_{p1}	f_{p2}	$f_{p1} - 10\text{MHz}$	$f_{p2} + 10\text{MHz}$
23	4.12	2.22	3.63	3.17	62.0	62.7
39	6.97	1.64	2.34	2.92	45.4	45.2
54	9.62	1.55	2.24	2.76	38.6	37.4

$C = 300\text{pF}$, $ESR = 0.04\Omega$, which can be substituted into (4.1) to give

$$Q_c = \frac{1}{2\pi(20 \times 10^6)(300 \times 10^{-12})(0.04)} = 663 \quad (5.19)$$

at 20MHz. Analogously the Q_u factor of the varactor can be computed as

$$Q_{\text{diode}} = \frac{1}{2\pi(20 \times 10^6)(100 \times 10^{-12})(0.25)} = 318 \quad (5.20)$$

also at 20MHz. This SMD capacitor will perform much better than the varactor. However, the component limiting the Q_u of the resonator is the inductor. The inductor has $Q_u = 60$ at 20MHz which put the total resonator Q_u at

$$Q_{\text{res}_c} = \left(\frac{1}{60} + \frac{1}{663} \right)^{-1} = 55 \quad (5.21)$$

$$Q_{\text{res}_v} = \left(\frac{1}{60} + \frac{1}{318} \right)^{-1} = 50 \quad (5.22)$$

This difference in Q_u values at 20MHz correspond to a 0.16dB difference in passband loss at the centre frequency. And at 50MHz the difference is slightly larger, 0.2dB. A big improvement in resonator capacitor Q_u has a very small impact on the resonator Q_u because of the bad inductor Q_u . A continuously tuned filter using varactor diodes is therefore a good choice when compared to using discrete tuning or switching between fixed filters for this band.

5.5 High side filter

This filter showcases the best available technologies to achieve 80dB of attenuation 10MHz from the passband edge at the high-end of the 20-500MHz band. An eighth order Chebyshev filter is the best choice when designing for minimum insertion loss, as argued in section 5.3 (see figure 5.17), but a sixth order filter was chosen to reduce tuning complexity. Figure 5.17 shows filters of different orders with identical resonators designed achieve 80dB of attenuation 10MHz from the upper passband edge (500MHz).

5.5.1 Filter design procedure

A sixth order Chebyshev prototype is used with quarter wavelength transmission lines loaded with varactor diodes as resonators. The prototype is designed for 10dB return loss to maximise the cut-off rate. Component values are obtained by applying the CR bandpass design equations as stated in section 2.5.

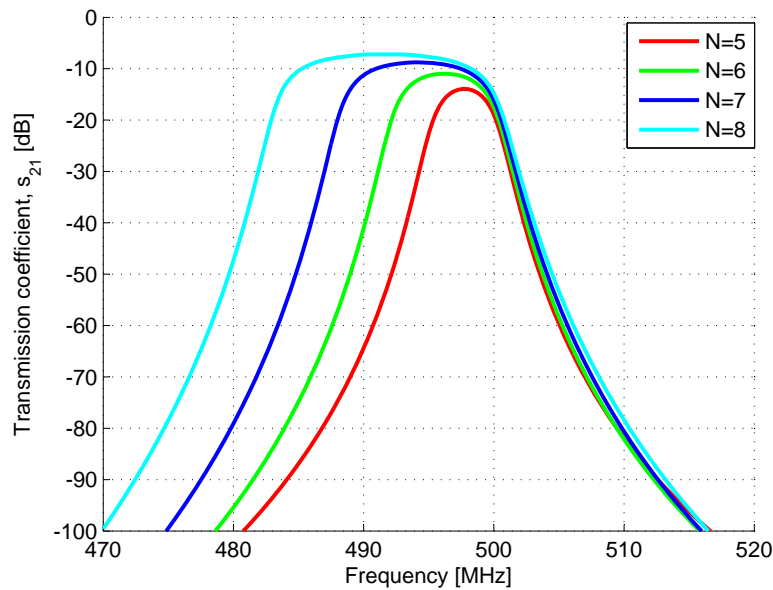


Figure 5.17: Effect of different filter order on passband insertion loss

The maximum bandwidth was selected, while still meeting the cut-off specifications. This translates to a fractional bandwidth in the order of 1.6%, which is very narrow. The main practical complication is that the coupling between resonators needs to be very weak. Consequently very small capacitors or very large inductors are needed. Inductors would have to be in the order of a couple of mH and capacitors have to be in the order of tenths of a pF. Inductors this large are not practical at 500MHz, so capacitive coupling was selected.

Inter-resonator coupling

The sub pF capacitance values required for inter-resonator coupling is below the range of single varactor diodes, as their minimum capacitance is in the order of a couple of pF. A series combination could work, but more than two diodes would be required for a single coupler. SMD capacitors that have such low values do exist and are a viable option. Ultimately, microstrip interdigital capacitors were chosen because of the ability to design for a wide range of capacitor values.

Using fixed capacitors means the bandwidth and the filter response will change as the filter is tuned. Considering that the coupling is capacitive, $J = \omega C$, the bandwidth will increase as the filter is tuned higher, and consequently decrease the cut-off rate. The filter will have the slowest cut-off rate at the highest tuned frequency, and therefore the filter is designed at the highest frequency to ensure that the cut-off specification is met.

Resonators

Shorter transmission lines will provide more tuning with the same change in capacitance, but requires larger capacitances, as explained in section 3.1.2. Varactors with large capacitance values that work at 500MHz are not readily available and a compromise was made by using physically shorter lines.

The ceramic coaxial resonators that are discussed in section 4.2, are used in this filter for their high Q -value. Specifically, the HP series with 9000 ($\epsilon_r = 90$) material is used, which can be cut to have quarter wavelength

resonance at 400MHz to 600MHz (see appendix B.1.1). The shortest line ($f_0 = 600\text{MHz}$) was chosen so that small varactor diodes may be used.

NXP BB179 varactor diodes were used because they are readily available and have low series resistance, in the order of 0.6Ω , see appendix B.3.1. Also, the series resistance is specified at 470MHz, which is convenient for predicting the insertion loss. M/A-Com diodes (MA4ST1300 series) were also considered, and found to be only slightly better with series resistance in order of 0.4Ω (see figure 4.7), but were not implemented because the large cost difference did not outweigh the slight improvement in series resistance.

Varactor biasing was done with a circuit similar to the one used in the low-side filter, see figure 5.11a. The difficulty at the high end of the band is in finding large DC blocking capacitors that resonate above 500MHz. The largest available RF capacitors (130pF) that were found resonate close to 1GHz (data in appendix B.2.2), and two were used in parallel to provide a good short circuit to the RF signal. The MWO simulation circuit of the resonator is shown in figure 5.18.

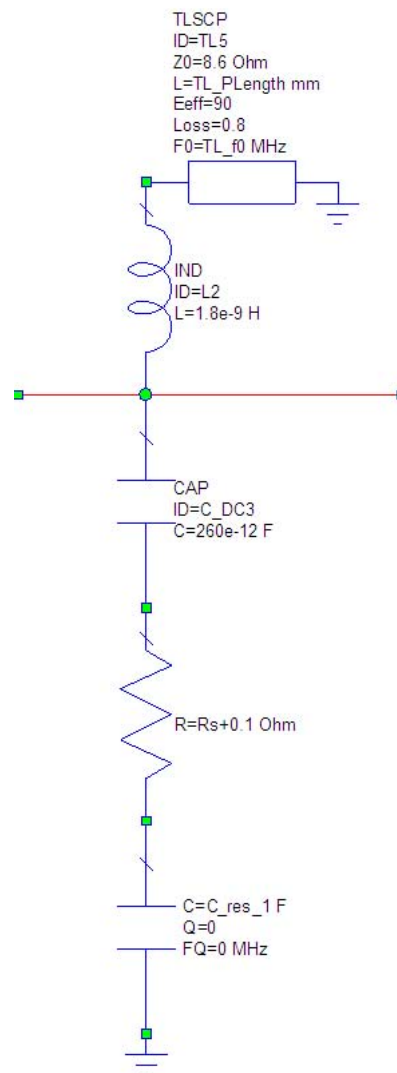


Figure 5.18: Single resonator as simulated in MWO

The required capacitance curves for the resonator capacitors as predicted by simulation is shown in figure 5.19.

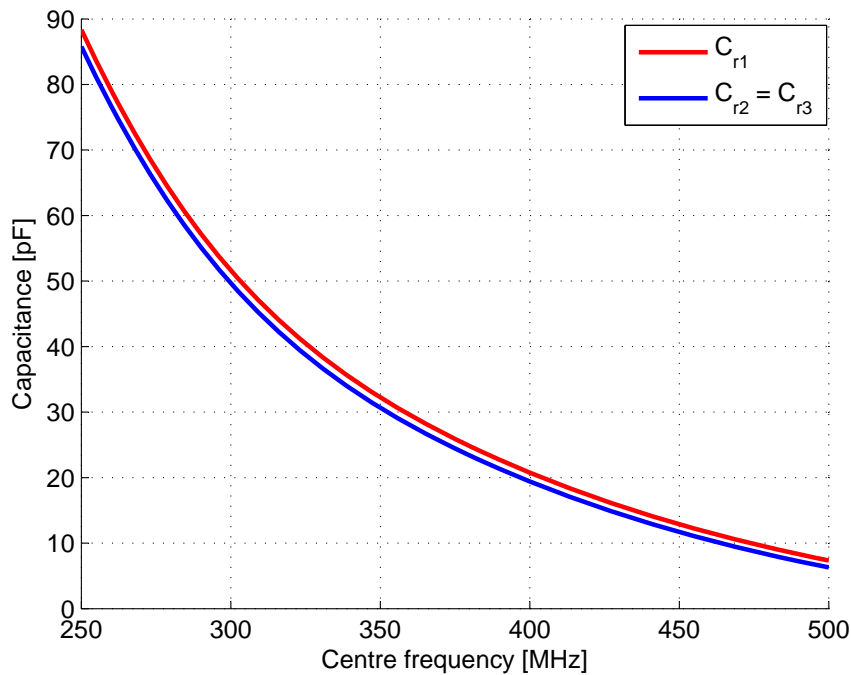


Figure 5.19: Resonator capacitor tuning curves

5.5.2 Implementation of inter-resonator coupling

Interdigital microstrip capacitors were designed for the inter-resonator couplings with the aid of the design equations as published by Alley [28]. The design values are shown in table 5.4. The ‘length’ and ‘gap’-parameters are shown in figure 5.20. These values were obtained with approximate equations fitted onto the data provided by Alley [29]. All the gaps and finger widths are 0.38mm, as this clearance can be etched quite accurately. The input/output capacitors are large enough to be implemented with SMD capacitors, as seen in table 5.4, and will require a physically large interdigital capacitor.

Table 5.4: Summary of coupling capacitors and their interdigital capacitor design values

	Capacitance [pF]	N	length
$C_{01} = C_{67}$	1.422	16	7.54
$C_{12} = C_{56}$	0.347	8	3.88
$C_{23} = C_{45}$	0.281	8	3.14
C_{34}	0.274	8	3.06

Electromagnetic (EM) simulations were done in AWR AXIEM to verify the designs. The EM model of an AXIEM simulation is shown in figure 5.20.

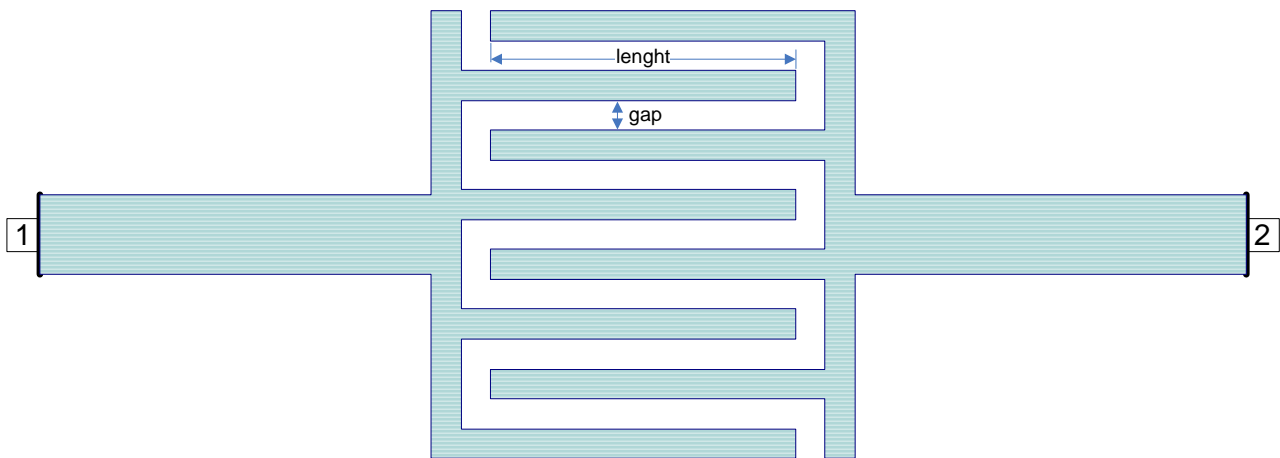


Figure 5.20: EM simulation of interdigital capacitor

The equivalent circuit model for an interdigital capacitor is a capacitor pi-network. The series capacitance (between ports one and two in figure 5.20) is the designed value. Capacitance to ground is also present, but can be tolerated by adjusting the resonator capacitors. Acceptable correlation was found between the design values and simulated results, as seen in the comparison in table 5.5.

Table 5.5: Capacitance values [pF] of interdigital capacitors according to design equations and simulations

	Design	AXIEM	error %	MWO MICAP	error %
C_{12}	0.347	0.423	22	0.492	42
C_{23}	0.281	0.356	27	0.412	47
C_{34}	0.274	0.348	27	0.404	48

The PCB was fabricated with the designed values, with a slightly wider bandwidth measured than was simulated. A photo of the filter is shown in figure 5.21.

5.5.3 Simulations and Measurements

Initial measurements showed that the filter was not functioning as expected. The bandwidth was more than twice the designed value, the passband had pronounced ripples and the lower cut-off rate was much too gradual. The more gradual cut-off at the lower band-edge bears some resemblance to the effect caused by an inductor-pi inverter in figure 3.6, pointing to inductive coupling. As the filter was designed for purely capacitive coupling, adding inductive coupling will degrade the response. Tin plates were fashioned around the resonators to shield them from each other and reduce the unwanted magnetic coupling. This proved to be quite successful, but was not able to completely inhibit all magnetic coupling. The results of the shielding is shown in figure 5.22.

Uncertainty exists regarding the losses of the resonator. The ceramic transmission lines are simply modelled as a physical line with an attenuation constant, and was only measured at its resonant frequency of 600MHz. The series resistance of the varactor is only specified at one frequency-bias point and is known to vary with biasing voltage, but may also vary with frequency. Accurately measuring the series resistance of the varactor

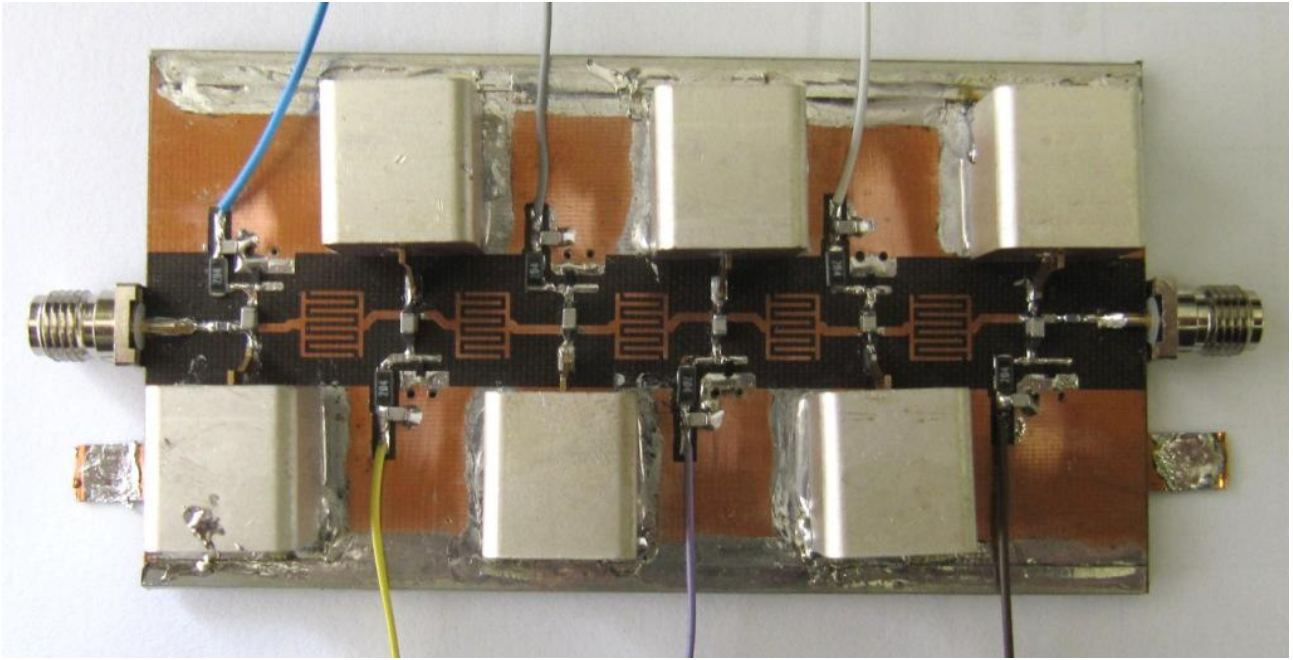


Figure 5.21: Photo of high side filter

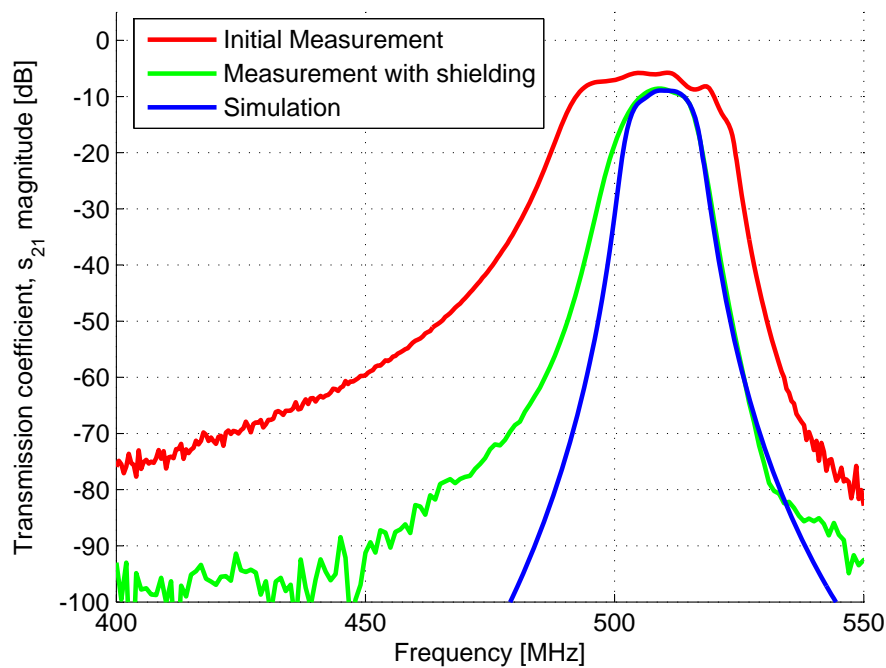


Figure 5.22: Filter response before and after the resonators were shielded from each other

diode is also difficult as it is so small compared to the other impedances in the circuit. The simulation was modified to adjust the series resistance of the varactor to fit the measured results. To match the measurements this resistance was scaled from $R_s = 0.75$ at $f_0 = 498\text{MHz}$ to $R_s = 0.4$ at $f_0 = 400\text{MHz}$. The measured and simulated results are shown in figure 5.23.

Unwanted magnetic coupling still exists between resonators, as can be seen from the more gradual cut-off rate at the lower band-edge. Room for improvement exists by improving the shielding between resonators. The

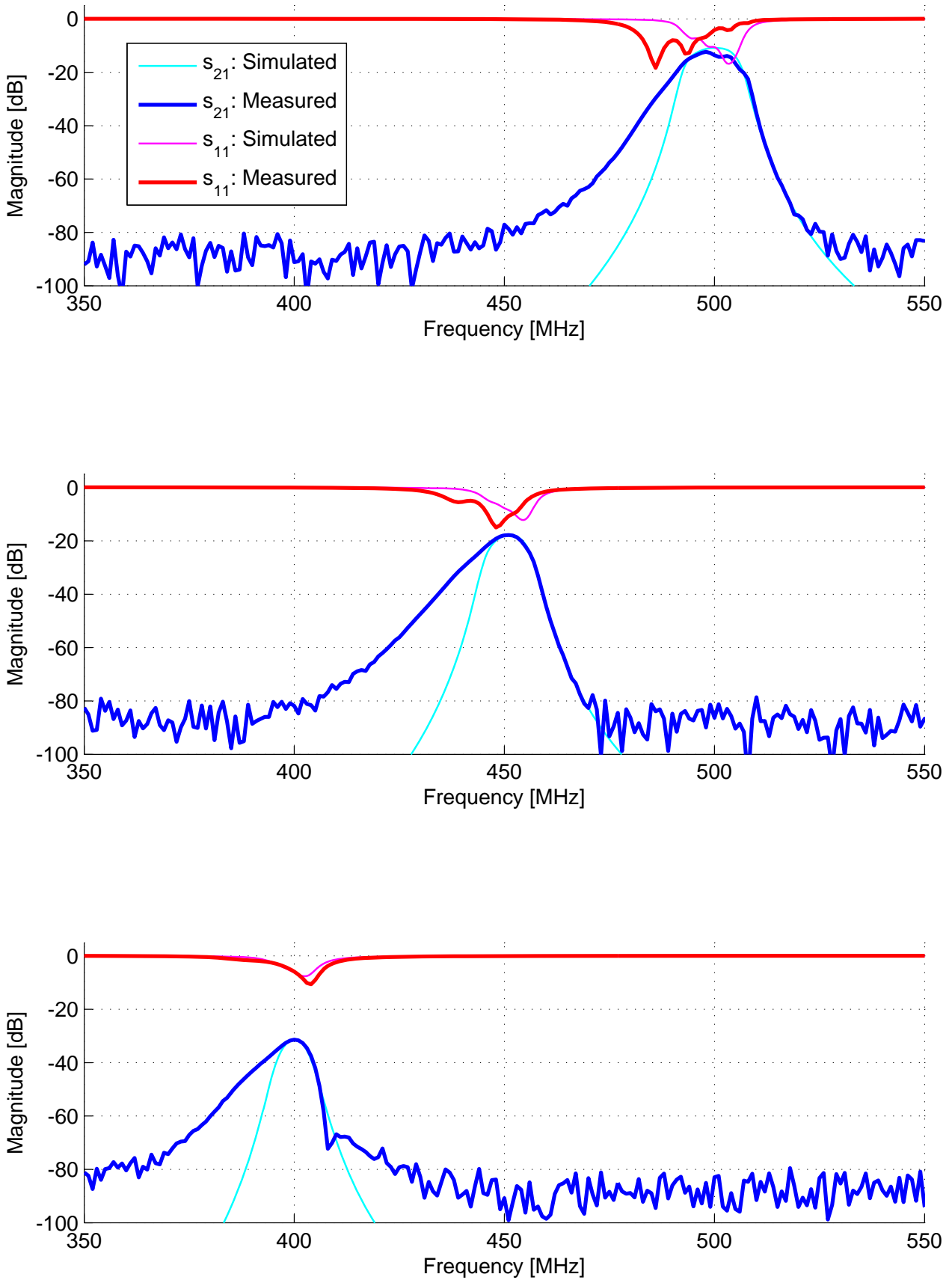


Figure 5.23: Simulated and measured results when filter is tuned to $f_0 = 498$ MHz, $f_0 = 450$ MHz and $f_0 = 400$ MHz

problem with increasing the shielding too much is that the interdigital capacitors may inadvertently be shielded as well, which will also degrade the filter response.

Measurements also revealed that the MWO simulation with MICAP model approximated the built filter the best. The capacitance of the interdigital capacitors were more than AXIEM simulation predictions. Consequently the fractional bandwidth was measured to be approximately 2.7% compared with 1.6%, as in the original design.

The measurements are only shown where the filter is tuned from 400-500MHz. In fact, the varactors are able to tune the filter down to 250MHz, achieving an octave tuning range. At this frequency the insertion loss in the passband is 65dB, 15dB above the noise floor, and the filter functions as an attenuator.

A filter using fixed capacitors in the resonator circuit instead of tunable elements will perform much better, as seen in table 5.6. The simulation assumes capacitors with ESR of 0.1Ω and also uses the ceramic transmission lines. This is not a viable option, as the ceramic lines are expensive, and if the bandwidth of the filter is less than 10MHz, more than ten filters are needed to cover the 400-500MHz band.

Table 5.6: Comparison of tunable and non-tunable filters in terms of their insertion loss

f_0 [MHz]	Insertion loss at f_0 [dB]	
	Simulated fixed filter	Measurement of tunable filter
400	12.9	31.4
450	7.1	17.8
500	4.2	12.4

5.6 Conclusion

The filter at the lower band-edge was quite successful in terms of insertion loss and tuning range. It was not able to meet the cut-off specification. This filter shows what can be achieved if the insertion loss specification is regarded as a higher priority than the cut-off specification. Almost no improvement is visible when compared to a similar filter with fixed resonators.

The high side filter proved to be less successful in achieving its goal cut-off specification goal. Improvement to this design using current varactor diode technology will be to use varactor as inter-resonator coupling. Alternatively, digitally tunable capacitors, as currently under development by Peregrine, will solve some of the problems encountered with inter-resonator coupling in this project. These capacitors have very small capacitance and will consequently enable construction of narrow band tunable filters. They can also be easily controlled by digital logic.

Tunable inter-resonator capacitors will significantly complicate tuning, but will enable the filter to keep the bandwidth constant when tuning the filter down, instead of decreasing it, as is the case with the built filter. In addition to the decreased losses from optimal bandwidth, good filter response can also be maintained when the inter-resonator coupling is tuned.

Another improvement of the built design is to increase the order of the filter to eight. The optimal bandwidth for an eight order filter is much more than a sixth order, and the insertion loss in the passband will decrease as shown in figure 5.17. This change has to be weighed against an increase in complexity as well.

The suggested improvements for this filter will increase the filter complexity. If this is not desired, relaxing the specifications should seriously be considered. The fact is that the current available components have too much inherent losses and are not able to perform to such high standards as set by the specifications.

Chapter 6

Conclusions and recommendations

A Software Defined Radio (SDR) system using a bank of tunable bandpass filters as Radio Frequency (RF) front-end is a worthy competitor to traditional superheterodyne receivers.

The inductor-capacitor pi-network inverter was shown to enable the design of a constant relative bandwidth filter. The cut-off rate at the lower band-edge decreased, as the cut-off rate at the higher edge increased, shifting the passband response to be symmetrical about f_0 . This behaviour caused by the inductive coupling implies that a filter of lower order is necessary, as the cut-off rate at the higher band-edge is faster when compared to an ideal Chebyshev prototype.

In the case of the high-end filter, minimal degradation of the filter response was shown when tuning only the resonators, and leaving the inter-resonator coupling constant. This filter also stressed the difficulty in designing for the project specifications with the available components.

The 3dB insertion loss specification cannot be met with current technology. The required resonator Q_u -factors are shown in figure 5.8. The best inductors have $Q_u = 150$ and the ceramic coaxial lines that were used in the high-end filter have $Q_u = 550$ at 500MHz. These values are much less than Q_u -factors in the order of thousands needed to meet the specifications.

Future developments of micro electromechanical systems (MEMS) promise better Q_u factors. Currently, the major drawbacks of these systems are their cost and reliability. Digitally tuned capacitors will work well as inter-resonator coupling in the narrow band high side filter, but these are still under development and not readily available.

Problems encountered during implementation proved that achieving 80dB of attenuation is difficult. Small amounts of signal power can couple through Direct Current (DC) biasing networks if these are not sufficiently isolated. Careful attention to printed circuit board (PCB) layout is required to ensure no unwanted coupling occurs. Experimentation with shielding showed that even with meticulous design, some unwanted coupling is still present.

Varactors diodes proved to be good candidates as tuning elements for the filters in this project. Very tight cut-off specifications required a narrow band filter at the high end of the band. In such a narrow band filter the series resistance of the diode causes significant attenuation in the passband. A moderate relaxation in stopband specification will enable much better passband performance, even at narrow bandwidths.

A fact that must also be emphasised is that the varactors used in this project enabled octave tuning. Substantial insertion loss (65dB) was measured with the high-end filter at 250MHz, but the passband was still visible.

If octave tuning can be achieved for all the filters in the bank, then a minimum of five filters will be required to cover the band from 20-500MHz. The tuning ranges for four and five filters covering the 20-500MHz range is shown in table 6.1.

Table 6.1: Minimum required tuning ranges for tunable filters in a filter bank covering the band from 20-500MHz

	Tuning range [MHz]	
	1:1.9	1:2.24
Filter 1	20-38	20-45
Filter 2	38-72	45-100
Filter 3	72-138	100-223
Filter 4	138-263	223-500
Filter 5	263-500	-

These are reachable tuning ranges, particularly considering that the low-end filter was able to tune from 23-54MHz, which is a tuning ratio of 1:2.3. Filters with a tuning range of 1:2.24 or more will be able to cover the whole range with only four filters.

6.1 Recommended filter bank design

The maximum fractional bandwidth is shown in figure 6.1, similar to figure 5.7, where the maximum absolute bandwidth was shown. The fractional bandwidth is directly used in the design equations (section 2.5) and determines if the filter is considered wide or narrow band.

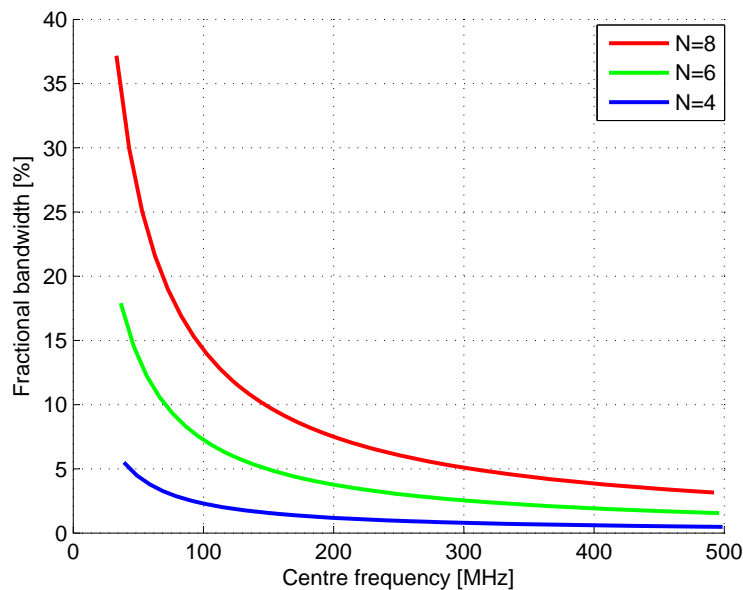


Figure 6.1: Maximum fractional bandwidth for different order Chebyshev filters to meet cut-off specification

Coupled Resonator (CR) designs are not well suited to wideband filters, as the frequency dependence of the inverters degrade the passband performance. Good results are obtained with filters with 10% fractional bandwidth or less [5].

If the filter bank consists of four filters (as shown in table 6.1, column 3), the following remarks apply:

Filter 1 & 2: These filters need to be relatively wide band. Optimise the resonator capacitors to compensate for the frequency variance of the inverters.

Filter 3: Use inductor-capacitor pi-network inverters and add variable capacitive cross coupling to form a cascaded quadruplet (CQ) filter. Such cross coupling is more suited to narrow bandwidths (see figure 6.1).

Filter 4: Transmission lines that have higher Q_u -factor when compared to lumped inductors can be used in this band. Varactors should be used as inter-resonator coupling to keep the bandwidth constant, and minimise losses in this way.

6.2 Future work

A tunable filter bank needs some form of digital control system to tune and select the correct filter. A digital control system was designed for this project and the schematics are shown in appendix D. Such a system will enable measurement of the tuning speed, an important aspect when compared with superheterodyne systems. Implementing automatic fine tuning with a computer aided system can also be investigated.

Comparing varactor tuned filters with superheterodyne receivers in terms of linearity will also prove interesting. The non-linear distortion caused by mixers in the superhet receivers is an important argument in favour of SDR systems. This advantage only holds if the RF front-end of the SDR does not add significant distortion.

Prospects for future work in tunable filters in the 250-500MHz band is promising. The development of MEMS varactors will be a great advancement for tunable filters in this band. Experimenting with these switches and varactors have already seen the development of a number of filters [11], but the technology is still maturing and not in full scale commercial production yet.

Appendix A

Lumped Element Inverter Implementations

Table A.1: Pi-network inverter implementations for use with resonators with parallel type of resonance

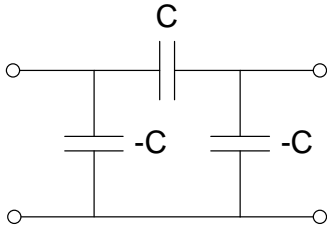
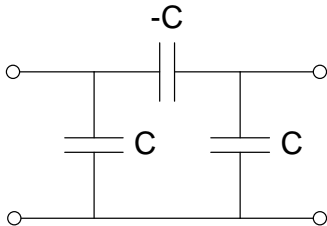
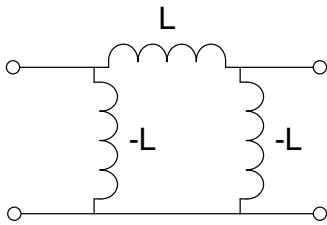
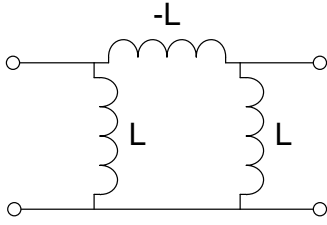
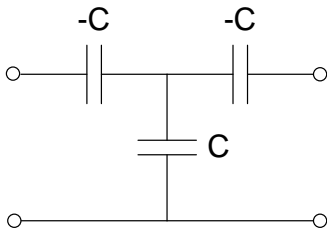
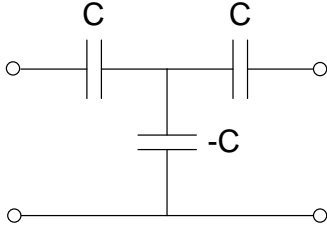
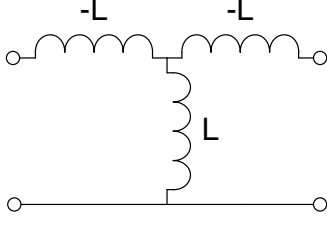
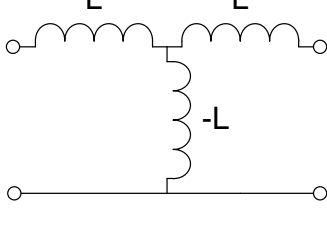
Inverter Circuit	Transmission matrix	K-values	J-values
<p>(a)</p> 	$\begin{bmatrix} 0 & \frac{-j}{\omega C} \\ -j\omega C & 0 \end{bmatrix}$	$K = -\frac{1}{\omega C}$	$J = -\omega C$
<p>(b)</p> 	$\begin{bmatrix} 0 & \frac{j}{\omega C} \\ j\omega C & 0 \end{bmatrix}$	$K = \frac{1}{\omega C}$	$J = \omega C$
<p>(c)</p> 	$\begin{bmatrix} 0 & j\omega L \\ \frac{j}{\omega L} & 0 \end{bmatrix}$	$K = \omega L$	$J = \frac{1}{\omega L}$
<p>(d)</p> 	$\begin{bmatrix} 0 & -j\omega L \\ -\frac{j}{\omega L} & 0 \end{bmatrix}$	$K = -\omega L$	$J = -\frac{1}{\omega L}$

Table A.2: T-network inverter implementations for use with resonators with series type of resonance

Inverter Circuit	Transmission matrix	K-values	J-values
 <p>(a)</p>	$\begin{bmatrix} 0 & \frac{j}{\omega C} \\ j\omega C & 0 \end{bmatrix}$	$K = \frac{1}{\omega C}$	$J = \omega C$
 <p>(b)</p>	$\begin{bmatrix} 0 & -\frac{j}{\omega C} \\ -j\omega C & 0 \end{bmatrix}$	$K = -\frac{1}{\omega C}$	$J = -\omega C$
 <p>(c)</p>	$\begin{bmatrix} 0 & -j\omega L \\ -\frac{j}{\omega L} & 0 \end{bmatrix}$	$K = -\omega L$	$J = -\frac{1}{\omega L}$
 <p>(d)</p>	$\begin{bmatrix} 0 & j\omega L \\ \frac{j}{\omega L} & 0 \end{bmatrix}$	$K = \omega L$	$J = \frac{1}{\omega L}$

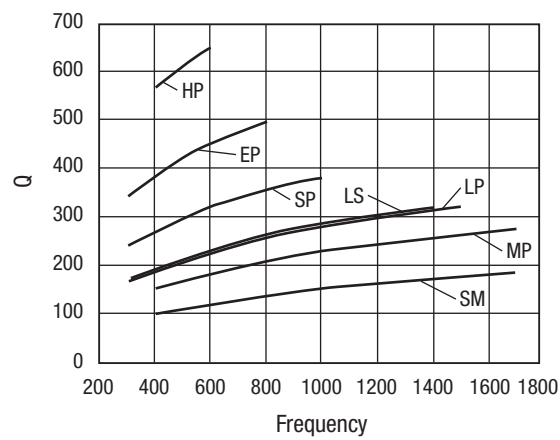
Appendix B

Selected information from datasheets

B.1 Transmission lines

B.1.1 Trans-Tech™ ceramic resonators

9000 Series Q Curves



D9000 Quarter Wave Q Curves

Recommended Frequencies 9000 Series ($\epsilon_R = 90 \pm 3$, $T_F = 0 \pm 10$)

Type	Profile	Recommended Range f_0 (MHz)	Nominal Length (in.) ± 0.030 in.	Nominal Length Range (in.)	Characteristic Impedance (Ω)		
$\lambda/4$ Quarter wave length	HP	400–600	$L = 311/f_0$ (MHz)	0.518–0.778	8.6		
	EP	300–800		0.389–1.037	7.7		
	SP	300–1000		0.311–1.037	6.3		
	LS	300–1500		0.207–1.037	6.3		
	LP	300–1400		0.222–1.037	9.4		
	MP	400–1700		0.183–0.778	8.8		
	SM	400–1700		0.183–0.778	6.3		
	$\lambda/2$ Half wave length	HP		800–1200	$L = 622/f_0$ (MHz)	0.518–0.778	8.6
		EP		800–1700		0.366–0.778	7.7
		SP		800–2100		0.296–0.778	6.3
LS		800–3100	0.201–0.778	6.3			
LP		800–2800	0.222–0.778	9.4			
MP		800–3400	0.183–0.778	8.8			
SM	800–3400	0.183–0.778	6.3				

B.1.2 Micro-coax semi-rigid line

MICRO-COAX
Leading the way in transmission line solutions.

206 Jones Blvd. Pottstown, PA 19464 USA
Phone: 610-495-0110 : 800-223-2629
www.micro-coax.com

UT-141C-LL
()

Semi-Rigid Coaxial Cable

MECHANICAL CHARACTERISTICS

Outer Conductor Diameter, inch (mm)	0.141+/-0.002 (3.581+/-0.0508)		
Dielectric Diameter, inch (mm)	0.1175 (2.985)		
Center Conductor Diameter, inch (mm)	0.0403+/-0.001 (1.024+/-0.0254)		
Maximum Length, feet (meters)	20 (6.1)		
Minimum Inside Bend Radius, inch (mm)	0.5 (12.7)		
Weight, pounds/100 ft. (kg/100 meters)	3.2 (4.76)		

ELECTRICAL CHARACTERISTICS

Impedance, ohms	50+/-1.5		
Frequency Range GHz	DC-36		
Velocity of Propagation %	77		
Capacitance, pF/ft. (pF/meter)	26.6 (87.3)		
Typical Insertion Loss, dB/ft. (dB/meter) and Average Power Handling, Watts CW at 20 degrees Celsius and Sea level	Frequency	Insertion Loss	Power
	0.5 GHz	0.07 (0.23)	821
	1.0 GHz	0.10 (0.33)	576
	5.0 GHz	0.23 (0.75)	249
	10.0 GHz	0.33 (1.09)	172
20.0 GHz	0.49 (1.59)	117	
Corona Extinction Voltage, VRMS @ 60 Hz	1900		
Voltage Withstand, VRMS @ 60 Hz	5000		

ENVIRONMENTAL CHARACTERISTICS

Outer Conductor Integrity Temperature, Deg Celsius	Not Applicable		
Maximum Operating Temperature, Deg Celsius	250		

MATERIALS

Outer Conductor	Copper		
Dielectric	LD PTFE		
Center Conductor	SPC		

CUTAWAY

B.1.3 SRC semi-rigid lines

Semi-Rigid		0.023	0.047	0.085	0.141	0.250	0.047	0.085	0.141	0.250	0.047	0.085	0.141
Shield		SnPlateCu	SnPlateCu	SnPlateCu	SnPlateCu	SnPlateCu	SnPlateAl	SnPlateAl	SnPlateAl	SnPlateAl	SnPlateAl	SnPlateAl	SnPlateAl
Center Conductor		Silver Covered Copper Clad Steel	Silver Covered Copper Clad Steel	Silver Covered Copper Clad Steel	Silver Covered Copper Clad Steel	Silver Covered Copper Clad Steel	Silver Covered Copper Clad Steel	Silver Covered Copper Clad Steel	Silver Covered Copper Clad Steel	Silver Covered Copper Clad Steel	Silver Covered Copper Clad Steel	Silver Covered Copper Clad Steel	Silver Covered Copper Clad Steel
Dimension in. (mm)		.005 (.127)	.011 (.288)	.020 (.51)	.036 (.91)	.064 (1.62)	.0113 (.288)	.020 (.51)	.036 (.91)	.064 (1.62)	.0113 (.288)	.020 (.51)	.036 (.91)
Dielectric		PTFE .017	PTFE .037	PTFE .066	TFE .116	PTFE .209	PTFE .037	PTFE .066	PTFE .118	PTFE .209	PTFE .037	PTFE .066	PTFE .118
Min. Inside Bend	in. rad	0.05	0.05	0.05	0.075	0.375	0.05	0.07	0.125	0.375	0.05	0.07	0.125
Outside Dia	in. (mm)	.023 (.584)	.047 (1.19)	.085 (2.16)	.141 (3.58)	.250 (6.35)	.047 (1.19)	.085 (2.16)	.141 (3.58)	.250 (6.35)	.047 (1.19)	.085 (2.16)	.141 (3.58)
Impedance		50	50	50	50	50	50	50	50	50	50	50	50
Capacitance		29	29	29	29	29	29	29	29	29	29	29	29
Max Voltage	vrms	750	2,000	5,000	5,000	7,500	2,000	5,000	5,000	7,500	2,000	5,000	5,000
Temperature range	°C	+125	+150	+125	+125	+100	+150	+125	+125	+100	+150	+125	+125
Cutoff Frequency		245GHz	109GHz	61GHz	34GHz	19GHz	108GHz	64GHz	34GHz	19GHz	108GHz	64GHz	34GHz
Attenuation (dB/100ft)													
	.5GHz	53.3	24	13.6	7.8	4.6	25.8	13.4	8.3	4.6	25.8	13.4	8.3
	1GHz	75.6	34.2	19.5	11.3	6.8	36.7	19.1	12.1	6.8	36.7	19.1	12.1
	5GHz	171	78.8	45.9	27.7	17.4	84.5	43.3	30.1	17.4	84.5	43.3	30.1
	10GHz	245	113.8	67.5	41.5	27	121.9	62	45.5	27	121.9	62	45.5
	20GHz	351	165.9	100.3	63.6	NA	177.3	89.1	70	NA	177.3	89.1	70
Power (W)													
	.5GHz	20	67.4	232	484	1061	96.8	298	600	1061	96.8	298	600
	1GHz	14	47.4	162	336	728	68.1	210	450	728	68.1	210	450
	5GHz	6.0	21	70	140	290	29.9	93	180	290	29.9	93	180
	10GHz	5.0	14.4	48	95	190	20.8	65	120	190	20.8	65	120
	20GHz	3.0	10	33	63	NA	14.4	45	70	NA	14.4	45	70

B.2 Passive lumped elements

B.2.1 Coilcraft® Micro spring™ air core inductors

Part number ¹	Turns	L ² (nH)	Percent tol ³	Q ⁴ min	SRF min ⁵ (GHz)	DCR max ⁶ (mOhm)	I _{rms} ⁷ (A)
0906-2KL_	2	1.65	10	100	10.0	4.0	1.6
0906-3JL_	3	2.55	5	100	8.2	5.0	1.6
0906-4_L_	4	3.85	5,2	100	7.5	6.0	1.6
0906-5_L_	5	5.40	5,2	100	7.0	8.0	1.6
1606-6_L_	6	5.60	5,2	100	6.5	9.0	1.6
1606-7_L_	7	7.15	5,2	100	6.0	10	1.6
1606-8_L_	8	8.80	5,2	100	6.0	12	1.6
1606-9_L_	9	9.85	5,2	100	5.2	13	1.6
1606-10_L_	10	12.55	5,2	100	4.6	14	1.6

1. When ordering, specify **tolerance, termination and packaging** codes:

1606-10 **G L C**

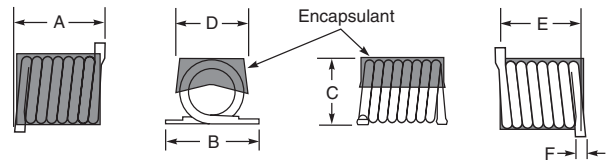
Tolerance: **G** = 2% **J** = 5% **K** = 10% (Table shows stock tolerances in bold.)

Termination: **L** = RoHS compliant tin-silver (96.5/3.5) over copper. Special order: **T** = RoHS tin-silver-copper (95.5/4/0.5) or **S** = non-RoHS tin-lead (63/37).

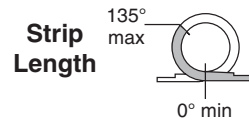
Packaging: **C** = 7" machine-ready reel. EIA-481 embossed plastic tape, 500 parts per full reel.

B = Less than full reel. In tape, but not machine-ready. To have a leader and trailer added (\$25 charge), use code letter C instead.

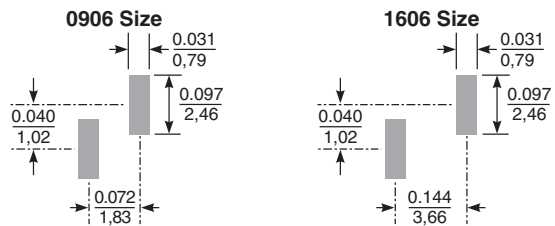
- Inductance measured using Agilent/HP 4286 with Coilcraft SMD-A fixture and correlation.
 - Tolerances in bold are stocked for immediate shipment.
 - Q measured at 800 MHz, using an Agilent/HP 4291A with an Agilent/HP 16193A test fixture.
 - SRF measured using an Agilent/HP 8720D with a Coilcraft SMD-D fixture.
 - DCR tested on the Cambridge Technology Model 510 Micro-ohmmeter.
 - Current that causes a 15°C temperature rise from 25°C ambient.
 - Electrical specifications at 25°C.
- See Qualification Standards section for environmental and test data.
Refer to Doc 362 "Soldering Surface Mount Components" before soldering.



Size	A max	B max	C max	D	E	F max
0906	0,095 2,41	0,135 3,43	0,060 1,52	0,055 ± 0,010 1,40 ± 0,25	0,072 ± 0,010 1,83 ± 0,25	0,020 0,51
1606	0,165 4,19	0,135 3,43	0,062 1,58	0,055 ± 0,010 1,40 ± 0,25	0,144 ± 0,012 3,66 ± 0,30	0,020 0,51

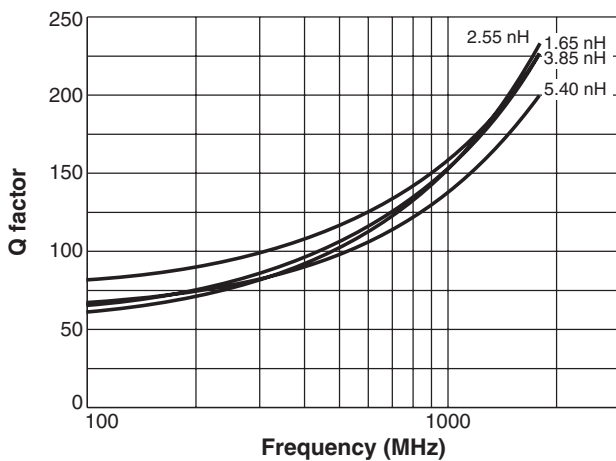


Recommended Land Patterns

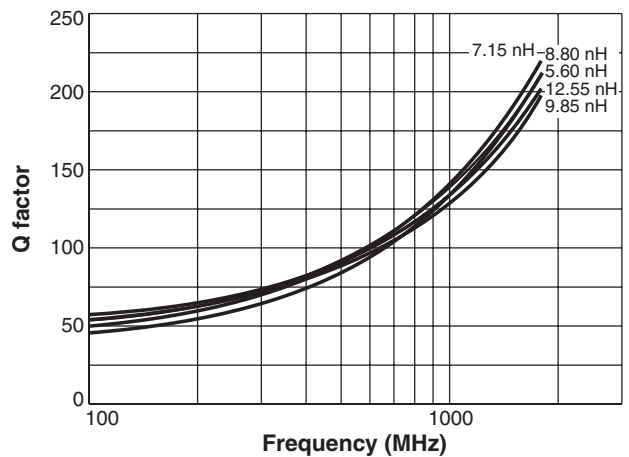


Dimensions are in $\frac{\text{inches}}{\text{mm}}$

Typical Q vs Frequency – 0906 Series

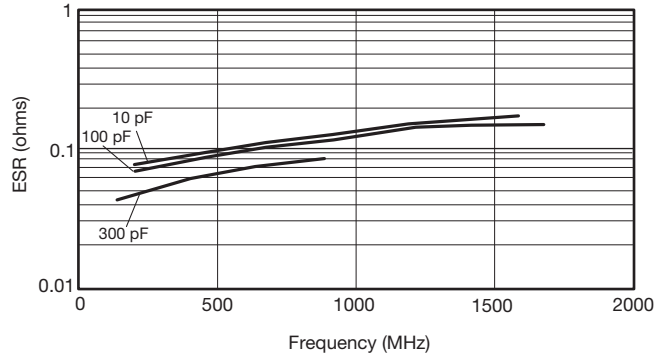


Typical Q vs Frequency – 1606 Series

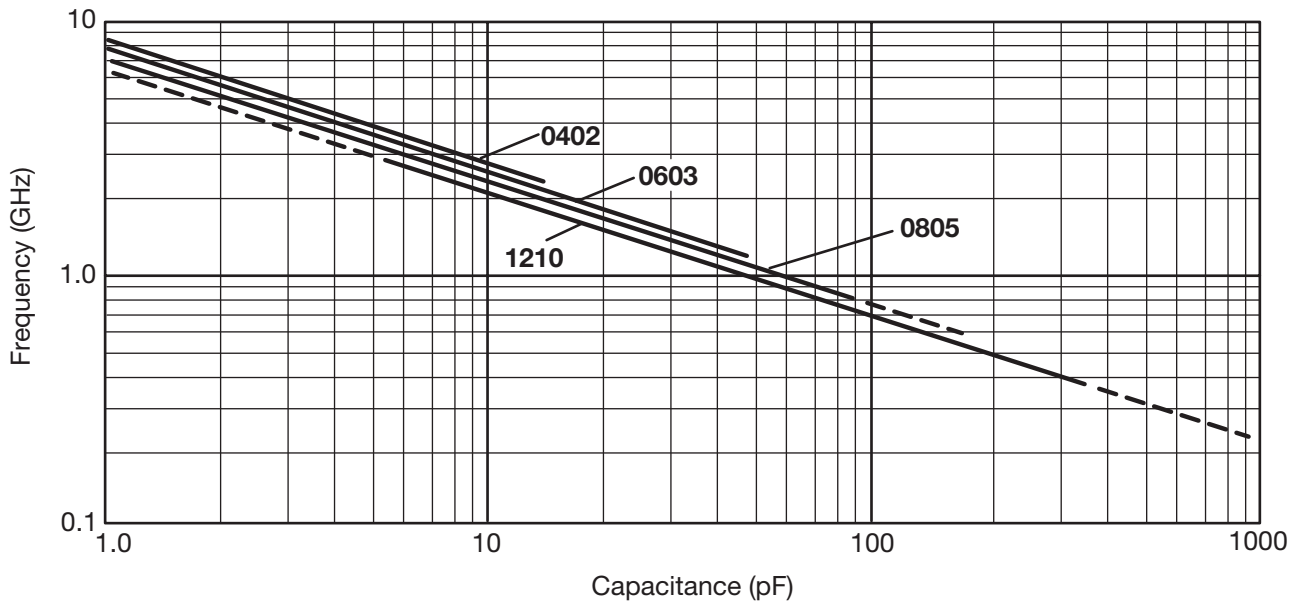


B.2.2 AVX Microwave MLC C0G (NP0)

**TYPICAL ESR vs. FREQUENCY
1210 "U" SERIES**



**TYPICAL
SERIES RESONANT FREQUENCY
"U" SERIES CHIP**



B.3 Varactor diodes

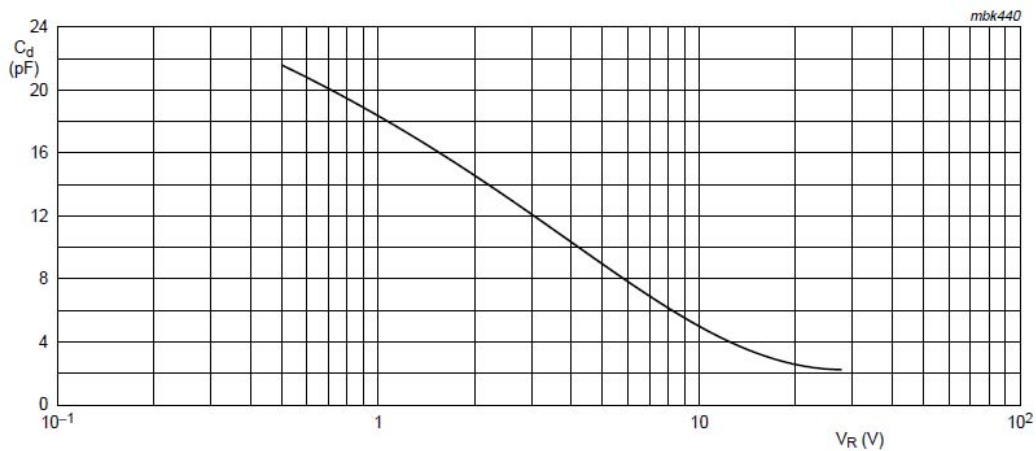
B.3.1 NXP BB179

Table 5: Characteristics

$T_j = 25\text{ }^\circ\text{C}$ unless otherwise specified.

Symbol	Parameter	Conditions	Min	Typ	Max	Unit
I_R	reverse current	see Figure 2				
		$V_R = 30\text{ V}$	-	-	10	nA
		$V_R = 30\text{ V}; T_j = 85\text{ }^\circ\text{C}$	-	-	200	nA
r_s	diode series resistance	$f = 470\text{ MHz}$	[1]	0.6	0.75	Ω
C_d	diode capacitance	$f = 1\text{ MHz}$; see Figure 1 and 3				
		$V_R = 1\text{ V}$	18.22	-	21.26	pF
		$V_R = 28\text{ V}$	1.951	2.1	2.225	pF
$\frac{C_d(1V)}{C_d(2V)}$	capacitance ratio	$f = 1\text{ MHz}$	-	1.27	-	
$\frac{C_d(1V)}{C_d(28V)}$	capacitance ratio	$f = 1\text{ MHz}$	8.45	9	10.9	
$\frac{C_d(25V)}{C_d(28V)}$	capacitance ratio	$f = 1\text{ MHz}$	-	1.05	-	
$\frac{\Delta C_d}{C_d}$	capacitance matching	$V_R = 1\text{ V to }28\text{ V}$; in a sequence of 10 diodes (gliding)	-	-	2	%

[1] V_R is the value at which $C_d = 9\text{ pF}$



$f = 1\text{ MHz}; T_j = 25\text{ }^\circ\text{C}$.

Fig 1. Diode capacitance as a function of reverse voltage; typical values.

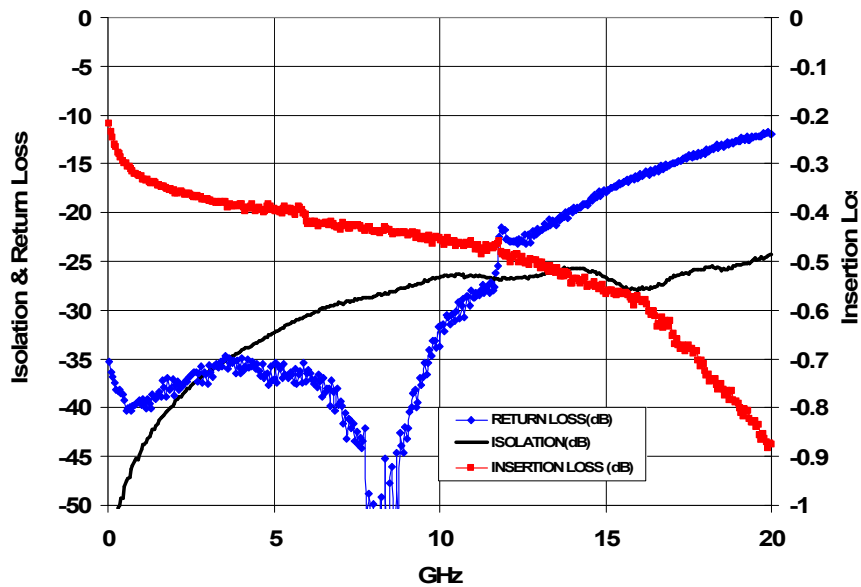
B.4 RF switches

B.4.1 Randant MEMS

SPDT High Isolation RF-MEMS Switch, DC to 20 GHz

RMSW221™

Typical RF Performance



- Measured characteristics between RF ports Drain and Source 1. Similar characteristics were measured between Drain and Source 2.
- Measurement results include bond wires.

Appendix C

Numerical computation

```

function cheby_proto(N,La)
% cheby_proto Chebyshev low pass prototype values
% @ N = order of the filter
% @ ripple_dB is the passband ripple

% from insetion loss to ripple:
s11_2 = 10^(-La/10);
s12_2 = 1 - s11_2;
ripple_dB = 10*log10(1/s12_2);

beta = log( coth( ripple_dB/17.37 ) );
gamma = sinh(beta/(2*N));

% g0 and gn+1
g0 = 1;
if mod(N,2)      % if odd
    gnp1 = 1;
else            % if even
    gnp1 = coth(beta/4)^2;
end

k = 1:N;
a = sin( (2*k-1)*pi/(2*N) );
b = gamma^2 + sin(k*pi/N).^2;

g = zeros(1,N);

g(1) = 2*a(1)/gamma;
for k=2:N
    g(k) = 4*a(k-1)*a(k)/( b(k-1)*g(k-1) );
end

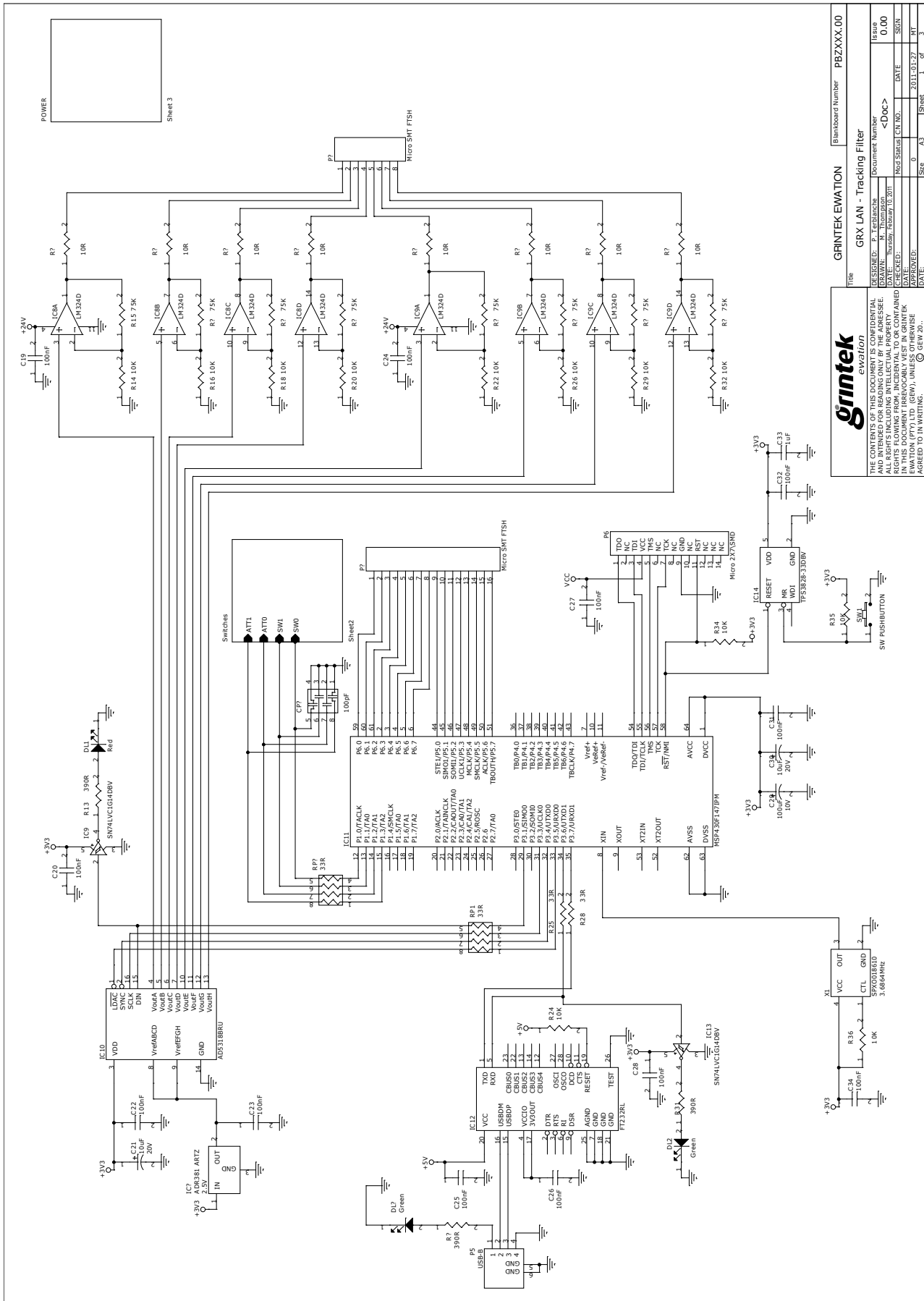
g = [g0 g gnp1];

```

Figure C.1: MATLAB® code for computation of chebyshev prototype values

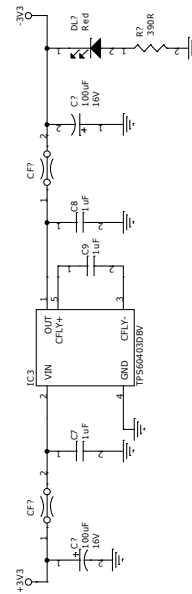
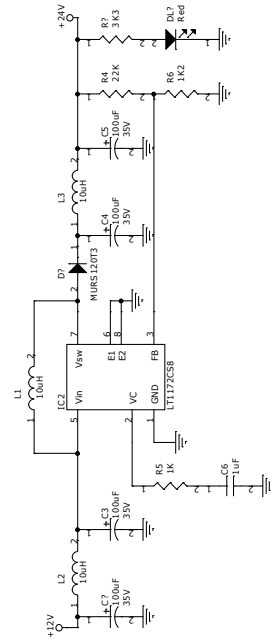
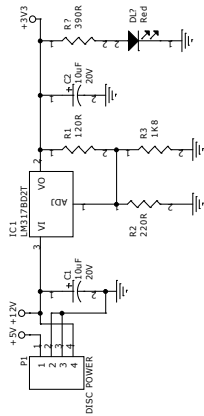
Appendix D

Digital control system schematics

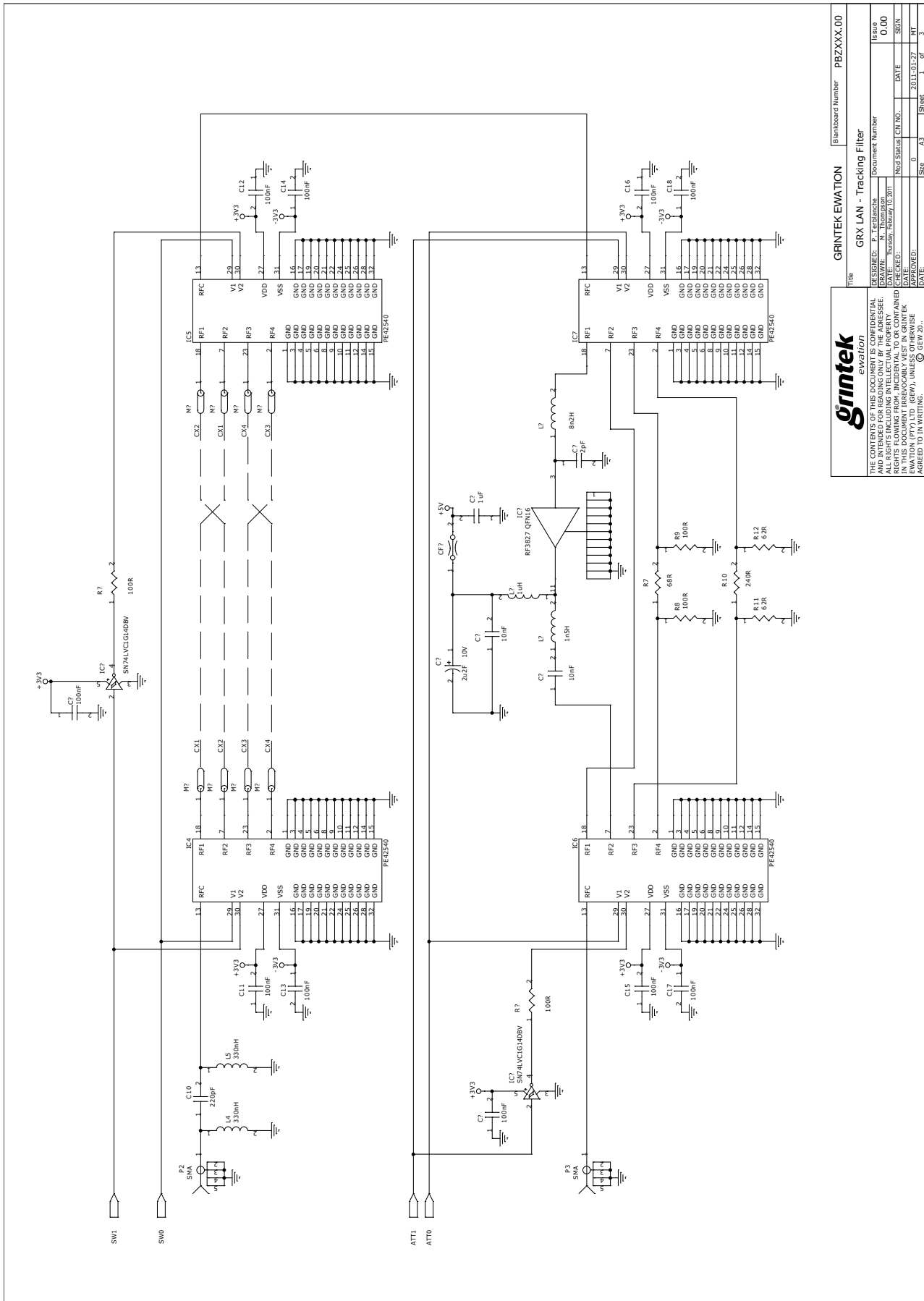


Title		GRINTEK EMATION		Revision Number		PBZXXX.00	
DESIGNED - P. T. van den Bosch		Document Number		GRX LAN - Tracking Filter		Issue	
DATE: Tuesday, 15 March 2011		Checked		DATE: Tuesday, 15 March 2011		0.00	
APPROVED:		Checked		DATE: 2011-01-27		SIGN	
DATE:		Checked		DATE:		WT	
Sheet		A3		1		of 3	

Grintek
 ewg10701
 THE GRINTEK LOGO, THE GRINTEK NAME, AND RELATED OR HANGING ONLY BY THE ADDRESS. ALL RIGHTS INCLUDING INTELLECTUAL PROPERTY RIGHTS IN SOFTWARE, FIRMWARE, AND COMPANIED EMATION (PTY) LTD. (GEM), UNLESS OTHERWISE AGREED TO IN WRITING. © GEM 20...



Grintek ewatton		Title	GRINTEK EWATTON	Sheet Number	PEZXXX.00
THE CONTAINED INFORMATION IS UNCLASSIFIED AND INTENDED FOR READING ONLY BY THE ADDRESSEE. ALL RIGHTS INCLUDING INTELLECTUAL PROPERTY RIGHTS ARE RESERVED FOR THE COMPANY AND/OR EWMATON (PTY) LTD (GRV), UNLESS OTHERWISE AGREED TO IN WRITING. © GRV 2011.		Document Number	GRX LAN - Tracking Filter	Issue	0.00
DESIGNED BY	P. Terblanche	DATE	Tuesday, February 05, 2013	Doc No.	<DOC>
CHECKED BY	Boyd Shurutt	DATE		Sheet	1 of 3
APPROVED BY		DATE	2011/01/27		



List of References

- [1] J.G. Proakis and D.G. Manolakis. *Digital signal processing*. Pearson Prentice Hall, 2007. viii, 1, 2
- [2] R.G. Vaughan, N.L. Scott, and D.R. White. The theory of bandpass sampling. *Signal Processing, IEEE Transactions on*, 39(9):1973–1984, sep 1991. viii, 3
- [3] G.M. Rebeiz and J.B. Muldavin. RF MEMS switches and switch circuits. *Microwave Magazine, IEEE*, 2(4):59–71, dec 2001. ix, 4, 42, 43
- [4] J.Y. Park, G.H. Kim, K.W. Chung, and J.U. Bu. Electroplated RF MEMS capacitive switches. In *Micro Electro Mechanical Systems, 2000. MEMS 2000. The Thirteenth Annual International Conference on*, pages 639–644, jan 2000. ix, 46
- [5] G.L. Matthaei, L. Young, and E.M.T. Jones. *Microwave filters, impedance-matching networks, and coupling structures*. Artech House microwave library. Artech House Books, 1980. 3, 8, 9, 11, 12, 16, 17, 19, 21, 28, 38, 45, 49, 72
- [6] D.E. Johnson. *Introduction to filter theory*. Prentice-Hall electrical engineering series. Prentice-Hall, 1976. 3, 8, 49
- [7] J.A.G. Malherbe. *Microwave transmission line filters*. Artech Microwave Library. Artech House, 1979. 3, 20, 49
- [8] I.C. Hunter and Institution of Electrical Engineers. *Theory and design of microwave filters*. IEE electromagnetic waves series. Institution of Electrical Engineers, 2001. 3, 9, 10, 23, 26, 49
- [9] D.M. Pozar. *Microwave engineering*. J. Wiley, 2005. 3, 8, 11, 12, 33, 40, 42, 43, 44, 45, 47, 49
- [10] I.C. Hunter and J.D. Rhodes. Electronically tunable microwave bandpass filters. *Microwave Theory and Techniques, IEEE Transactions on*, 30(9):1354–1360, sep. 1982. 3, 32, 33, 38, 45, 49
- [11] G. Rebeiz, K. Entesari, I. Reines, S.-j. Park, M. El-tanani, A. Grichener, and A. Brown. Tuning in to RF MEMS. *Microwave Magazine, IEEE*, 10(6):55–72, oct. 2009. 4, 40, 43, 45, 46, 72
- [12] J. Uher and W.J.R. Hoefer. Tunable microwave and millimeter-wave band-pass filters. *Microwave Theory and Techniques, IEEE Transactions on*, 39(4):643–653, apr 1991. 4, 45
- [13] A.R. Brown and G.M. Rebeiz. A varactor-tuned RF filter. *Microwave Theory and Techniques, IEEE Transactions on*, 48(7):1157–1160, jul 2000. 4, 45

LIST OF REFERENCES

- [14] Ikuo Awai. Meaning of resonator's coupling coefficient in bandpass filter design. *Electronics and Communications in Japan (Part II: Electronics)*, 89(6):1–7, 2006. 12
- [15] J.B. Ness. A unified approach to the design, measurement, and tuning of coupled-resonator filters. *Microwave Theory and Techniques, IEEE Transactions on*, 46(4):343–351, apr 1998. 12
- [16] B.S. Guru and H.R. Hızıroğlu. *Electromagnetic field theory fundamentals*. Cambridge University Press, 2004. 13
- [17] P.W. van der Walt. Microwave networks lecture notes. June 2010. 15
- [18] R.J. Wenzel. Exact design of TEM microwave networks using quarter-wave lines. *Microwave Theory and Techniques, IEEE Transactions on*, 12(1):94–111, jan 1964. 26, 27
- [19] G.D. Vendelin, A.M. Pavio, and U.L. Rohde. *Microwave circuit design using linear and nonlinear techniques*. Wiley, 2005. 41, 43, 44, 45
- [20] K. Entesari, K. Obeidat, A.R. Brown, and G.M. Rebeiz. A 25 to 75 MHz RF MEMS tunable filter. *Microwave Theory and Techniques, IEEE Transactions on*, 55(11):2399–2405, nov. 2007. 43
- [21] D.A. Neamen. *Microelectronics: circuit analysis and design*. McGraw-Hill, 2007. 43
- [22] Skyworks Solutions, Inc. *Application Note: Varactor Diodes*, Rev. A edition, August 2008. 43
- [23] P.S. Carter. Magnetically-tunable microwave filters using single-crystal yttrium-iron-garnet resonators. *Microwave Theory and Techniques, IRE Transactions on*, 9(3):252–260, may 1961. 45
- [24] T. Reeves, N. Van Stigt, and C. Rossiter. A method for the direct synthesis of general sections. In *Microwave Symposium Digest, 2001 IEEE MTT-S International*, volume 3, pages 1471–1474 vol.3, 2001. 47
- [25] J.B. Thomas. Cross-coupling in coaxial cavity filters - a tutorial overview. *Microwave Theory and Techniques, IEEE Transactions on*, 51(4):1368–1376, apr 2003. 47
- [26] A.I. Zverev. *Handbook of filter synthesis*. Wiley, 1967. 47
- [27] R. Levy. Direct synthesis of cascaded quadruplet (cq) filters. *Microwave Theory and Techniques, IEEE Transactions on*, 43(12):2940–2945, dec 1995. 47
- [28] G.D. Alley. Interdigital capacitors and their application to lumped-element microwave integrated circuits. *Microwave Theory and Techniques, IEEE Transactions on*, 18(12):1028–1033, dec 1970. 64
- [29] B.C. Wadell. *Transmission line design handbook*. Artech House - Antennas and Propagation Library. Artech House, 1991. 64